THE GALACTIC NOVA RATE: ESTIMATES FROM ALL-SKY TIME DOMAIN SURVEYS

By

Adam Kawash

A DISSERTATION

Submitted to
Michigan State University
in partial fulfillment of the requirements
for the degree of

Astrophysics and Astronomy−Doctor of Philosophy

2022

ABSTRACT

THE GALACTIC NOVA RATE: ESTIMATES FROM ALL-SKY TIME DOMAIN SURVEYS

By

Adam Kawash

There is a significant discrepancy between recent predictions of the Milky Way classical nova rate of ~ 60 per year and the annual discovery rate of ~ 10. Why the recovery fraction of these events is $\sim 15\%$ even with large advancements to observational time domain astronomy remains largely unexplained. Because of the location of Earth within the Galaxy, discovering Galactic transients requires a large field of view. For the past few decades, observations from a network of amateur astronomers were largely responsible for discovering classical novae, so the sky-coverage as a function of position and depth was difficult to model. Fortunately, in the past decade, many time domain surveys with fields of view that cover large areas of the sky have been commissioned, making the sky-coverage more well defined. To date, there are no Galactic nova rate predictions made using data from a time domain survey that is capable of observing the entire sky. In this thesis, the first estimate of the Galactic nova rate using observations from two all-sky surveys is made.

The All-Sky Automated Survey for Supernovae (ASAS-SN) is the first survey to systematically observe the entire sky every night, providing unprecedented cadence of the sky for transients and variable stars. The space-based survey *Gaia* has a broad observing filter and a fine (~ 0.1 arcsecond) pixel scale, so it is capable of detecting Galactic plane transients in crowded fields that are heavily affected by extinction. These are the only two all-sky surveys to report classical nova candidates, and they have contributed to marginally increasing

the discovery rate of Galactic novae to 13 per year on average since 2017. In addition to the increase in discoveries, this thesis exploits the systematic observing patterns to estimate what fraction of the Galaxy's novae these surveys detect. To make this estimate, I have constructed a statistical model of Galactic classical novae by utilizing the recently published models of stellar density and extinction of the Milky Way. Using ASAS-SN photometry, I measure the outburst amplitude of novae to be normally distributed with mean and standard deviation $\mu = 11.43 \pm 0.25$ mag and $\sigma = 2.57 \pm 0.20$ mag, respectively. By using recently available all-sky 3D dust maps, I estimate that $\sim 50\%$ of Galactic novae are hidden by extinction from being detected by ASAS-SN. Finally, I estimate that the recovery fraction of the global population of Galactic novae for ASAS-SN $\approx 33\%$, *Gaia* $\approx 42\%$, and a joint effort of the two surveys $\approx 54\%$, predicting that the Galactic nova rate is 26 ± 5 yr^{-1}, significantly lower than recent estimates.

To my Dad, who will probably be the only person to read this from front to back. I hope you like it.

ACKNOWLEDGMENTS

I am extremely grateful for all of my family, friends, and colleagues that supported me during my time at Michigan State University. I genuinely thought I would not finish my Ph.D., so thank you to everyone who helped me get this far.

To Laura, thank you for being an intelligent, supportive, and considerate advisor. Thank you for funding me as a research assistant and still agreeing to advise me even when I decided to work on an optical time-domain survey. I realize these past few years have been tough, but you have been an amazing mentor to me in the face of all of life's obstacles.

To my undergraduate advisor Maura, thank you for encouraging me to go to graduate school. I can confidently say I would not be here without you. Thank you to Elias, Jay, and Kirill for being excellent nova experts who I could always bug with questions. Thank you to everyone I shared an office with from the Bunker, BPS 4260, and to Slim and Tig in the home office.

Thank you to Claire, Justin, and Mike for struggling alongside me over the past five years and for helping me (almost) pass the qualifying exam. I am very grateful for the friends I have made during my time here that have made Lansing a fun place to live.

Brynn, thank you for moving to Michigan with me and keeping the past four years interesting and enjoyable. All of this was a lot easier with you here with me.

TABLE OF CONTENTS

LIST OF TABLES . . . . . **viii**

LIST OF FIGURES . . . . . **ix**

KEY TO ABBREVIATIONS . . . . . **xvi**

Chapter 1 Introduction **1**
1.1 What is a Classical Nova? 2
1.2 The Galactic nova rate problem 5
1.3 How can this thesis better estimate the Galactic nova rate? 7
1.3.1 ASAS-SN 7
1.3.2 mwdust 10
1.3.3 Gaia 12
1.4 Why is it important to study novae? 14
1.5 Outline 15

Chapter 2 Classical Novae Masquerading as Dwarf Novae? Outburst Properties of Cataclysmic Variables with ASAS-SN **17**
2.1 Introduction 18
2.2 Methods 23
2.2.1 Catalog 23
2.2.2 Light curves 24
2.2.3 Outburst Peak Magnitude and Decline Time 27
2.2.4 Outburst Amplitude 28
2.3 Results 29
2.3.1 Detected DN and CN Outbursts 29
2.3.2 Outburst vs. Quiescent Brightness 32
2.3.3 Outburst amplitude vs. t2 33
2.4 Which Dwarf Novae might be mis-classified Classical Novae? 40
2.5 Conclusions 44
2.6 Appendix 49
2.6.1 Filter Transformations 49
2.6.2 Quiescent Magnitude Measurements 51
2.6.3 Astrometry and Catalog Matching 52
2.6.4 Sensitivity/Contamination 54
2.6.5 Classical and Reccurent Nova Outburst Properties 58

Chapter 3 Galactic Extinction: How Many Novae Does it Hide and How Does it Affect the Galactic Nova Rate? **62**
3.1 Introduction 63

3.2 Nova Model/Results . . . 66
3.2.1 Stellar Density Profile . . . 66
3.2.2 Extinction Model . . . 67
3.2.3 Positions and Distances . . . 68
3.2.4 Brightness Distribution . . . 71
3.2.5 Reddened Novae . . . 74
3.3 Global Nova Rate Estimates . . . 79
3.4 How Sensitive Are The Results to our Assumptions? . . . 87
3.4.1 Extinction Models . . . 87
3.4.2 Mass Model . . . 88
3.4.3 Differing Bulge and Disk Populations . . . 89
3.5 Conclusions . . . 92
3.6 Appendix . . . 94
3.6.1 Besancon Mass Model . . . 94
3.6.1.1 Thin Disk . . . 94
3.6.1.2 Thick Disk . . . 96
3.6.1.3 Bulge/Bar . . . 96
3.6.1.4 Stellar Halo . . . 97

Chapter 4 The Galactic Nova Rate: Estimates from the ASAS-SN and *Gaia* Surveys . . . 98
4.1 Introduction . . . 99
4.1.1 History of Nova Discoveries . . . 101
4.1.2 Galactic nova rate predictions . . . 104
4.2 Discovered Samples . . . 108
4.2.1 Gaia Discovery Rate . . . 110
4.2.2 ASAS-SN Discovery Rate . . . 113
4.2.3 The joint ASAS-SN and Gaia Discovery Rate . . . 114
4.3 Monte Carlo Simulations . . . 114
4.3.1 Positions . . . 114
4.3.2 Peak Apparent Magnitude . . . 115
4.3.3 Lightcurves . . . 118
4.3.4 Gaia Simulation . . . 124
4.3.5 ASAS-SN Simulation . . . 127
4.4 Global Nova Rate Estimates . . . 130
4.5 Comparisons to Previous Results . . . 135
4.5.1 Bulge vs. Disk Rates . . . 135
4.5.2 Comparison to Palomar Gattini-IR . . . 137
4.5.3 Extragalactic Comparisons and Faint/Fast Novae . . . 140
4.6 Conclusions . . . 141

Chapter 5 Conclusions and Future Work . . . 146

BIBLIOGRAPHY . . . 150

LIST OF TABLES

Table 2.1: Outburst Properties of Dwarf Novae 31

Table 2.2: Classical and Rapid Recurrent Nova Candidates 44

Table 2.3: Outburst Properties of Classical and Recurrent Novae 60

Table 2.3: Outburst Properties of Classical and Recurrent Novae 61

Table 3.1: Galactic Nova Rates For Various Parameters 86

Table 3.2: Mass and Normalization values for the various components of the Galactic model 95

Table 4.1: Confirmed Galactic Classical Novae 2019–2021 109

Table 4.1: Confirmed Galactic Classical Novae 2019–2021 110

Table 4.2: Unconfirmed Classical Nova Candidates 2019–2021 111

LIST OF FIGURES

Figure 1.1: Artist's rendtition of a nova eruption. credit: Krzysztof Ulaczyk / Warsaw University Observatory 2

Figure 1.2: Example of a set of grey scale images automatically generated to vet the legitimacy of an ASAS-SN candidate. The scale is denoted at the bottom showing lighter pixels as having higher flux, grey having no flux, and darker pixels having negative flux. The top left panel is the reference image of the field with a green circle centered on the position of the candidate. The rest of the panels show this reference image subtracted by the observations on an individual epoch (i.e., image subtraction). The second through fourth column of the top row show the three individual exposures taken on the latest night and the panel below the reference image shows the result of adding these three images. The rest of the panels show the coadded images from the most recent epochs before the alert was generated at the position of this candidate. This example is the nova ASASSN-21fh or V1710 Sco, first detected by ASAS-SN on 2021-04-12. 9

Figure 1.3: Credit: Figure 1 from Bovy et al. (2016). This shows how the three dust maps were stitched together to create an all-sky 3D dust map. The grey scale shows the amount of extinction in *Gaia* G-band out to 5 kpc. 12

Figure 2.1: The ASAS-SN light curve of the dwarf nova ASASN-14fu. The $\geq$5-sigma detections are shown for V-band and g-band observations in blue and orange, respectively. The black triangles denote 5σ upper limits derived from non-detections, and the gaps in the data are due to seasonal the Solar constraints. 25

Figure 2.2: Galactic (top) and equatorial (bottom) coordinate positions of CVs with outburst property estimates. Dwarf novae are shown in blue, and classical novae are shown in red. The gap in the data for dwarf novae is due to the survey limits of Pan-STARRS 30

Figure 2.3: Peak magnitude of outburst versus measured brightness in quiescence for all outbursts discussed in this work. Dwarf nova outbursts are shown in blue, and classical nova outbursts without companion information are shown in red. Those classical novae where the companion type is known are denoted as green X's, orange stars, and cyan crosses for main sequence, red giant, and sub-giant companions, respectively. The non-shaded region indicates where our analysis can measure outburst properties by combining ASAS-SN and Pan-STARRS observations. Only these surveys were used to study DNe, but AAVSO V-band observations were utilized to study CNe that peak above the saturation limit of ASAS-SN. The dashed line shows an outburst amplitude of 8 mag. The "amplitude-limited" diagonal shaded region shows the requirement that outbursts in our catalog must have amplitudes >2 mag, and quiescent brightness measurements in this region are likely contaminated by outbursts. The horizontal gray shaded region at top denotes the saturation limit of ASAS-SN ($g \lesssim 10$ mag). The horizontal shaded region at bottom signifies two magnitudes brighter than the sensitivity limit of ASAS-SN ($g \gtrsim 18$ mag). Finally, the vertical shaded region at right represents the saturation limit of the Pan-STARRS 3π survey ($g \lesssim 13$ mag). . 34

Figure 2.4: Amplitude of outburst versus the time t_2 to decline by two magnitudes from maximum for both CNe and DNe. A filled circle signifies that both the outburst amplitude and t_2 were estimated for that object. A triangle signifies that a lower limit was placed on the outburst amplitude, and an open symbol shows the upper limit that was placed on t_2. Though we are able to place lower and upper limits on t_2, we only show the upper limit for visualization purposes. Blue objects denote DN outbursts, while CNe analyzed in this work and Strope et al. (2010) are represented with symbols as in Figure 2.3. The top and right panels show the distributions of t_2 and outburst amplitude, respectively, with DNe shown in blue and CNe shown in red. The dashed histograms show the distributions of only measured values, not limits, and the solid lines shows the fits to the measured values including the limits. 35

Figure 2.5: The outburst amplitude versus $\log t_2$ for the CNe analyzed in this work. The markers are the same as Figure 2.4. The red dashed line and the red shaded region show our best-fit relation for CNe, with values and uncertainty given in §2.3.3. The dotted black lines show the expected theoretical correlation derived from the MMRD relationship from Figure 5.4 of Warner (1995). 39

Figure 2.6: The brightest possible peak g-band absolute magnitude an outburst could have while still being in the Galaxy, as a function of the amount of g-band extinction. The objects with 3σ parallax detections in *Gaia* are assumed to be at the distances in Bailer-Jones et al. (2018) and are plotted in green. The violet points are objects that do not have significant *Gaia* parallaxes, so we place a limit on the brightest peak absolute magnitude by assuming a maximum Galactic distance of 30 kpc. In order to be luminous enough to be a CN, the absolute magnitude needs to be brighter than $M_g \approx -4.2$ mag, and this cutoff is shown as the dashed black line. The peak absolute magnitude presented here is not an accurate measurement especially for objects with no reliable distance estimates and those with large amounts of dust extinction; the plotted values are only used to select CN candidates. 42

Figure 2.7: ASAS-SN Light curves for 4 of the candidates listed in Table 2.2. The left column shows all observations of these objects and the right column shows the observations around the brightest outburst. Blue and orange points denote the $\geq$5-sigma detections from V-band and g-band observations, respectively, and the black triangles signify the $\geq$5-sigma upper limits from non-detections. 45

Figure 2.8: Same as Figure 2.7 for the remaining 4 candidates in Table 2.2. . . . 46

Figure 2.9: Top: Distribution of observed time to decline by two magnitudes for detected DN outbursts in blue and the probability distribution for measuring the decline as a function of t_2 in red. Both distributions are normalized so that the area under the curve is unity, but the red curve is then multiplied by a factor of four for visualization purposes. Bottom: Peak g magnitudes of DN outbursts vs. measurements and limits of the time to decline by two magnitudes from maximum. Real DN outbursts are shown as blue circles. The red contours show the fraction of time the decline time of fake transients could be successfully measured or constrained with an upper limit in our analysis. . 56

Figure 2.10: Outburst amplitude for the dwarf novae as a function of duty cycle. 57

Figure 2.11: Light curves of four classical novae analyzed in this work. The $\geq$5-sigma detections for ASAS-SN g-band, ASAS-SN V-band and AAVSO V-band observations are shown in orange, blue, and green respectively after converting to brightness in g-band. The black triangles denote 5-sigma upper limits from non-detections These show examples of faint outbursts (top left), flares causing multiple peaks (top right), outbursts during solar conjunction (bottom left), and smooth declines (bottom right). 59

Figure 3.1: Distributions of Galactic positions in cylindrical radii (top) and height above the disk (bottom) for 1000 randomly sample novae distributed by randomly sampling from the Robin et al. (2003) shown as the blue dashed line and from the Cautun et al. (2020) model shown as the red solid line. 69

Figure 3.2: Top: positions of N = 1000 simulated novae in Galactic coordinates, distributed by randomly sampling the Robin et al. (2003) stellar density model. Bottom: same as top but in an external face-on view of our Galaxy. Novae are plotted in blue, and the position of the Sun is as an orange cross. 70

Figure 3.3: Distribution of distances from the Sun for N = 1000 simulated novae. The top panel shows a cumulative distribution, and the bottom panel is a normalized histogram. 72

Figure 3.4: Cumulative distributions of peak apparent magnitudes of N = 1000 simulated novae compared to the distribution of observed novae discovered since 2000 (orange dash dotted line) 75

Figure 3.5: Galactic coordinate positions of N = 1000 simulated novae around the Galactic center. The blue points indicate novae that reach a peak brightness of $g = 15$ mag or brighter, and would likely be discovered by optical observations. The red points indicate novae that never reach g = 15 mag and have a much lower chance to be discovered by optical observations. The amount of extinction integrated out to 15 kpc from the `mwdust` model is shown as a grey scale color map. The resolution of the map is 0.25 degrees with a maximum extinction value of 28 mag for visualization purposes. 76

Figure 3.6: Positions of known, optically discovered novae in Galactic coordinates around the Galactic center as orange dots. Nova candidates reported by VVV and OGLE observations are shown as red stars. VVV and OGLE should be better suited for finding reddened novae in the plane than bluer optical observations, but OGLE has a lower cadence in these highest extinction regions. The dust map is the same as Figure 3.5. Lines of constant declination are shown in blue to highlight the lack of optically discovered novae at the most southern declinations. 78

Figure 3.7: Normalized cumulative distribution (top) and normalized histogram (bottom) of novae as a function of Galactic latitude. All simulated novae are plotted in red, while simulated novae that reach a brightness of $g = 15$ mag are shown in blue. Optically discovered novae are plotted as an orange dashed line. The discovered sample more closely resembles the bright m ¡ 15 mag model, suggesting a bias against discovering novae in regions of heavy extinction and a severe historic lack of novae discovered at low Galactic latitude. 80

Figure 3.8: Distribution of the Galactic nova rate from 1000 iterations of our primary 85

Figure 3.9: Same as Figure 3.8 for various combinations of stellar density models, extinction models, and ratio of disk to bulge novae per unit mass (θ). Top Left: Galactic nova rate distributions resulting from using the Cautun et al. (2020) mass model. Top Right: Galactic nova rate distributions resulting from changing the `mwdust` model to an exponential disk; this results in rate estimates inconsistent at the one-sgima level. Bottom Left: Galactic nova rate distributions from an elevated rate of nova production in the bulge using the Cautun et al. (2020) mass model. Bottom Right: same as bottom left but for the Robin et al. (2003) model Overall, the ASAS-SN and OGLE derived rates are sensitive to the model assumptions but the PGIR rate is not. 90

Figure 4.1: Galactic nova rate predictions as a function of the year published, compared with the number of novae confirmed each year since 1980. The rate predictions made using the Galactic or direct method are shown as red circles and using the extragalactic or indirect method are shown as black diamonds, along with error bars if the uncertainty was estimated. The prediction from this work is shown as the magenta square. The number of discovered and confirmed Galactic novae each year is plotted as a blue histogram, and was derived using Koji Mukai's List of Galactic Novae, Bill Gray's Database of Galactic Novae, and AAVSO's VSX. Citations for published rates from left to right: Liller & Mayer (1987); Ciardullo et al. (1990); van den Bergh (1991a); della Valle & Livio (1994a); Shafter (1997); Hatano et al. (1997); Shafter et al. (2000); Shafter (2002); Darnley et al. (2006); Shafter (2017); Özdönmez et al. (2018); De et al. (2021). 102

Figure 4.2: The normalized extinction distributions of 10,000 simulated novae in the ASAS-SN g-band filter (blue) and *Gaia* G-band filter (red). These distributions are estimated from the `mwdust` package (default values shown as dotted lines), and we add additional extinction if the line of sight is not complete out to the distance of the nova (solid line).117

Figure 4.3: The normalized distributions of peak apparent magnitude of 10,000 simulated novae in the g-band filter (blue) and G-band filter (red). Also shown is the distribution with zero extinction with the peak scaled to fit (black dashed line). This demonstrates that dust is a much larger factor than the luminosity or distance in determining the peak apparent magnitude of a nova. 119

Figure 4.4: Distribution of the peak absolute magnitude versus time to decline by two magnitudes from maximum (t_2) for 10,000 model novae (black dots). The peak absolute magnitudes are sampled from a normal distribution, and the t_2 values are sampled from a log-normal distribution. The patchiness in the t_2 distribution is the result of a limited number of nova lightcurve templates. The allowed values in this parameter space are shown below the blue dashed line, and this is compared to real Galactic nova values estimated from *Gaia* distances (Schaefer 2018; denoted with green stars), extragalactic measurements (pink diamonds, cyan crosses, and orange diamonds; Shafter et al. 2011; Kasliwal et al. 2011; Shara et al. 2016), and the MMRD correlation derived in della Valle & Livio (1995) (shown as the red shaded region). 122

Figure 4.5: The recovery fraction of model novae in ASAS-SN and *Gaia* as a function of peak absolute magnitude and t_2. The recovery fraction values are calculated on a grid of 0.5 mag by 0.25 $\log_{10}(t_2)$ days, and are shown on each square, with darker grey-scale indicating a higher recovery fraction. While novae that adhere to the supposed MMRD relation are on average easier to detect, they are only recovered about twice as efficiently as faint fast novae, implying that all-sky surveys would have detected a substantial population of faint fast novae if they were present. 123

Figure 4.6: Three examples of simulated novae in ASAS-SN (left) and *Gaia* (right). The detections are shown in blue for ASAS-SN and red for *Gaia*, with non-detections shown as black triangles. The epoch of eruption is denoted by the vertical dashed line and the peak apparent magnitude and t_2 are listed in each panel. The top row shows a fast reddened nova, the middle row shows a nearby and slow nova (the non-detections shortly after the eruption indicate that the transient has saturated the ASAS-SN detectors), and the bottom row shows a reddened nova that was only detected by *Gaia*. 126

Figure 4.7: The predicted Galactic nova rate based on 1,000 Monte Carlo trials, from ASAS-SN (blue histogram), *Gaia* (red histogram), and a combination of both surveys (purple histogram). We give the median values of the distributions as the most likely Galactic nova rate, and include the 16% and 84% confidence regions. The redundancy of the three distributions is low, as the combined results are sensitive to when a nova is detected by both, just one, or neither surveys. The results are all consistent at the 1σ level, with the most likely rate from both surveys predicting a Galactic nova rate of $R = 26 \pm 5$ yr^{-1}. 131

Figure 4.8: The positions of simulated novae that are discovered in our model (blue dots) compared to the real sample discovered between 2019 − 2021 (orange stars). The simulated positions are derived assuming novae trace the stellar density of the Galaxy. The elongated bulge, oriented at a roughly 20° angle from the Sun–Galactic center line, appears to place more recoverable bulge novae at $l > 0°$ compared to $l < 0°$. 134

Figure 4.9: Comparison of the month of first detections of model novae (solid histograms) vs. discovered samples (scatter points with Poisson error bars). Both surveys have a seasonal gap while the Sun is in Sagittarius from November to January, and *Gaia* (shown in red) has an additional seasonal gap six months later because of the rotation direction of the satellite. When a field comes out of Solar constraint, the model predicts an excess of nova discoveries. 136

KEY TO ABBREVIATIONS

- AAVSO - American Association of Variable Star Observers
- ASAS-3 - All Sky Automated Surve
- ASAS-SN - All-Sky Automated Survey for Supernovae
- CBAT - Central Bureau for Astronomical Telegrams
- CCD - Charge Coupled Device
- CMOS - Complementary Metal Oxide Semiconductor
- CRTS - Catalina Real-time Transient Survey
- CN(e) - Classical Novae(e)
- CTIO - Cerro Tololo International Observatory
- CVs - Cataclysmic Variables
- DN(e) - Dwarf Novae(e)
- DR - Data Release
- DREAMS - Dynamic REd All-sky Monitoring Survey
- EDR - Early Data Release
- FWHM - Full-width at Half Maximum
- GSA - *Gaia* Science Alerts
- *HST - Hubble Space Telescope*
- LAT - Large Area Telescope
- LMC - Large Magellanic Cloud
- LSST - Large Synoptic Survey Telescope
- MMRD - Maximum Magnitude vs. Rate of Decline
- MS - Main Sequence
- NMW - New Milky Way Survey
- OGLE - Optical Gravitational Lensing Experiment
- Pan-STARRS - Panoramic Survey Telescope and Rapid Response System

- PGIR - Palomar Gattini-IR
- PRIME - PRime-focus Infrared Microlensing Experiment
- RG - Red Giant
- SG - Sub-giant
- SN(e) - Supernova(e)
- WD - White Dwarf
- SAAO - South African Astrophysical Observatory
- VRO - Vera Rubin Observatory
- VSX - Variable Star Index
- VVV - Vista Variables in the Via Lactea

Chapter 1

Introduction

Transient or time-domain astronomy refers to the the study of astrophysical phenomena that lasts a limited amount of time, and ironically, this field is more challenging to study in our own Galaxy, the Milky Way, in some aspects compared to other galaxies. When considering if the next Galactic type Ia supernova will be detected, or conversely, if the last one was missed, two major concerns come to mind: sky coverage and dust. Are there enough observations covering the whole sky for transients? Is there enough foreground dust to make bright transients, like supernovae, too faint for discovery? These questions are of the upmost importance for transient astronomy and vast improvements have been made to answer both in the past decade. In this thesis, these improvements are utilized to better understand another longstanding question about the Milky Way: how often do thermonuclear runaways on accreting white dwarfs, or classical novae, occur in the Galaxy?

This question, though difficult to answer, is easy to comprehend. A basic grasp of the nature of classical novae is the only piece of information needed to understand the problem at hand. This chapter is broken down into subsections to explore the following questions. What is a classical nova (Section 1.1)? What are the past limitations in estimating the Galactic nova rate (Section 1.2)? How can this thesis better understand and predict the Galactic nova rate (Section 1.3)? Why is it important to study novae (Section 1.4)? And finally, the rest of the chapters are outlined in Section 1.5, which consist of three articles submitted to peer reviewed journals.

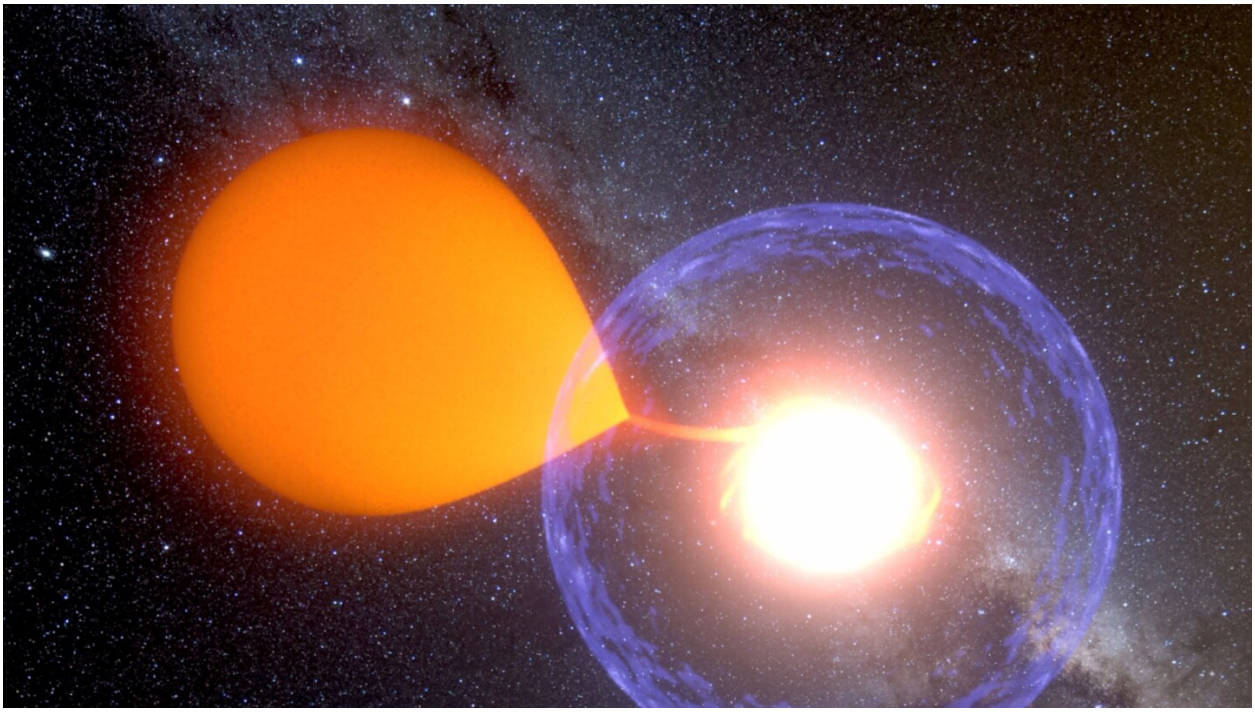

Figure 1.1 Artist's rendtition of a nova eruption. credit: Krzysztof Ulaczyk / Warsaw University Observatory

1.1 What is a Classical Nova?

Classical novae occur in binary star systems consisting of a white dwarf primary and a non-degenerate secondary star (Gallagher & Starrfield, 1978). The WD accretes Hydrogen rich material from the secondary, forms an accretion disk, and gains this material on its surface. As the material is built up on the surface, the temperature and density at the base of the accreted layer increase to the point where nuclear fusion can begin, commonly referred to as a thermonuclear runaway (Starrfield et al., 1972). This causes the accreted layer to expand and the system to brighten by many magnitudes for weeks to years (see Bode & Evans 2008; Chomiuk et al. 2021a for a review).

This eruption does not significantly disrupt the WD or the secondary, because the mass ejected is relatively low, and after some time, the whole process starts over again. The time

between multiple nova eruptions in a single system is referred to as the recurrence time, and largely depends on the mass of the WD and the accretion rate (Yaron et al., 2005). If a binary is observed to exhibit more than one nova eruption it is then referred to as a recurrent nova. In the Galaxy, there are 10 known recurrent novae with recurrence times ranging from 10 to 80 years (Schaefer, 2010), though it is expected that all novae recur, if only on longer timescales of thousands to millions of years. In M31 the remarkable nova M31N 2008-12a has been observed to erupt at a frequency of one year.

This is unquestionably an exciting time to study novae. A wide effort to observe novae across the electromagnetic spectrum has been put forth to understand the physics of the nova eruption, yielding key discoveries regarding the mass ejection mechanisms and shocks contributing to the luminosity of novae Chomiuk et al. (2021a). For the scope of this thesis, we are largely interested in the observational properties of the nova eruption and how that relates to our ability to find them. The peak luminosity is arguably the most import intrinsic aspect of a nova. The luminosity function has been well measured by studying M31 novae, where the distances are well constrained, to be normally distributed with mean $\mu = -7.2$ mag and $\sigma = 0.8$ mag. The luminosity function of Milky Way novae is harder to measure as the distances are usually poorly constrained, but this M31 luminosity function is consistent both with early Galactic estimates (Mclaughlin, 1945) and with Galactic novae with *Gaia* Data Release 2 (DR2) distances (Della Valle & Izzo, 2020), suggesting it is a reasonable model.

The next most important aspect of the nova eruption is the length of time the eruption lasts, generally referred to as the speed of a nova. This speed is usually parameterized by the time a nova takes to decline some number of magnitudes from peak brightness (e.g., t_2 is the time it takes for a nova to decline two magnitudes from maximum brightness). However,

this speed parameter does not always describe the entire eruption well, as nova lightcurves show a variety of characteristics (Strope et al., 2010).

There has been great effort put forth to determine if the maximum magnitude or peak luminosity and the rate of decline of novae are correlated (usually referred to as the MMRD; Capaccioli et al. 1989a; della Valle & Livio 1995; Kasliwal et al. 2011; Shara et al. 2017a) with evidence found both for and against this postulation that more luminous novae decline more quickly. These studies are performed on extragalactic nova populations as their distances are more well constrained compared to their Galactic counterparts. Related to the peak luminosity is the change in brightness between the peak and quiescent state, referred to as the outburst amplitude. This is much easier to measure for Galactic novae, as in many cases the quiescent counterpart is either detectable or is able to be constrained by photometric observations prior to the eruption, while quiescent counterparts are only rarely detected for extragalactic novae. There has only been one previous study looking at the relationship between outburst amplitude and the rate of decline for Galactic novae (Warner, 1987), and it concluded that they are strongly anti-correlated, similar to the studies of the MMRD. I revisit the outburst amplitude rate of decline relationship with modern data in Chapter 2 of this thesis.

Because of their extreme luminosities, the discovery of classical novae long predates any physical understanding. "Nova" is abbreviated from *stella nova* simply meaning *new star* (Duerbeck, 2008). Historical records suggest that humans have been discovering novae for thousands of years (Patterson et al., 2013). Understanding the luminosity of novae played a key role in what became known as the *Great Debate* about the size of the universe and whether nebulae were inside or outside the Galaxy, by Lundmark (1920) noting S Andromedae, the 1885 'nova' in the M31 nebula, was an outlier in brightness from other novae.

Later, novae were suggested to belong to three distinct classes in Lundmark (1935), where they were partitioned into three categories based on the absolute magnitude: *upper-class Novae*, or *super-Novae* having $M_{\max} \sim -15$, *middle-class Novae*, or *ordinary Novae*, having $M_{\max} \sim -7$, and *lower-class Novae*, or *dwarf Novae* having $M_{\max} \sim +3$ or $+4$. The goal of this thesis is to estimate the frequency of middle-class novae, referred to now as classical novae, in the Milky Way. It was in Lundmark (1935) that the first attempt to estimate the frequency of ordinary novae in the Galaxy was postulated: "It seems that the number of outbursts of ordinary Novae in our galaxy is at least 50 a year, but probably much higher." Lundmark (1935). Though crude, this estimation is remarkably consistent with recent, more robust estimates of the Galactic nova rate (Shafter, 2017); however, the uncertainty is still large. Reducing this uncertainty is the key goal of this thesis. In the following section, the problems contributing to the uncertainty in the Galactic nova rate are explored.

1.2 The Galactic nova rate problem

Since the first estimate of the Galactic nova rate in 1935, there have been roughly 20 additional estimates ranging from ~ 16 yr^{-1} (van den Bergh & Younger, 1987a) to as high as 259 per year (Sharov, 1972) (a complete history of nova rate predictions can be found in Section 4.1.2). The variance in predictions is undoubtedly large but smaller in recent years with estimates all agreeing at the 1σ level on a rate of ~ 60 novae per year (Shafter, 2017; Özdönmez et al., 2018; De et al., 2021). However, the number of novae discovered in the Galaxy is much lower, with only $9-17$ novae discovered per year over the past since 2017(see Figure 4.1). If these predictions are correct, this would mean that only $15\% - 30\%$ of the Galactic nova population are discovered. Herein lies the problem. Are there explanations

for the reason why a majority of nova eruptions would go undetected or has the global rate been overestimated?

The typical nova eruption lasts for weeks to months, but because of the location of Earth within the Milky Way, a large portion of the sky needs to be observed to discover these transients. The vast majority of nova discoveries from the past forty years have been made by a Global network of amateur astronomers, with the largest number of observers residing in Japan. Because the discoveries are made inhomogeneously, with varying cadence, depths, and are not stored in one accessible database, it is difficult to quantify the degree to which novae are missed because of lack of sky coverage. Hence, until very recently, it was not possible to quantitatively estimate the completeness of nova searches, except perhaps for the brightest novae that can be seen by the naked eye (e.g., Shafter 2002, 2017).

Another way a large fraction of Galactic novae can go undetected is if foreground dust extinction is sufficiently large enough to obscure the light from distant novae from reaching Earth. All-sky dust maps have been common use for decades (e.g., Schlegel et al. 1998), but they only attempt to estimate the total extinction along a line of sight and are inadequate at low Galactic latitude where extinction is large and complex with multiple dust clouds. Therefore these maps are unreliable for large Galactic distances near the plane and fail to differentiate between the extinction differences of a star at 5, 10, or 15 kpc. For these reasons, previous nova rate estimates were limited to small samples of nearby, and therefore bright, novae unaffected by dust extinction, and no study has quantified what fraction of novae are unobservable because of dust.

Fortunately, major advancements in time domain surveys and modeling of Galactic dust have occurred in recent years, allowing for this thesis to make major improvements to nova rate estimations.

1.3 How can this thesis better estimate the Galactic nova rate?

As stated above, the Galactic nova rate is difficult to estimate because (1) discovery observations for novae are inhomogenous and hard to model and (2) extinction as a function of distance was historically unknown for nova studies. Luckily both of these issues have been addressed in recent years, shedding new light of the Galactic nova rate problem.

1.3.1 ASAS-SN

The All-Sky Automated Survey for SuperNovae (ASAS-SN or "Assassin"; Shappee et al. 2014) started scanning the extragalactic sky for transients visible from the single Hawaii facility every five nights in 2013. Then, in mid-2017 a facility at Cerro Tololo International Observatory (CTIO, Chile) was added, unlocking an all-sky field of view (Kochanek et al., 2017). By the end of 2017, ASAS-SN added an additional facility at CTIO, a facility at McDonald Observatory (Texas), and a facility at the South African Astrophysical Observatory (SAAO, Sutherland, South Africa). Now with five facilities in operation, ASAS-SN is capable of scanning the entire sky every night for transients.

Each facility consists of four 14 cm aperture Nikon telephoto lenses, yielding a field of view of 4.5 deg^2, pixel scale of 8.0", and a full-width at half maximum (FWHM) of $\sim 1.5-2$ pixels. Observations at the original two facilities were made in a V-band filter and with a g-band filter in the newer three facilities. In 2018, the original two facilities switched to observing in a g-band filter (400 nm – 540 nm), so ASAS-SN now dithers 90s exposures across the entire night sky to look for transients down to a median depth of $g \lesssim 18.5$ mag.

The primary goal of ASAS-SN is to conduct a survey with minimal observational bias, and

in particular, discover nearby extragalactic supernovae to characterize the local supernova rate (Shappee et al., 2014). Because ASAS-SN also observes the Galactic plane regularly, it discovers many Galactic events, including classical novae.

ASAS-SN uses image subtraction to find variable stars and transients. This is carried out by building up reference images of each field, then subtracting these from observations on individual epochs. The difference images are then analyzed for changes in flux that could be real or from artifacts in the subtraction. Pipelines have been built to look for transients of certain types, including the `Outburst` pipeline, specifically designed to search for Galactic nova candidates. This pipeline creates a stream of images for a human to judge if the image contains an artifact, a known variable, or a newly discovered variable. An example of an ASAS-SN candidate image is shown in Figure 1.2. If the image is from a real and previously unknown variable star or transient, it is publicly reported to the ASAS-SN transient page[1]. The likelihood of artifacts increases for fainter candidates, so only $g < 15$ mag candidates are placed in the `Outburst` stream. Also, a automated email alert is generated for these bright candidates candidates, quickly alerting the user of potential nova candidates. The ASAS-SN detectors typically saturate at $g < 10$ mag, and photometry can be unreliable brighter than this threshold.

The advantages of having a survey like ASAS-SN are monumental. If one finds a variable object of interest, how the brightness of that star has changed over the last 5 to 9 years can be immediately accessed from one database. In the context of nova modeling, the cadence that the entire sky was scanned is now precisely known, information that was not available a decade ago. The question of whether $\sim 80\%$ of novae are missed by amateur observations was automatically answered by ASAS-SN's ongoing observations: the addition of ASAS-SN

[1] https://www.astronomy.ohio-state.edu/asassn/transients.html

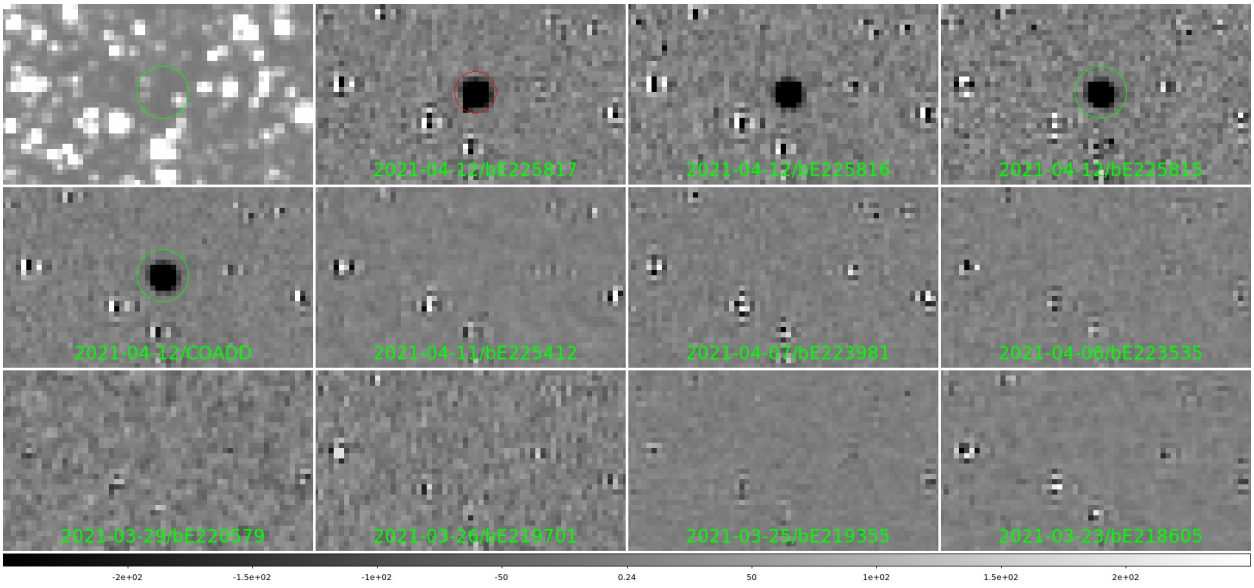

Figure 1.2 Example of a set of grey scale images automatically generated to vet the legitimacy of an ASAS-SN candidate. The scale is denoted at the bottom showing lighter pixels as having higher flux, grey having no flux, and darker pixels having negative flux. The top left panel is the reference image of the field with a green circle centered on the position of the candidate. The rest of the panels show this reference image subtracted by the observations on an individual epoch (i.e., image subtraction). The second through fourth column of the top row show the three individual exposures taken on the latest night and the panel below the reference image shows the result of adding these three images. The rest of the panels show the coadded images from the most recent epochs before the alert was generated at the position of this candidate. This example is the nova ASASSN-21fh or V1710 Sco, first detected by ASAS-SN on 2021-04-12.

has not significantly increased the discovery of Galactic novae, putting further pressure on claims of a nova rate of ~ 60 per year and instead making it likely the true Galactic nova rate is lower. It is clear that lack of observations is not the reason for missed novae.

One caveat to the ASAS-SN observations is that they are now carried out only in the g-band, since typical extragalactic transients (supernovae and nuclear transients) are rather blue. However, this is not the ideal band for a Galactic survey, since foreground extinction due to dust is worse in g than redder filters. Indeed, as I discuss in the next subsection, extinction is commonly asserted as the next reason for the discrepancy between observed and predicted rates.

1.3.2 mwdust

Simply stated, novae are bright. A typical nova with a peak absolute magnitude of $M \sim -7$ mag at an extreme Galactic distance of $d = 30$ kpc would have an apparent magnitude of $m \sim 10$ mag, easily detectable by most observers. Therefore, dust has long been thought to play a role in determining how bright a nova appears, but it has been difficult to quantify this effect.

In past nova studies, it is common to assume smooth single or double exponential disks of extinction within the Galaxy. Extinction that decreases at a larger radius from the Galactic center and height from the plane seems like a safe assumption, but this model will be sensitive to the assumed normalization and scaling and does not allow for the presence of dust clouds. To be able to use ASAS-SN to study Galactic novae, an all-sky extinction estimation is needed, especially with reliable measurements in the plane. Furthermore, a distant dependent extinction is of key interest but such a dust map has never been used in the context of nova modeling.

This is likely because of the lack of availability of an all-sky three dimensional map of interstellar dust. Three dimensional dust maps are created through a variety of methods but typically involve measuring the colors of a sample of stars along different lines of sight. Though stars can have intrinsically different colors, the more dust the light from the star has to pass through, the redder it will appear. Large photometric surveys completed in recent years allow for larger sample of color measurements of stars and therefore the creation of more robust 3D dust maps.

Examples of these maps include: the Marshall et al. (2006) map of the inner Galactic plane derived from 2MASS data, the Sale et al. (2014) map of the northern Galactic plane derived from the INT/WFC Photometric $H\alpha$ Survey, and the Green et al. (2019) map of the Northern Hemisphere derived from 2MASS, *Gaia*, and the Panoramic Survey Telescope and Rapid Response System (Pan-STARRS) data. No single map covers the entire sky, but Bovy et al. (2016) created the `mwdust` all-sky 3D extinction map by combining the Marshall et al. (2006) map and the Green et al. (2019) map and filled in the remaining gap with analytic model from Drimmel et al. (2003). The Marshall et al. (2006) map covers a Galactic longitude $-100^\circ < l < 100^\circ$ and latitude $-10^\circ < b < 10^\circ$ and is sampled with a resolution of 15'. The Green et al. (2019) map covers the sky north of declination $\delta > -30^\circ$ not covered by the Marshall et al. (2006) map and has a variable resolution of $4' - 14'$ The remaining region around the south celestial pole is covered by the Drimmel et al. (2003) map with a resolution of $20'$. A figure from Bovy et al. (2016) showing `mwdust` estimating extinction across the entire sky is shown here in Figure 1.3. `mwdust` is able to estimate extinction in different observing bands by assuming a reddening law of $A_V/E(B-V) = 3.4$.

By utilizing `mwdust`, this thesis is able to estimate the extinction to a nova at any position in the Galaxy and should make larger improvements over previous, less data motivated

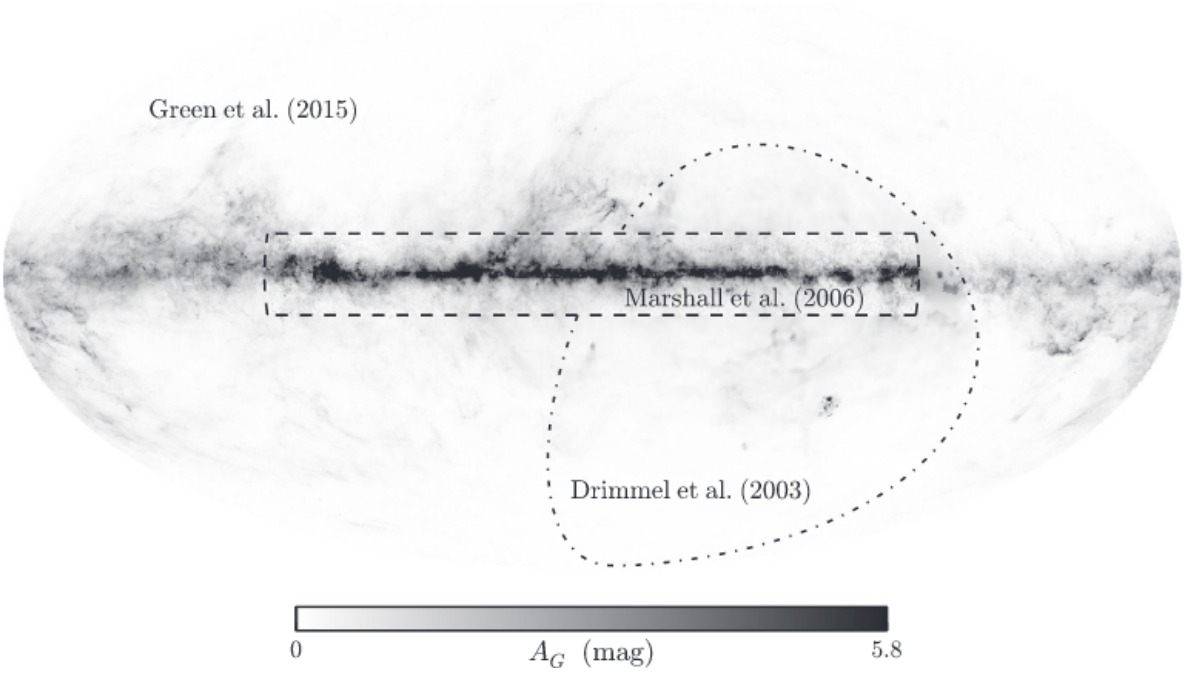

Figure 1.3 Credit: Figure 1 from Bovy et al. (2016). This shows how the three dust maps were stitched together to create an all-sky 3D dust map. The grey scale shows the amount of extinction in *Gaia* G-band out to 5 kpc.

distributions of dust. What fraction of Galactic novae are missed due to dust extinction can be answered more robustly than ever before with `mwdust`.

1.3.3 Gaia

The newest source of data used in `mwdust` is from the *Gaia* satellite. In addition to its usefulness in understanding the distribution of dust in the Galaxy, it also has use as a transient survey that can be added to the ASAS-SN measurements to make a more well informed estimate of the Galactic nova rate.

The *Gaia* satellite was launched in 2013 with the goal of making precise position, parallax, and proper motion measurements of > 1 billion sources down to $G < 20.7$ mag (Gaia Collaboration et al., 2016). With each data release, DR1 in 2016 (Gaia Collaboration et al.,

2016), DR2 in 2018 (Gaia Collaboration et al., 2018a) and the early data release EDR3 in 2021 (Gaia Collaboration et al., 2021), larger samples of photometric and astrometric measurements of stars across the entire sky are made available. These precise measurements of brightness, color, position, and distances can be used to shed led on the probability of transients belonging to the classical nova class. *Gaia* unlocks a wealth of information to nova studies and even discovers many novae.

Gaia repeatedly scans the sky to make astrometric measurements of a large sample of stars. It typically takes two observations separated by 106.5 minutes and then follows up with another pair of observations 2-4 weeks later (Hodgkin, S. T. et al., 2021). When succeeding observations occur, sometimes new sources or flux changes from known sources are detected, also known as transients. These transients are publicly reported to the Gaia Science Alerts website[2], and the first confirmed Galactic nova *Gaia* discovered occurred in 2019 when GSA reported Gaia19dum (Aydi et al., 2019). Because the cadence of *Gaia* is much lower than ASAS-SN, it was not predicted to be a proficient discovery source of novae, but there are key features to the *Gaia* design that make it an excellent contributor to nova science.

Gaia uses a broad white-light G-band filter (400 nm – 900 nm), making it less affected by reddening from dust than ASAS-SN. The pixel scale is extremely fine (~ 0.1 arcseconds), allowing stars to be differentiated in crowded fields. It also has a large dynamic range, capable of detecting novae across > 10 magnitudes and to relatively faint depths of $G < 19$ mag. The space-based mission is not affected by the lunar cycle, clouds, and variable seeing that plague ground based observatories. And, just like ASAS-SN, it observes the entire sky including the Galactic plane, where most of the stars and novae reside. For these reasons, *Gaia* has discovered many novae over the past few years, and, in this this thesis, the recovery

[2] gsaweb.ast.cam.ac.uk/alerts

efficiency of this survey is also studied to estimate the Galactic nova rate.

1.4 Why is it important to study novae?

Because novae are relatively common, they have been an excellent resource to study nearby and highly energetic events across the electromagnetic spectrum (see Chomiuk et al. 2021a for recent highlights). Novae are typically discovered in the optical, and have exhibited a wide range of features in their lightcurves (Strope et al., 2010). As the ejecta expands, it becomes transparent at shorter wavelengths, with more flux transitioning to the ultraviolet (Gallagher & Code, 1974). This phenomena continues until eventually the WD can be observed through X-ray emission from residual nuclear burning (Kahabka & van den Heuvel, 1997). Recently, the first detection of x-ray emission has been found from the fireball phase of a nova before its optical brightening (König et al., 2022). At even higher wavelengths, GeV gamma-ray emission has been detected in novae during the first days to weeks of the eruption by Large Area Telescope (LAT) on NASA's *Fermi Gamma-Ray Space Telescope* (Abdo et al., 2010; Ackermann et al., 2014). This gamma-ray emission has even been found to have been correlated with the optical lightcurve, suggesting that shocks may dominate the emission of novae, contra a long-standing view that thermal emission dominated (Aydi et al., 2020).

Weeks to months after the eruption, some novae show strong evidence of the formation of dust in their ejecta, seen by a sudden drop in the optical brightness coincident with a increase in the infrared brightness (Gehrz, 1988), and at even longer wavelengths, radio emission is detected from the WD photo-ionizing the nova ejecta (Chomiuk et al., 2021b). These are just a few examples of how novae are studied across the electromagnetic spectrum.

Understanding the physics of nova eruptions by piecing this information together that is captured at different regimes is an active area of research. Discovering more novae not only provides more opportunities to study these phenomena, but it also sheds light on the current selection effects. For example, if current nova surveys miss novae that are preferentially faint or fast-evolving, our overall view of novae may be biased. Understanding the diverse nature of novae will require a more complete sample and a comprehension of which and how many novae are still going undiscovered.

The importance of the nova rate goes beyond understanding novae and is a key input in many nuclear and astrophysical models. Radionuclides found in novae like ^{22}Na (Friedman et al., 2020), ^{26}Al (Bennett et al., 2013), and ^{7}Be (Arnould & Norgaard, 1975; Starrfield et al., 1978a) are detectable in gamma-rays during decay and therefore estimates of the amount novae contribute to Galactic abundances are able to be made. For example, there has been a keen interest in determining if novae are responsible for Li abundances in the Milky Way, with studies concluding for (Molaro et al., 2016) and against (Kemp et al., 2022) this assertion. The Galactic nova rate is a major input in these studies and consequently is vital to constrain the contribution of novae to Galactic isotopes (see Section 4.1 for further discussion).

1.5 Outline

The subsequent chapters of this thesis contain the work to provide insights to the observational properties of nova eruptions in the Galaxy, the time domain surveys capable of detecting them, and then ultimately predict the Galactic nova rate. Chapter 2 consists of the peer reviewed article written by Kawash et al. (2021b) and published in the Astrophysi-

cal Journal where the outburst properties of a large sample of classical novae were compared to the most similarly appearing class of transient: the dwarf nova. By using ASAS-SN to measure these properties, the discovery rate of classical novae is more well constrained by quantifying the amount of confusion between transient classes.

These lessons are then built upon in Chapter 3, consisting of the peer reviewed article written by Kawash et al. (2021c) and published in the Astrophysical Journal, where a model of classical novae and dust is constructed to estimate what fraction of the population are detectable by various time domain surveys. This is the first work to incorporate three dimensional dust information on an all-sky scale for nova modeling, better quantifying the effects that extinction has on the discovery rate of optically discovered novae.

The information from Chapter 2 is combined with the model built in Chapter 3 to make the first all-sky time domain survey prediction of the Galactic nova rate in Chapter 4. This chapter contains the article written by Kawash et al. (2022) and submitted to the Astrophysical Journal, and it is the first Galactic nova rate to be made using all-sky surveys. The conclusions from this work are outlined in Chapter 5 along with a discussion of the future work to constrain the Galactic nova rate.

Chapter 2

Classical Novae Masquerading as Dwarf Novae? Outburst Properties of Cataclysmic Variables with ASAS-SN

Abstract

The unprecedented sky coverage and observing cadence of the All-Sky Automated Survey for SuperNovae (ASAS-SN) has resulted in the discovery and continued monitoring of a large sample of Galactic transients. The vast majority of these are accretion-powered dwarf nova outbursts in cataclysmic variable systems, but a small subset are thermonuclear-powered classical novae. Despite improved monitoring of the Galaxy for novae from ASAS-SN and other surveys, the observed Galactic nova rate is still lower than predictions. One way classical novae could be missed is if they are confused with the much larger population of dwarf novae. Here, we examine the properties of 1617 dwarf nova outbursts detected by ASAS-SN and compare them to classical novae. We find that the mean classical nova brightens by $\sim$11 magnitudes during outburst, while the mean dwarf nova brightens by only $\sim$5 magnitudes, with the outburst amplitude distributions overlapping by roughly 15%. For the first time, we show that the amplitude of an outburst and the time it takes to decline

by two magnitudes from maximum are positively correlated for dwarf nova outbursts. For classical novae, we find that these quantities are negatively correlated, but only weakly, compared to the strong anti-correlation of these quantities found in some previous work. We show that, even if located at large distances, only a small number of putative dwarf novae could be mis-classified classical novae suggesting that there is minimal confusion between these populations. Future spectroscopic follow-up of these candidates can show whether any are indeed classical novae.

2.1 Introduction

Interacting binary systems that consist of a white dwarf accreting material from a close companion star are known as Cataclysmic Variables (CVs). The secondary, usually a low-mass main-sequence star, transfers matter through Roche-lobe overflow, which forms an accretion disk around the white dwarf (see Warner 1995 and Hellier 2001 for reviews).

A Dwarf Nova (DN) outburst is a common event that occurs in a CV, and is generally thought to be caused by a thermal instability in the accretion disk (see Hameury 2020 for a review). The disk rapidly transitions from neutral to ionized, leading to a sudden increase in disk viscosity and mass-accretion rate, and a dramatic brightening of the accretion disk (Hellier, 2001). DNe are one of the most common types of Galactic transients, with new objects being discovered generally every week (see Kato et al. 2020 and previous papers for examples). Individual systems will typically outburst every 20–300 days (Osaki, 2001). The peak absolute magnitude of a DN depends mostly on the physical size and inclination of the accretion disk, and ranges from $M_{V,\mathrm{max}} \approx 7$ to 2 mag, with long orbital period systems viewed face-on producing brighter outbursts (Harrison et al., 2004; Patterson, 2011).

A Classical Nova (CN) is another type of event that occurs in a CV, and is caused by a thermonuclear runaway on the surface of the white dwarf (see Bode & Evans 2008 for a review). Accreted material builds up on the surface of the white dwarf over time, until a critical pressure is reached, which triggers explosive thermonuclear burning and the puffing up and expulsion of the accreted envelope. Recent studies of CNe in M31 with well-constrained luminosities show that the absolute magnitude at peak brightness can range from $M_V \approx -4$ to -10 mag, much more luminous than DNe (Shafter, 2017). This is consistent with early estimates of the Galactic nova luminosity function (Mclaughlin, 1945) even with more precise distances from *Gaia* DR2 (Della Valle & Izzo, 2020). Outbursts of CNe are expected to recur on a timescale that depends on the white dwarf mass and accretion rate (Yaron et al., 2005), and if a CN has been observed to erupt more than once, it is referred to as a recurrent nova. Of the ten recurrent novae known in our Galaxy, the recurrence time ranges from 10 to 80 years (Schaefer, 2010). However, in other galaxies, more rapidly recurring novae are being discovered (Darnley, 2019), with a nova in M31 that has been found to recur every year (Darnley et al., 2016), and nova LMC V1341 (= Nova LMC 1968) recently exhibiting a four year recurrence time (Kuin et al., 2020; Page et al., 2020). For the purposes of this work, we are interested in both recurrent and singular classical novae and do not distinguish between the two classes, considering them both thermonuclear-powered CNe.

There have been many estimates of the Galactic nova rate (see Della Valle & Izzo 2020 for a review), but it remains poorly constrained. Recently, (Shafter, 2017) derived a rate of 50^{+31}_{-23} novae per year from Galactic observations and a rate between ~ 50 and ~ 70 novae per year from extragalactic observations. These rates, though mutually consistent, are larger than previous estimates, and significantly higher than the discovered rate. Historically,

amateur astronomers have played a leading role in the discovery and observations of CN eruptions, and found only a small fraction of the predicted population. The average number of discovered Galactic novae increased from about 3 per year in the mid 20th century (when many discoveries were made visually) to 4 per year in the 1980s and 1990s (when film photography was often used) to 8 per year in the 2000s and 2010s (when digital cameras became widely available)[1]. Amateur observers use a variety of equipment, which often include an astronomical CCD camera attached to a telephoto lens or small telescope with typical detection limits down to $V \approx 12$ mag. As amateur observations do not systematically cover the entire sky down to a well defined limiting magnitude, one explanation for the discrepancy between the number of predicted and discovered CNe in the Galaxy is that most CNe eruptions go undiscovered. To test this possibility, a deep wide-field survey with high observing cadence is needed. Fortunately, such a survey now exists.

The All-Sky Automated Survey for SuperNovae (ASAS-SN) is the only survey to date observing the entire night sky with nearly nightly cadence (Shappee et al., 2014; Kochanek et al., 2017). Early ASAS-SN observations were conducted at two facilities in Hawaii and Chile, using a V filter with a few day cadence down to a depth of $V \approx 17$ mag. In 2017, ASAS-SN added facilities in Texas, South Africa, and an additional facility in Chile, switched to observing in a g filter down to a median depth of $g \approx 18.5$ mag and became able to observe the entire night sky (including the Galactic plane) with nearly nightly cadence (Kochanek et al., 2017; Jayasinghe et al., 2020). The primary goal of ASAS-SN is to discover bright, extragalactic supernovae, but due to the all-sky nature of the survey, there are a wide variety of transients discovered, including CV outbursts. The observing capabilities of ASAS-SN

[1]Up-to-date lists of novae may be found at `https://asd.gsfc.nasa.gov/Koji.Mukai/novae/novae.html` and `https://github.com/Bill-Gray/galnovae`

make it uniquely suited for monitoring fast outbursts from CVs brighter than $g \approx 18\,\mathrm{mag}$, considerably deeper than most amateur observations. Various models from Shafter (2017) predict anywhere from 30 to 110 CNe brighter than $V \approx 18$ in the Galaxy each year, but so far ASAS-SN observations have yielded no large increase in the number of discovered novae.

With no increase in the discovery rate. another explanation must exist if the rate estimates are correct. One possibility is that CNe are being confused with the more numerous DN outbursts. Due to the high frequency of nearby DN outbursts, it is not feasible to obtain a classification spectrum of even a substantial fraction of DN candidate outbursts in the Galaxy. This problem will only be exacerbated by next generation time domain surveys like the Large Synoptic Survey Telescope (LSST; Ivezić et al. 2019). The default assumption for a fainter CV outburst ($g_{\mathrm{peak}} > 13\,\mathrm{mag}$) is that it is a DN; this is usually a safe assumption since a Galactic CN should be very bright, even when observed on the other side of the Galaxy unless the dust extinction is very high.

The main goal of this work is to investigate the possibility that some Galactic CNe are being mistaken for DNe by inspecting the outburst properties of a large sample of both types of transients. For extragalactic CNe, the association with a well-studied nearby galaxy means that the CN distances— and therefore absolute magnitudes— are well constrained. Although the luminosity function of CNe is reasonably well-measured (e.g., Shafter, 2017), it has limited utility in the Galaxy where nova distances are usually poorly constrained; many Galactic CN progenitors are too faint in quiescence or too distant for an accurate parallax measurement even with *Gaia* (Schaefer, 2018; Selvelli & Gilmozzi, 2019). However, photometry of the field prior to outburst often exists for Galactic events, making it possible to estimate how much the object brightened during outburst—typically called the outburst amplitude. The outburst amplitude has the potential to be a powerful discriminant between

CNe and other transients but is relatively little studied.

Significant effort that has been invested in understanding the potential relationship between absolute magnitude of peak outburst and its rate of decline for CNe (MMRD; Capaccioli et al. 1989a; della Valle & Livio 1995; Kasliwal et al. 2011; Shara et al. 2017a). There are far fewer studies of the relationship between outburst amplitude and decline time for CNe. Warner (1987) found that CNe exhibit outburst amplitudes ranging from 8 to 15 magnitudes in V-band, with large-amplitude CNe fading quickly and small-amplitude CNe sometimes taking years to fade back to quiescence, and this relationship has been used to identify potential recurrent nova candidates from the sample of known CNe (Pagnotta & Schaefer, 2014). Recurrent novae are expected to occur on massive white dwarfs and have short decline times (Yaron et al., 2005). Given the large luminosity differences between CNe and DNe, this relationship could also be useful in identifying potential CNe candidates hiding in the large population of DNe. DNe typically have outbursts that last roughly a week with amplitudes of 2–5 mag, much lower than CNe. However, WZ Sge type DNe (Ortolani et al., 1980; Kato, 2015; Hellier, 2001; Howell et al., 1995) show rare (once in decades) accretion-powered superoutbursts with amplitudes reaching 9 magnitudes and lasting for weeks (e.g., Tampo et al., 2020). Although the vast majority of DNe should have lower outburst amplitudes than CNe, WZ Sge type superoutbursts could be confused with CNe if only the outburst amplitude but not the absolute magnitude is known. It is a goal of this paper to better understand this potential for confusion, and to investigate possibilities for alleviating it in order to more confidently identify CNe.

Recently, time-domain surveys have found large numbers of DN outbursts due to their high frequency. A few examples of these include the Sloan Digitial Sky survey (SDSS: Gänsicke et al. 2009), the Catalina Real-time Transient Survey (CRTS: Coppejans et al.

2016), and the Optical Gravitational Lensing Experiment (OGLE; Mróz et al. 2015a). These have resulted in large sample studies of a multitude of DN outburst properties, but we have found no previous discussion of the relationship between outburst amplitude and decline time from maximum for DNe.

In this work, we focus on the relationship between outburst amplitude and decline time as a potential tool for distinguishing CNe from DNe. To do this, we estimate the outburst properties of DNe, along with CNe that have erupted since ASAS-SN started observing in 2013 and compare the two samples. In Section 2.2, we describe how the sample of CVs was obtained, how the light curves were generated, and how the various outburst properties were measured. In Section 2.3, we present the outburst properties of the CN and DN populations, fit the distributions of outburst amplitudes and decline times, measure the correlation between these two properties, and discuss the observable differences between the two types of outbursts. We then assess in Section 2.4 whether CNe could be hiding amongst DNe, and how we can ensure in the future that the two types of transients are not confused.

2.2 Methods

2.2.1 Catalog

The list of CVs analyzed in this work was obtained from the AAVSO International Variable Star Index (VSX; Watson et al. 2006), which contains the most up-to-date and comprehensive list of known CVs, including CVs discovered by ASAS-SN. VSX was queried using `TAPVizieR` (Landais et al., 2013) for any objects flagged as[2]:

- U Geminorum-type variables ("UG" flag), including all the sub-classes in the VSX

[2] `https://www.aavso.org/vsx/index.php?view=about.vartypes`

catalog. These are CVs that have been typed as DNe.

- DQ Herculis-type variables ("DQ" flag), which are CVs with intermediate-strength magnetic fields, and are also known as intermediate polars. Given the right orbital period, accretion rate, and magnetic field strength, these systems can still produce DN outbursts (Hameury & Lasota, 2017).

- CVs of unknown type ("CV" flag). These are often CVs that have recently been discovered in surveys like ASAS-SN, and which have not yet been assigned a type in VSX.

A total of 9333 objects had these flags in the VSX catalog at the time the catalog was queried (December 2019). There were a total 62 CN eruptions discovered in the Galaxy between January 2013 and April 2020. The positions of these CNe, like the sample of DNe, were obtained from VSX.

2.2.2 Light curves

Image-subtraction light curves were generated using ASAS-SN observations for all objects in our sample following the procedures described in Jayasinghe et al. (2018a, 2019, see also Alard & Lupton 1998; Alard 2000). ASAS-SN light curves for most fields outside of the Galactic plane span back to 2013. In 2017, ASAS-SN switched from observing in a V-band filter to a g-band filter and started more regularly monitoring the Galactic plane. For the purposes of our analysis, g-band is used as the standard filter; the conversions of V-band measurements to g-band are outlined in Section 2.6.1. An example of an ASAS-SN light curve for a DN is shown in Figure 2.1 and additional light curves are shown in Figure 2.7, Figure 2.8, and Figure 2.11.

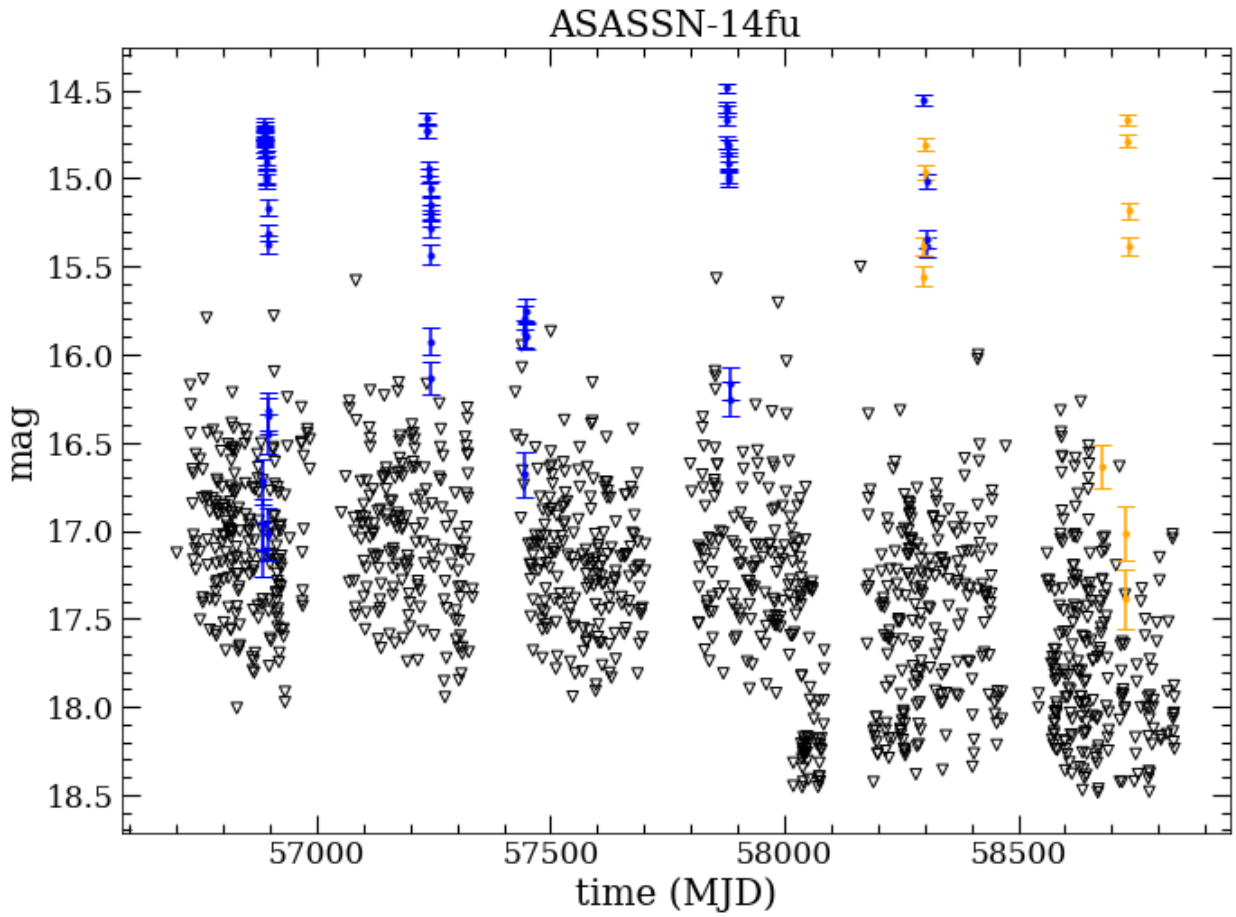

Figure 2.1 The ASAS-SN light curve of the dwarf nova ASASN-14fu. The ≥5-sigma detections are shown for V-band and g-band observations in blue and orange, respectively. The black triangles denote 5σ upper limits derived from non-detections, and the gaps in the data are due to seasonal the Solar constraints.

Image-subtraction photometry is preferred over aperture photometry for studying CV outbursts. Reference images are created using the best images of each field with outlier rejection before the final average, which automatically rejects any outbursts. By subtracting this reference image from individual epochs, any flux at the position of a CV in the individual observations should be from an outburst. Contaminating flux from nearby stars, a problem given ASAS-SN's angular resolution (2 pixel full width at half maximum = 16 arcseconds), is removed by the subtraction, although bright stars are not always subtracted cleanly. All the light curves used to measure the outburst properties were inspected for contamination. Some CVs within a few pixels of a bright star ($g < 14\,\mathrm{mag}$) show artifacts due to reference image subtraction errors. These were flagged and ultimately dropped, leading to the elimination of $\sim 2\%$ of the sample. Higher resolution photometry of the environment was provided by the Panoramic Survey Telescope and Rapid Response System (Pan-STARRS; Chambers et al. 2016).

ASAS-SN light curves for objects near the edge of a detector chip can have problems. These sources often lie in the overlap regions between fields, so data from one camera were flagged if the median magnitude was more than two magnitudes different from other cameras or if the flux limit of the ASAS-SN image was much lower than expected based on the observation duration.

Light curves of Galactic CNe that have erupted since 2013 were also generated using image-subtraction photometry from ASAS-SN. These data were combined with V-band observations from the American Association of Variable Star Observers (AAVSO; Kafka 2020) to increase the cadence and expand the sensitivity of our analysis for the CNe brighter than the saturation limit of ASAS-SN ($g \approx 10\,\mathrm{mag}$). The AAVSO data were visually inspected, and observations from individual observers were discarded if they were inconsistent with

data from other contributors. These erroneous observations, though rare, likely occur when one object is mistaken for another in a crowded field.

2.2.3 Outburst Peak Magnitude and Decline Time

Various aspects of the outburst can be measured directly from the light curve. To measure the maximum brightness, it is common to smooth the light curves of CNe (e.g., Burlak & Henden, 2008). This allows jitters and short flares to be ignored when estimating the peak. However, for the purposes of this work, we define the peak brightness simply as the brightest observation in the light curve, as done by Strope et al. (2010). For most objects, the cadence of ASAS-SN provides observations very close to maximum brightness, but for transients evolving on a timescale less than a day, the maximum brightness can be underestimated. Also, outbursts that are discovered immediately after a field emerges from its Solar conjunction can have significantly underestimated peak brightness.

Another quantity that we are able to measure directly from the light curve is the decline time, t_2, defined as the time in days it takes for the light curve to decline by two magnitudes from maximum brightness. For DN outbursts, this is relatively straightforward, as they typically exhibit smooth declines, though we consider any plateaus in the light curve after maximum brightness to be part of the decline. CN light curves can exhibit jitters, flares, and cusps (see Figure 2.11 and Strope et al. 2010), which can cause t_2 to change depending on the definition (e.g., first decline by two magnitudes versus final fade by two magnitudes). We define t_2 as the last time the light curve drops below two magnitudes from maximum in order to be consistent with the estimates by Strope et al. (2010).

To measure t_2, we first assumed that the brightest detection was the peak of an outburst. Then, we required that the decline have at least two detections separated by more

than one hour to automatically eliminate satellite trails and asteroids. Next, we required that all data used to measure t_2 be brighter than the independently measured quiescent magnitude (discussed in §2.6.2). This eliminates objects with outburst amplitudes less than 2 magnitudes, but was necessary to distinguish outbursts, CV variability in quiescence, and contamination from nearby bright stars. We also required that there is no gap between consecutive observations longer than 40 days to eliminate artificially extended t_2 values due to Solar conjunctions. Linear interpolation between the two data points above and below the two-magnitude threshold was used to estimate t_2.

We are able to tightly constrain t_2 when ASAS-SN observations are able to detect the outburst below the two-magnitude threshold. In these cases, we consider this a measurement of t_2. For some faint and fast outbursts close to the ASAS-SN detection limit, the outburst decline is not tracked all the way to the two magnitude threshold, but a subsequent non-detection places a limit fainter than the two-magnitude threshold. In this case, we limit t_2 to be bounded by these two epochs.

2.2.4 Outburst Amplitude

Observations of the brightest outburst of a DN from ASAS-SN were combined with observations from The Pan-STARRS 3π Steradian Survey (Chambers et al., 2016) of the same object in quiescence to estimate the amplitude of outburst. We estimate the quiescent magnitude of the CNe in the same way for those in the observing field of Pan-STARRS (declination $> -30°$); otherwise we use *Gaia* DR2 photometry (Gaia Collaboration et al., 2018b) for CNe that erupted after *Gaia* DR2 observations were completed (2016 May 23). The details of the quiescent magnitude measurements are discussed in §2.6.2 and §2.6.3.

If an object is unambiguously detected in quiescence, we make a measurement of its

outburst amplitude. However, if an object is clearly not detected (no match within four arcseconds for DNe and 2 arcseconds for CNe), we place a lower limit on its outburst amplitude. The outburst amplitude we estimate is simply the difference between the peak magnitude of the outburst detected by ASAS-SN or AAVSO observations and the magnitude obtained from the Pan-STARRS or Gaia photometry catalogs, after correcting for filter transformations (§2.6.1). If a CN was detected immediately after Solar conjunction, it is likely that the peak brightness was missed (See Figure 2.11). We expect this is only an issue for CNe, since they can still be detected in outburst months after eruption. For these CNe, we place a lower limit on the outburst amplitude and an upper limit on t_2.

2.3 Results

2.3.1 Detected DN and CN Outbursts

In total, we find 2688 DNe with outbursts that declined by at least two magnitudes from maximum in the ASAS-SN data, around 30% of all DNe in VSX. This does not test the discovery and classification of DNe in ASAS-SN, as we have only searched for outbursts from known DNe discovered by a variety of surveys and techniques. In order to be detected in our analysis, a DN needs to have gone into outburst in a field ASAS-SN regularly monitored (the entire sky since 2017), and to have reached a peak outburst magnitude in the range $g \approx 10$–16 mag (a more detailed analysis of our detection capabilities is discussed in Section 2.6.4). From the subset of objects with detected outbursts, 1791 objects have declination greater than $-30°$, and are therefore in Pan-STARRS. We are able to unambiguously estimate or place a limit on the quiescent brightness for 1617 of these. The measured properties of these DNe are presented in Table 2.1 (the entirety of which is available online in a machine-readable

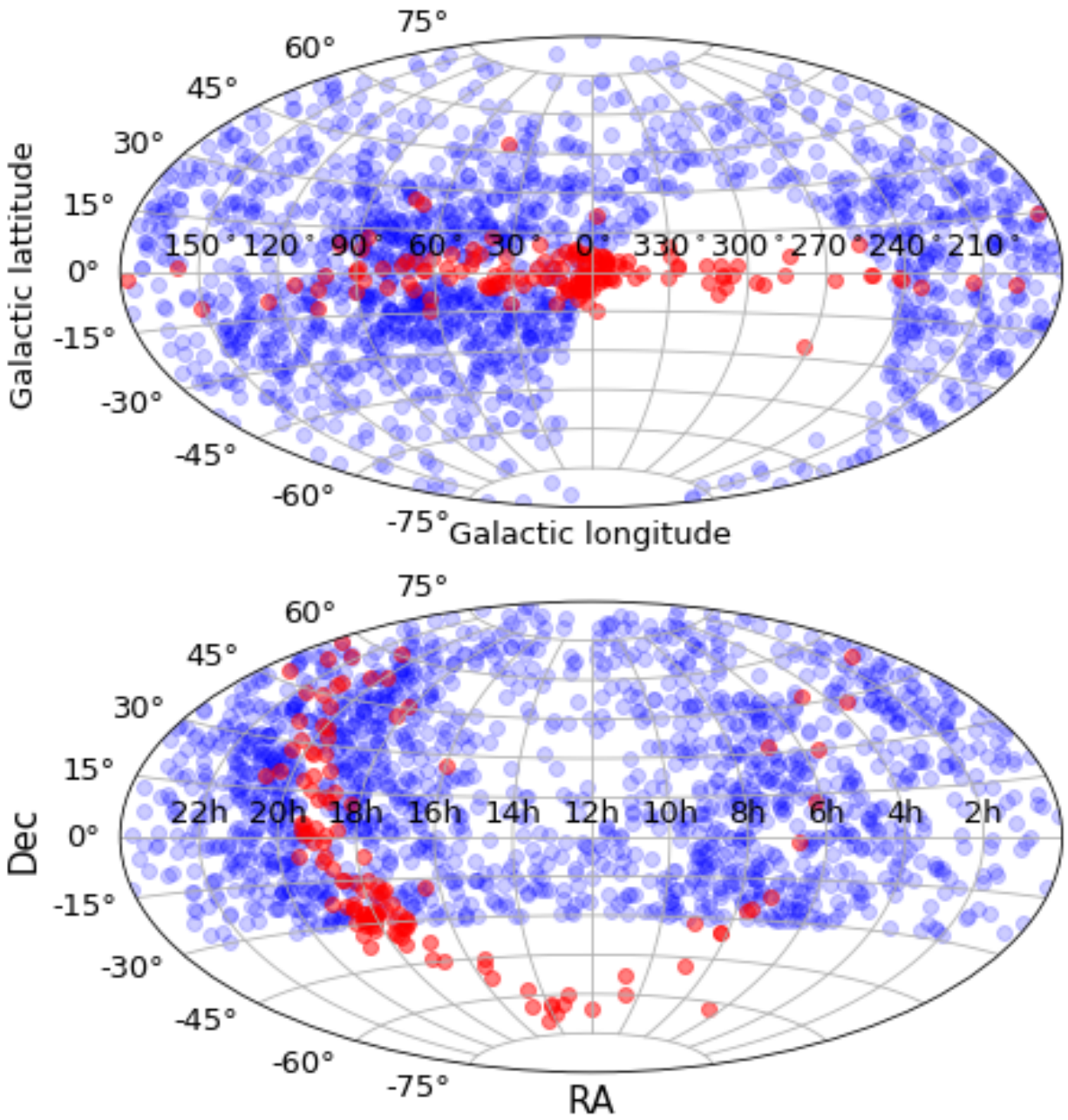

Figure 2.2 Galactic (top) and equatorial (bottom) coordinate positions of CVs with outburst property estimates. Dwarf novae are shown in blue, and classical novae are shown in red. The gap in the data for dwarf novae is due to the survey limits of Pan-STARRS

Table 2.1. Outburst Properties of Dwarf Novae

Name	RAJ2000 hms	DEJ2000 dms	Peak mag	Amp. mag	Amp. Flag boolean	t_2 days
ASASSN-18xt	2:25:06.37	8:06:38.6	14.1	6.4	1	12.1
CSS 091106 023638+111157	2:36:37.98	11:11:56.5	15.1	4.9	1	12.9
TCP J03005508+1802290	3:00:55.05	18:02:28.7	12.1	3.4	1	11.9
MLS 130110 034256+171739	3:42:56.18	17:17:40.1	16.0	4.7	1	3.8
MLS 130302 035906+175034	3:59:05.90	17:50:34.5	16.3	2.4	1	18.4
CSS 081118 041139+232220	4:11:38.58	23:22:20.3	15.0	4.6	1	11.0
CSS 081107 033104+172540	3:31:04.44	17:25:40.2	15.5	4.9	1	5.9
CSS 081107 033556+191119	3:35:55.78	19:11:19.1	15.6	5.3	1	14.2
CSS 090213 033031+201402	3:30:31.41	20:14:01.2	15.6	4.3	1	5.0
V0701 Tau	3:44:01.97	21:57:07.4	15.2	6.4	1	16.3

Note. — Names, positions, peak apparent brightness, amplitude of outburst, and t_2 for the dwarf novae in our sample. The Amp. Flag columns equals 1 when we are able to make a measurement of the outburst amplitude and 0 when we are able to place a lower limit. The t_2 Flag column is 1 when were are able to detect the object below the two magnitude threshold and 0 when there is only a non-detection below this threshold. When t_2 Flag = 0, the value listed for t_2 is likely larger than the true value. The $t_{2,low}$ column gives the time until last detection above the two magnitude threshold and the $t_{2,up}$ column gives the time until the first detection or non-detection below this threshold. These last two columns are lower and upper limits on t_2, respectively. The first 10 dwarf novae are shown here and the entirety of the this table is available in a machine readable format in the electronic paper.

format).

By combining data from ASAS-SN and AAVSO, we are able to measure or place a limit on t_2 for 50 CNe. We are able to unambiguously estimate the quiescent brightness for 40 of these objects. The measured properties of these CNe are presented in Table 2.3 in Section 2.6.5. In order to make a more robust comparison between DN and CN outbursts, previous CN outburst estimates and limits were also obtained from Strope et al. (2010). This yielded an additional 92 CNe for the sample, bringing the total number of CN outbursts studied to 132.

The positions of both the DNe and CNe are shown in Galactic and equatorial coordinates in Figure 2.2. The DNe in our sample are restricted to the Pan-STARRS observing field, but

we also used *Gaia* to have full sky coverage for the CNe. The CNe are generally restricted to within several degrees of the Galactic plane, as expected if CVs track the stellar mass density of the Galaxy (e.g., Shafter, 2017). However, as DNe are likely to be nearby, they often appear at higher Galactic latitudes. Without significant dust extinction, we expect to detect CNe even at the largest Galactic distances, but we do not expect to detect even the brightest DNe outbursts beyond $\sim$ 6 kpc. Since CNe are more luminous, we are still able to detect them down to latitudes near $b = 0^{\circ}$, although dust extinction can obscure CNe at the lowest latitudes.

2.3.2 Outburst vs. Quiescent Brightness

Figure 2.3 shows the distribution of the sources by plotting peak outburst brightness against brightness in quiescence. The peak outburst magnitudes of CNe are significantly brighter than for DNe, although this is largely due to selection effects. For DNe, the brightness in outburst were studied using data solely from ASAS-SN, so we do not include DN outbursts brighter than $\sim$10 mag (the saturation limit of ASAS-SN) in this study. The region with $g \gtrsim 10\,\mathrm{mag}$, where ASAS-SN is saturated, is populated only with CNe because we rely on AAVSO observations to measure brighter peak magnitudes for CNe. We also note that ASAS-SN is sensitive to transients as faint as $\sim$18 magnitude, but since we are interested in measuring t_2, the outburst has to reach at least two magnitudes brighter than the survey magnitude limit. This detection range is shown in the non-shaded region in Figure 2.3. Objects that are not detected in quiescence are indicated by leftward facing triangles at the expected 98% completeness limits. Where Darnley et al. (2012) classified the companion of a CN, we have included the classification as main sequence (MS), red giant (RG), and sub-giant (SG) stars. Luminous companions may contribute significantly to the quiescent

flux we measure (indeed, novae with giant companions are found to have bright quiescent magnitudes), which will lower the estimated outburst amplitude.

2.3.3 Outburst amplitude vs. t2

The amplitude of outburst is shown as a function of $\log_{10}(t_2)$ in Figure 2.4 for both CN and DN outbursts. As expected, the majority of DNe have smaller outburst amplitudes than CNe, although there is significant overlap for amplitudes of 5–10 mag. We find that the outburst amplitudes and decline times of both samples are well fit by normal distributions, with the exception of the decline times of DNe. These distributions were fit using censored statistics, as a fraction of our estimates for the amplitude of outburst and t_2 are limits and are shown along with histograms of measured values, not including limits, in Figure 2.4. For CNe, the normal distribution of the outburst amplitude has a mean and standard deviation of $\mu = 11.43 \pm 0.25$ mag and $\sigma = 2.57 \pm 0.20$ mag, respectively. This is in comparison with the amplitudes of DNe, where $\mu = 5.13 \pm 0.04$ mag and $\sigma = 1.55 \pm 0.03$ mag. There is a roughly 15% overlap in the outburst amplitude distributions of CNe and DNe, suggesting that this property alone is not sufficient to distinguish the two classes of objects.

The mean of the outburst amplitude distribution for DNe presented in this paper is larger than other measurements found using transient survey data alone (Coppejans et al., 2016; Mróz et al., 2015a). With typical CCD dynamic ranges of about 5 magnitudes, it is difficult to detect both the transient peak and the quiescent system in a single survey unless the amplitude is less extreme (Drake et al., 2014). By combining ASAS-SN and Pan-STARRS observations, we are able to measure and place lower limits on outburst amplitudes as high as 12 magnitudes.

We do not include error bars on Figure 2.4 for visualization purposes, but the lower and

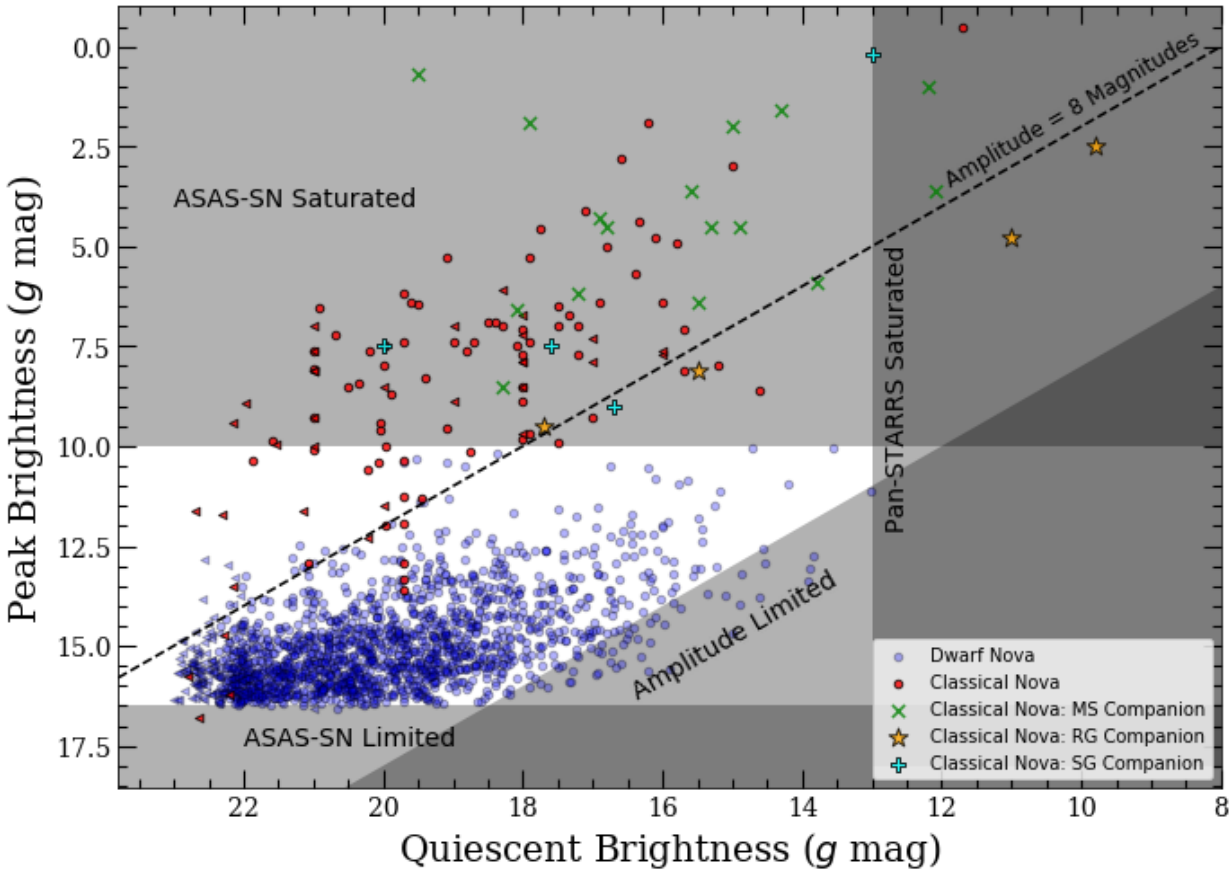

Figure 2.3 Peak magnitude of outburst versus measured brightness in quiescence for all outbursts discussed in this work. Dwarf nova outbursts are shown in blue, and classical nova outbursts without companion information are shown in red. Those classical novae where the companion type is known are denoted as green X's, orange stars, and cyan crosses for main sequence, red giant, and sub-giant companions, respectively. The non-shaded region indicates where our analysis can measure outburst properties by combining ASAS-SN and Pan-STARRS observations. Only these surveys were used to study DNe, but AAVSO V-band observations were utilized to study CNe that peak above the saturation limit of ASAS-SN. The dashed line shows an outburst amplitude of 8 mag. The "amplitude-limited" diagonal shaded region shows the requirement that outbursts in our catalog must have amplitudes >2 mag, and quiescent brightness measurements in this region are likely contaminated by outbursts. The horizontal gray shaded region at top denotes the saturation limit of ASAS-SN ($g \lesssim 10$ mag). The horizontal shaded region at bottom signifies two magnitudes brighter than the sensitivity limit of ASAS-SN ($g \gtrsim 18$ mag). Finally, the vertical shaded region at right represents the saturation limit of the Pan-STARRS 3π survey ($g \lesssim 13$ mag).

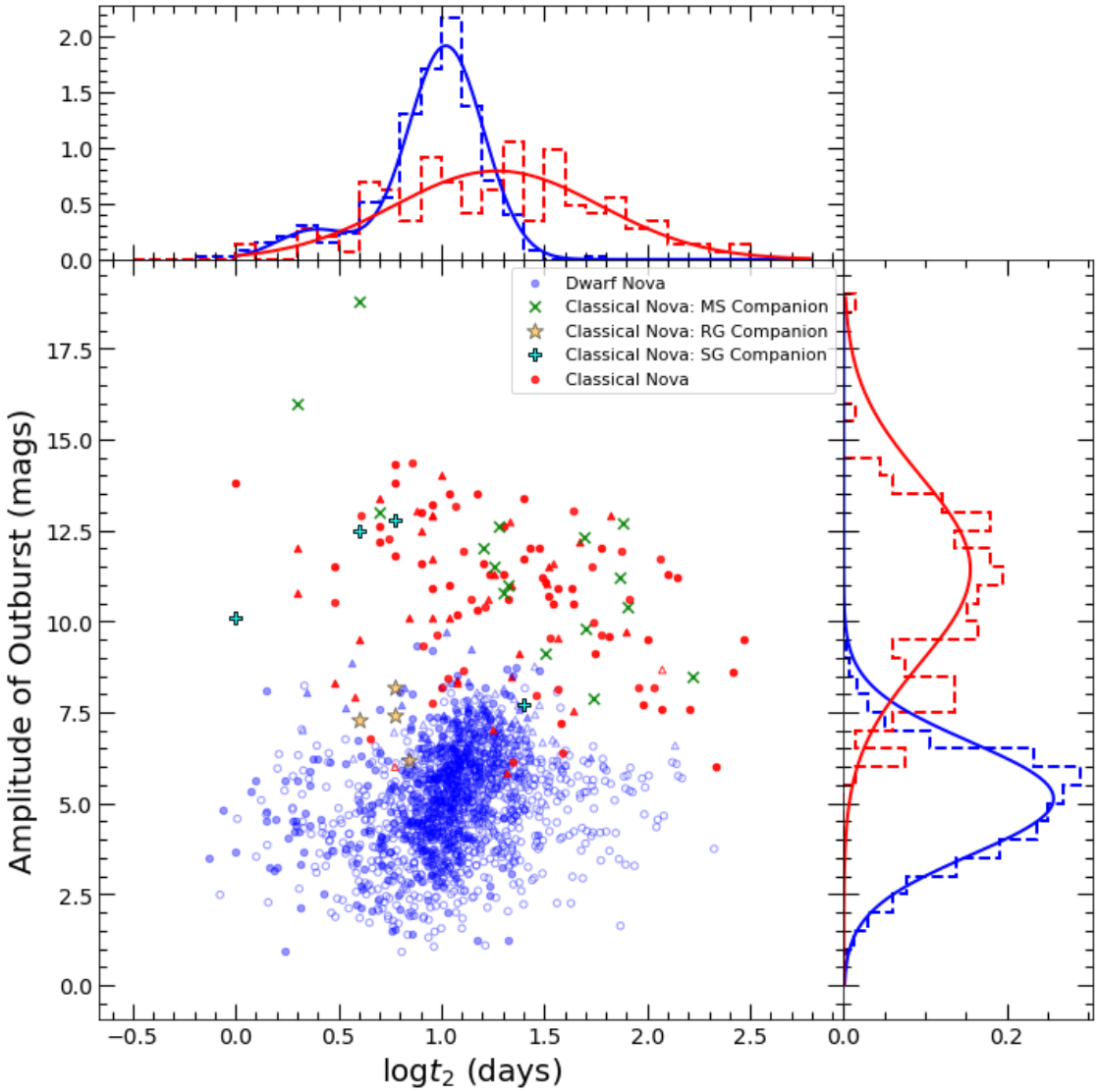

Figure 2.4 Amplitude of outburst versus the time t_2 to decline by two magnitudes from maximum for both CNe and DNe. A filled circle signifies that both the outburst amplitude and t_2 were estimated for that object. A triangle signifies that a lower limit was placed on the outburst amplitude, and an open symbol shows the upper limit that was placed on t_2. Though we are able to place lower and upper limits on t_2, we only show the upper limit for visualization purposes. Blue objects denote DN outbursts, while CNe analyzed in this work and Strope et al. (2010) are represented with symbols as in Figure 2.3. The top and right panels show the distributions of t_2 and outburst amplitude, respectively, with DNe shown in blue and CNe shown in red. The dashed histograms show the distributions of only measured values, not limits, and the solid lines shows the fits to the measured values including the limits.

upper bounds on t_2 for each DNe and CNe can be found in Tables 2.1 and 2.3, respectively. We have not estimated the error on the outburst amplitude and expect systematics to dominate. The error on the outburst amplitude should be relatively small in most instances, but for some small fraction of objects, the outburst amplitude may be significantly underestimated. The peak of the outburst can be missed if the object declines rapidly or occurs during a time of lower temporal cadence by ASAS-SN. In addition, for DNe that outburst frequently, there is a chance that the quiescent magnitude we measure from Pan-STARRS data is contaminated by outbursts. A more detailed discussion of possible errors, the sensitivity of our analysis, and possible selection effects is provided in Section 2.6.4. In considering the results presented in Tables 2.1 and 2.3, we encourage the reader to take these caveats into consideration.

Fitting a log-normal distribution to the CN decline times, we find a mean and standard deviation of $\langle t_2 \rangle = 18.7 \pm 1.9$ days and 3.2 ± 0.2 days, respectively. The distribution of t_2 values for DNe is not well fit by a single log-normal distribution, but can be described as a homoscedastic double-log-normal distribution, with mean values equal to 2.4 ± 0.2 days for 12% of the sample and 10.5 ± 0.2 days for the remaining 88% of the sample. The common standard deviation is 1.52 ± 0.02 days. Visual inspection of ASAS-SN images of these "fast" outbursts confirm that the transients are real.

The bimodality of the outburst durations in SU UMa dwarf novae is well documented, with normal outbursts lasting a few days and superoutbursts lasting roughly two weeks (Warner, 1995; Osaki, 1996). In our analysis, we only measure t_2 of the brightest outburst, so we expect our sample to be biased towards superoutbursts rather than normal outbursts. One explanation for a short outburst is that the heating wave fails to move fully throughout the accretion disk of the CV, and the unheated colder region pulls material from hotter

regions of the disk, shutting down the outburst (Smak, 1984). In the case of superoutbursts, the heating wave reaches the outer edge of the disk, causing the disk to remain hot for a longer amount of time.

In addition to finding that the distributions are well fit by Gaussians, we also find strong evidence of a relationship between the amplitude of outburst and t_2 for DNe, and modest evidence of an inverse correlation for CNe. We use censored statistics to measure a linear correlation of the form

$$\log_{10}(t_2) = \beta\,(\mathrm{Amp} - \langle \mathrm{Amp} \rangle) + \alpha \tag{2.1}$$

where Amp is the outburst amplitude and $\langle \mathrm{Amp} \rangle$ is the mean of only the measured outburst amplitudes ($\langle \mathrm{Amp} \rangle = 10.57$ for CNe and $\langle \mathrm{Amp} \rangle = 4.91$ for DNe). For DNe, we exclude the subset of fast DNe ($\log_{10}(t_2) < 0.4$), and we find a fit with $\alpha = 0.980 \pm 0.005$ and $\beta = 0.061 \pm 0.004$. This fit has a modest intrinsic scatter of $\sigma = 0.178 \pm 0.004$, and the correlation is highly significant, roughly 10σ.

We are unable to find a previous study of our observed correlation between amplitude and t_2 in DNe. However, Otulakowska-Hypka et al. (2016) studied the correlation between outburst duration (the total time of the outburst) and the amplitude of outburst for DNe. For normal outbursts of SU UMa stars they found no significant correlation between outburst duration and outburst amplitude. However, for superoutbursts, they did find evidence for a correlation. We make no distinction between subtypes of DN outbursts and expect this sample to contain a higher fraction of superoutbursts since our measurement is for the brightest observed outburst of an object since 2013 and excludes the faster outbursts from the fit.

For CNe, we find a less significant (roughly 3σ) correlation with best-fit parameters to

Equation 2.1 of $\alpha = 1.33 \pm 0.05$ and $\beta = -0.083 \pm 0.024$, and a large intrinsic scatter of $\sigma = 0.50 \pm 0.04$. This fit is shown in Figure 2.5 along with the predicted correlation derived from the MMRD relationship for various inclination angles and assuming an absolute magnitude in quiescence of $M_V = 3.8$ (Warner, 1995; Capaccioli et al., 1989b). Although the correlation for CNe is less significant than for DNe, the two populations have opposite slopes: amplitude and t_2 are anti-correlated for CNe, while they are positively correlated for DNe.

Warner (1987) noted the substantial scatter in the relation between amplitude and t_2 for CNe. He attributed it to observational errors, a random distribution of inclination angles, and/or nova outbursts depending on multiple binary parameters (e.g., white dwarf mass, accretion rate, and core temperature), but the measured values appeared to be in general agreement with predictions. Yaron et al. (2005) point out that their models predict a population of low-amplitude CNe (<7 mag). Both Warner (1987) and Yaron et al. (2005) analyzed novae from the Duerbeck (1987) catalog where few low amplitude novae are present. Our sample includes a larger population of such low-amplitude CNe (many of which also have small t_2), likely due to newer surveys that are more sensitive to fainter and faster CNe. This serves to steepen the slope of the fit and further increase the variance around the anti-correlation between amplitude and t_2, compared to the results of Warner (1987). Our findings are consistent with the recent results from Kasliwal et al. (2011) and Shara et al. (2017a), who find a class of novae that deviate from the proposed MMRD relationship.

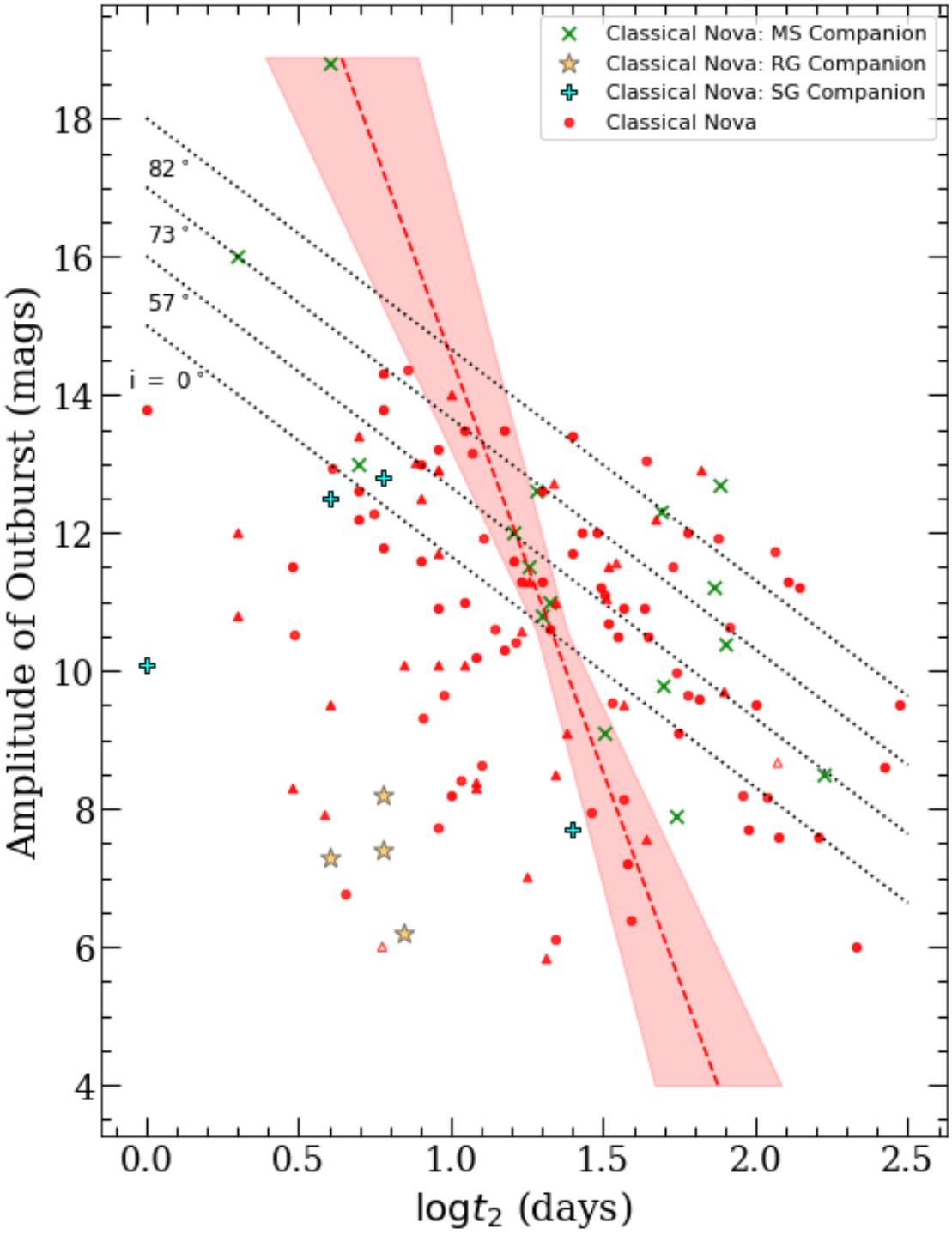

Figure 2.5 The outburst amplitude versus $\log t_2$ for the CNe analyzed in this work. The markers are the same as Figure 2.4. The red dashed line and the red shaded region show our best-fit relation for CNe, with values and uncertainty given in §2.3.3. The dotted black lines show the expected theoretical correlation derived from the MMRD relationship from Figure 5.4 of Warner (1995).

2.4 Which Dwarf Novae might be mis-classified Classical Novae?

To test the idea that some CNe commonly get mis-characterized as DNe, we search for possible CN candidates in our sample of DN outbursts. This is likely the first large-sample analysis of this kind, but there is at least one example of an ASAS-SN transient that was initially characterized as a DN candidate but turned out to be a highly reddened CN (ASASSN-20ga; De et al. 2020a). Because of their high luminosities, Galactic CN eruptions can only appear faint ($g \gtrsim 12\,\mathrm{mag}$) if they are affected by substantial dust extinction. For a Galactic transient to be a CN, it must have a peak absolute magnitude $M_{\mathrm{g,peak}}$ brighter than -4.2 mag ($M_{\mathrm{g,peak}} = -4.2$ mag is 3σ fainter than the mean of the log-normal CN luminosity function presented in Shafter 2017). The absolute magnitude is tied to the peak apparent magnitude $m_{g,peak}$ by

$$M_{\mathrm{g,peak}} = m_{\mathrm{g,peak}} - 5\log_{10}\left(\frac{d}{10\ \mathrm{pc}}\right) - A_g, \tag{2.2}$$

where d is the distance of the object in pc and A_g is the amount of extinction. To place an upper limit on how luminous a given transient can possibly be, we take the peak apparent magnitude of the transient measured from ASAS-SN, an upper limit on the distance given reasonable constraints, and the maximum g-band extinction in the direction of the transient from Schlafly & Finkbeiner (2011).

In our previous analysis, we only considered DNe in the Pan-STARRS field of view ($\delta > -30^\circ$), but here we apply those lessons learned to inspect all DN outbursts detected in ASAS-SN. This results in 2688 DNe with outbursts detected by ASAS-SN, spread over the entire sky. For 1039 of the objects, parallaxes were measured with *Gaia* at $\geq 3\sigma$ significance,

and for those, we use the 1σ upper limits on the distances given in Bailer-Jones et al. (2018). For those objects without significant distance estimates in Bailer-Jones et al. (2018), we used a Galactic upper limit of $d = 30$ kpc. This is likely too conservative for any direction in the Galaxy, but a directional upper limit on the distance is beyond the scope of this work. At this time, we are more focused on being complete than robust when identifying candidates and plan to investigate a more reasonable Galactic distance upper limit as a function of position in Kawash et al. (2021, in preparation).

We find that 201 (¡ 10%) objects classified as DNe in our sample could have $M_{\mathrm{g,peak}} \lesssim -4.2$ mag, if they were behind all of the dust estimated by Schlafly & Finkbeiner (2011), as shown in Figure 2.6. To be clear, these are not exact peak absolute magnitude measurements, especially for objects with no reliable distances (shown in purple) and high extinction, and are only being used to identify CN candidates. We further rule out objects where we have measured the outburst amplitude to be < 5 mag, the lower bound of CN amplitudes based on Figure 2.4, and objects with more than one detected outburst in an observing season (bounded by Solar conjunction). Though objects with multiple outbursts in ASAS-SN data are much more likely to be dwarf novae than recurrent novae, we can not rule out the latter. There are no known recurrent novae in the Galaxy that recur on timescales less than a decade, but M31 recurrent nova M31N 2008-12a erupts every year (Darnley & Henze, 2019). If objects like this, dubbed 'rapid recurrent novae,' exist in the Galaxy, they should be less luminous and evolve more quickly than a typical classical nova, making them easily confused with DNe. Therefore, we only eliminate objects with multiple outbursts in a year so our search is sensitive to rapid recurrent novae. Overall, we find that 94 objects have outburst amplitudes, recurrence times, and possibly luminosities consistent with that of a Galactic classical or recurrent nova.

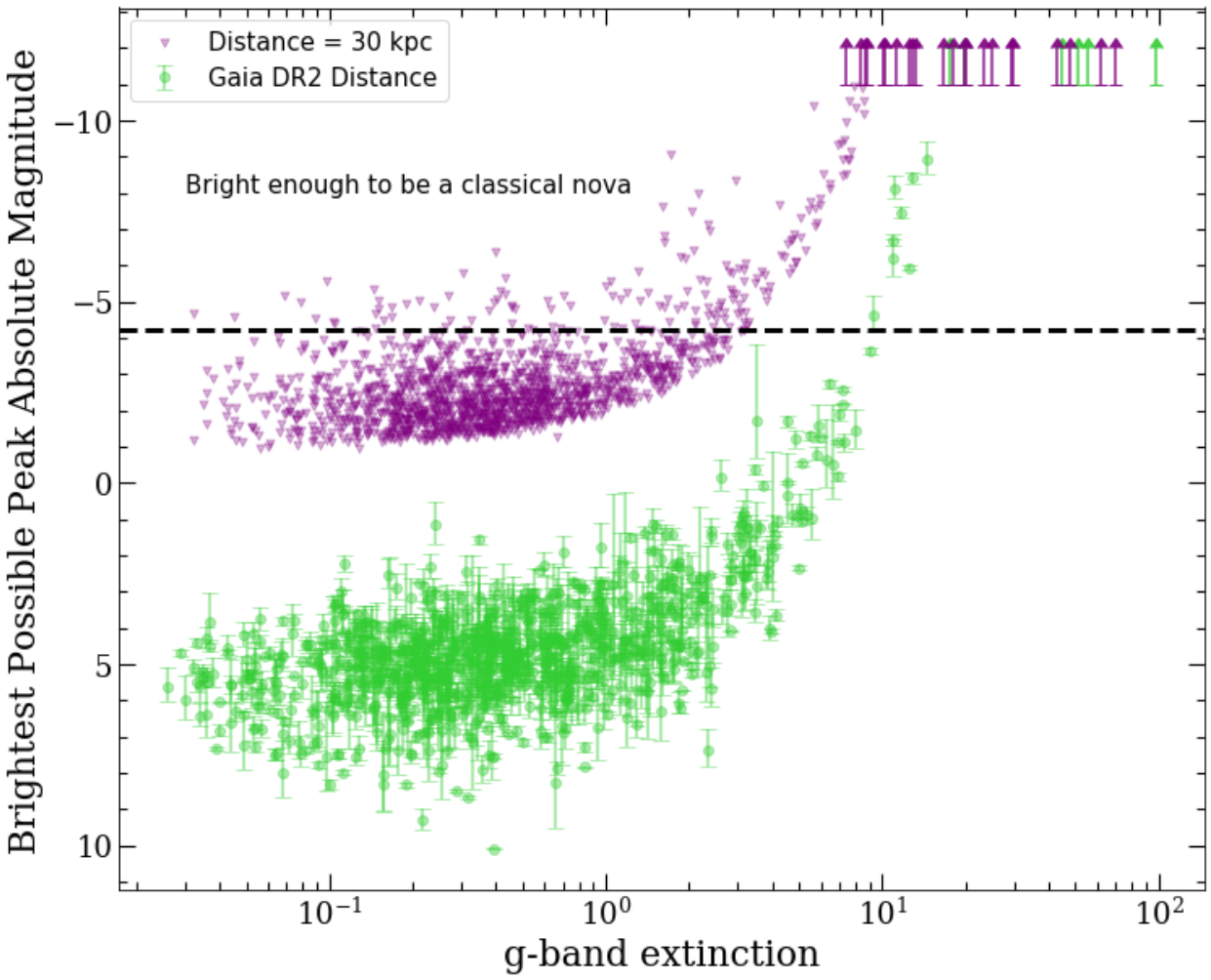

Figure 2.6 The brightest possible peak g-band absolute magnitude an outburst could have while still being in the Galaxy, as a function of the amount of g-band extinction. The objects with 3σ parallax detections in *Gaia* are assumed to be at the distances in Bailer-Jones et al. (2018) and are plotted in green. The violet points are objects that do not have significant *Gaia* parallaxes, so we place a limit on the brightest peak absolute magnitude by assuming a maximum Galactic distance of 30 kpc. In order to be luminous enough to be a CN, the absolute magnitude needs to be brighter than $M_g \approx -4.2$ mag, and this cutoff is shown as the dashed black line. The peak absolute magnitude presented here is not an accurate measurement especially for objects with no reliable distance estimates and those with large amounts of dust extinction; the plotted values are only used to select CN candidates.

Many of these objects have been confirmed as DNe through an identification spectrum or a measurement of the superhump period, but we find that 27 sources were not confirmed through any method. Quiescent multi-band photometry of these remaining candidates can provide insights to the distance and ultimately constrain the luminosity of the transient. In the Galactic plane, a candidate that is relatively blue is likely close by, and therefore will have a lower luminosity at peak brightness, suggesting a DN outburst. Conversely, a candidate that is brighter in redder filters is likely reddened by dust, implying a higher luminosity and a CN outburst. This strategy—identifying highly reddened quiescent counterparts—is only possible for candidates within a few degrees of the Galactic plane and that can be securely matched to multi-band optical catalogs. As described in §2.2.4, we find quiescent counterparts in Pan-STARRS, and also add in coverage of southerly declinations by using the DeCAPS catalog (Schlafly et al., 2018) (cross matching for both catalogs is as explained in Section 2.6.3). We use the *griz* photometry to estimate reddening by fitting the observed spectral energy distributions of the CVs in question to de-reddened SDSS CV colors from Kato et al. (2012) by varying the amount of reddening according to extinction laws (Cardelli et al., 1989; Mathis, 1990). For each of our candidates, this results in a distribution of extinction values that are plugged into the three-dimensional all-sky extinction map stitched together in Bovy et al. (2016) to find a range of plausible distances. This strategy only worked for 19 of the candidates: those that were able to be cross matched and in fields close to the plane, where the large amount of dust can constrain the distance. We find that all 19 are consistent with the peak luminosity of a dwarf nova, and zero are consistent with the peak luminosity of a classical nova. This analysis will also be useful to shed light on the nature of CV candidates that are discovered in the future, so it is made publicly available as an iPython notebook at `https://github.com/amkawash/CV_colors_luminosity`

Table 2.2. Classical and Rapid Recurrent Nova Candidates

Name ASASSN	RAJ2000 h m s	DEJ2000 ° ′ ″	l deg.	b deg.	Peak mag	Amp. mag	t_2 days	A_g mag	τ_R years
-17li	18:38:22.00	−09:43:47.4	22.790	−1.551	16.2	nan	[12 - 33]	10.2	> 3
-17ar	10:01:11.14	−55:11:56.3	280.224	−0.018	14.4	nan	20.7	7.6	> 3
-19nf	14:19:35.09	−59:58:24.0	313.755	1.033	16.1	> 7.5	[7 - 15]	19.8	0.9
-19am	09:30:39.31	−54:47:04.3	276.609	−2.521	16.3	nan	[11 - 18]	7.4	0.8
-17lq	17:29:28.81	−38:02:26.8	350.512	−2.042	15.4	> 8.2	[9 - 11]	10.1	> 3
-19pw	18:31:05.75	−14:47:52.6	17.469	−2.303	15.6	6.7	[14 - 17]	6.4	> 4
-17js	18:21:09.05	−19:24:47.6	12.275	−2.347	15.0	6.5	[6 - 9]	6.9	> 3
-19fd	17:03:19.29	−29:52:23.3	354.045	7.099	13.5	nan	7.9	1.4	> 4

Note. — Positions, peak brightness, extinction in the direction, and minimum recurrence time of unidentified CV outbursts with significant extinction and no optical quiescent detection. The minimum recurrence time is estimated as the shortest time between outbursts and is measured solely from ASAS-SN observations.

So, for all but 8 of the 2688 DN outbursts detected by ASAS-SN, we find evidence suggestive of their DN nature. An identification spectrum is needed to determine if any of the 8 remaining candidates are mis-classified classical or recurrent novae. These candidates are shown in Table 2.2 listing equatorial and Galactic coordinates, peak g apparent magnitude observed in the ASAS-SN light curve, a limit on outburst amplitude if able to be measured, t_2, extinction along the line of sight from Schlafly & Finkbeiner (2011), an estimate of the outburst recurrence time measured from the ASAS-SN light curve (τ_R), and if the outburst is luminous enough to be a CN as close as 10 kpc. The ASAS-SN light curves of all of these candidates are shown in Figures 2.7 and 2.8.

2.5 Conclusions

In this work, we characterize the brightest outburst of 1618 DN outbursts detected by ASAS-SN and 93 CNe observed by ASAS-SN and AAVSO contributors. In general agreement with

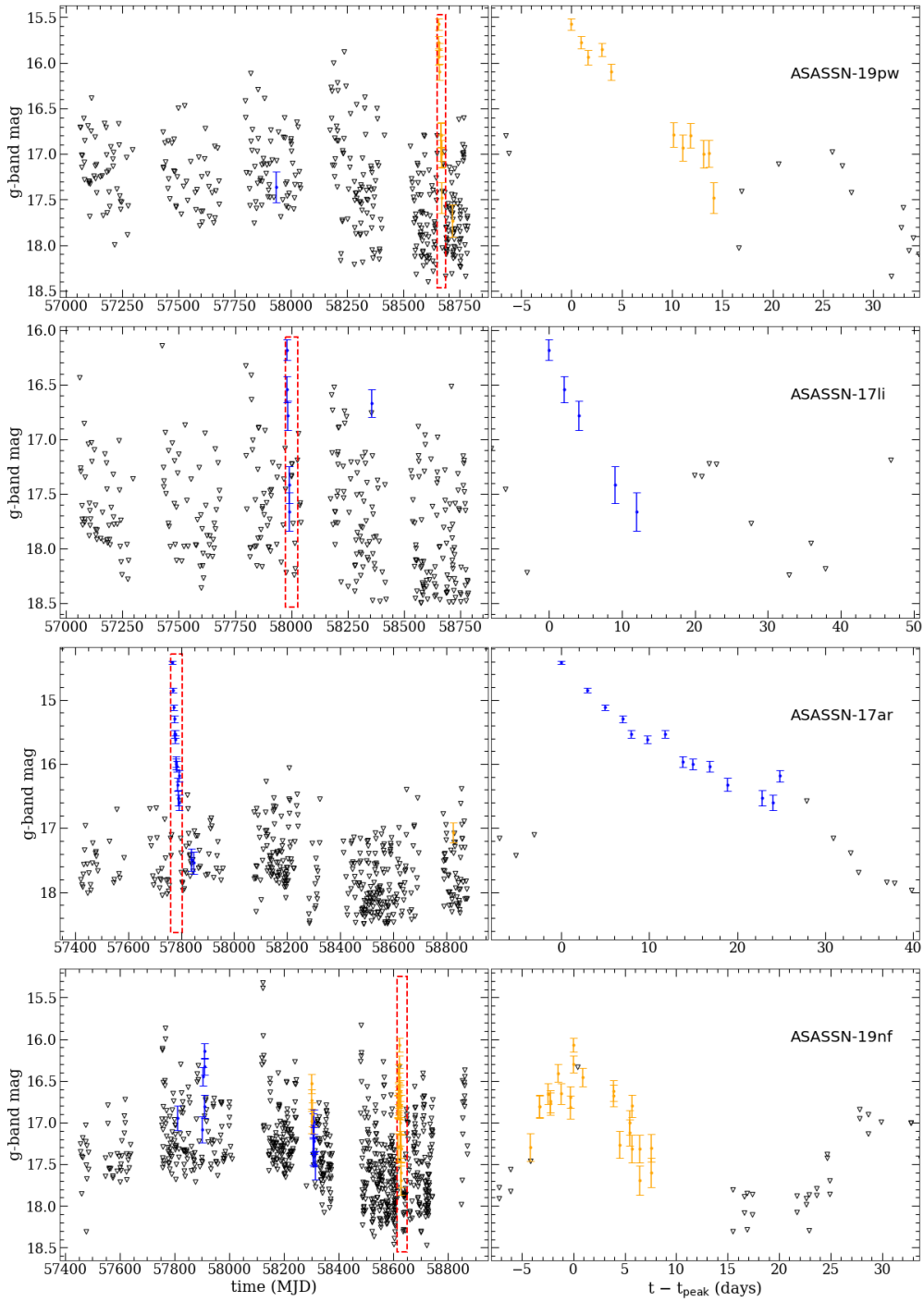

Figure 2.7 ASAS-SN Light curves for 4 of the candidates listed in Table 2.2. The left column shows all observations of these objects and the right column shows the observations around the brightest outburst. Blue and orange points denote the ≥5-sigma detections from V-band and g-band observations, respectively, and the black triangles signify the ≥5-sigma upper limits from non-detections.

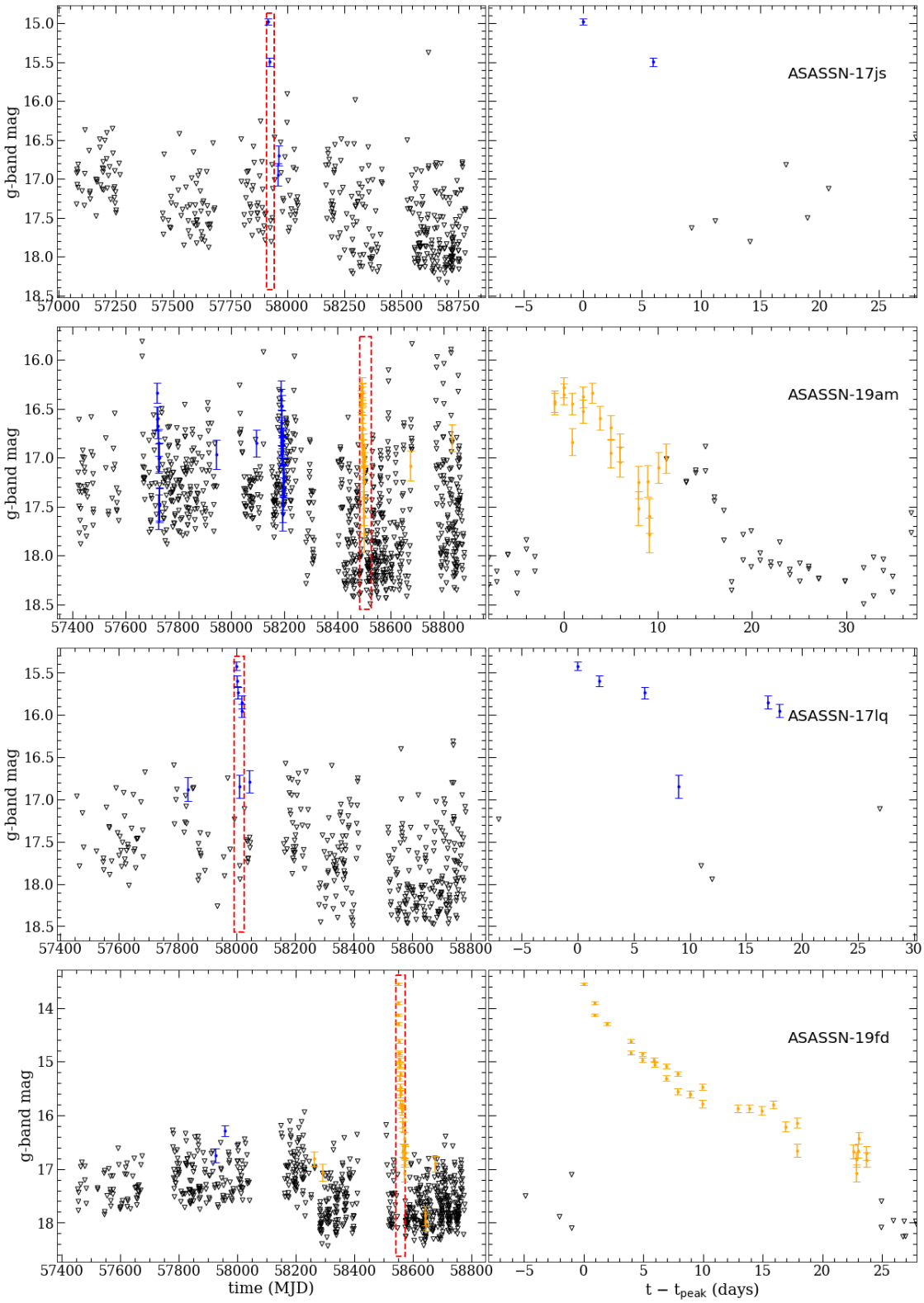

Figure 2.8 Same as Figure 2.7 for the remaining 4 candidates in Table 2.2.

previous results, we find that the mean outburst amplitude of CNe is 11.4 magnitudes, significantly larger than the mean DN outburst of 5.1 magnitudes. However, we find significant overlap in their distributions, at the $\sim$ 15% level. Although the outburst amplitude is a fairly good indicator for determining the nature of a CV outburst, it is clear that a CV outburst with amplitude in the range 5$-$10 mag is ambiguous in nature. Similarly, the mean decline time, or t_2, of CNe is larger than that of DNe, but a majority of the distributions overlap, especially at lower values. Because there is an overlap in parameter space between DN outbursts and CN eruptions, we have presented a technique to identify CN versus DN candidates based solely on photometric data. This will be a necessary tool to handle the large number of CV outbursts discovered in the LSST era.

The primary motivation for this work was driven by the possibility that CNe are being mis-characterized as DNe. To explore this prospect, we have investigated every DN that declines by two magnitudes from maximum in ASAS-SN. The majority of outbursts are inconsistent with the luminosity of a CN, but there is a small fraction that could be bright enough if they are behind most of the dust along the line of sight. We looked into this subset and found that only 8 objects (out of 2688) are still ambiguous based on available data. A classification spectrum will be needed to confirm if any of these candidates are CNe characterized as DNe, but it is clear that there is no significant number of Galactic classical novae hiding in the large sample of dwarf novae. The transient community appears to be doing an effective job classifying CV outbursts.

Our results suggest that either Galactic nova rate predictions are too high or there must be other factors than classical nova mis-classification causing the discrepancy between reported and predicted classical novae. Recent observations from Palomar Gattini-IR have revealed a sample of highly reddened and optically missed novae due to Galactic extinction (De et al.,

2021). We plan to explore to what degree interstellar dust has an effect on ASASN's, and other optical observer's, ability to discover classical novae.

Acknowledgments

This research has made use of the International Variable Star Index (VSX) database, operated at AAVSO, Cambridge, Massachusetts, USA. We acknowledge with thanks the variable star observations from the *AAVSO International Database* contributed by observers worldwide and used in this research.

A.K., L.C., E.A., and K.V.S. acknowledge financial support of NSF award AST-1751874 and a Cottrell fellowship of the Research Corporation. J.S. acknowledges support from the Packard Foundation. BJS, CSK, and KZS are supported by NSF grant AST-1907570. CSK and KZS are supported by NSF grant AST-181440.

We thank the Las Cumbres Observatory and its staff for its continuing support of the ASAS-SN project. ASAS-SN is supported by the Gordon and Betty Moore Foundation through grant GBMF5490 to the Ohio State University, and NSF grants AST-1515927 and AST-1908570. Development of ASAS-SN has been supported by NSF grant AST-0908816, the Mt. Cuba Astronomical Foundation, the Center for Cosmology and AstroParticle Physics at the Ohio State University, the Chinese Academy of Sciences South America Center for Astronomy (CAS- SACA), and the Villum Foundation.

The analysis for this work was performed primarily in `ipython` (Perez & Granger, 2007) using- `numpy` (Oliphant, 2006; Van Der Walt et al., 2011), `Astropy` (Price-Whelan et al., 2018), `Matplotlib` (Hunter, 2007), and `scipy` (Virtanen et al., 2020). The PanSTARRS1

Catalog was accessed using packages from `MAST CasJobs`[3] developed by the JHU/SDSS team.

We acknowledge the use of data from the AAVSO International Database and thank the observers for their contribution to this work.

We thank the anonymous referee for the useful feedback.

2.6 Appendix

2.6.1 Filter Transformations

The photometry utilized in this work makes use of a range of blue-green filters: the V filter used by AAVSO observers, the ASAS-SN V filter, the ASAS-SN g filter, the Pan-STARRS g_{P1} filter, and the Gaia G_{BP} filter. Although all of these filters are centered around a similar wavelength, the flux of a source in each filter band can be different, especially for reddened objects. To account for this, all V-band observations were transformed to g-band using

$$V - g = -0.017 - 0.508 \times (g - r)\,, \tag{2.3}$$

when g_{P1} and r_{P1} observations were available (Kostov & Bonev, 2018). Pan-STARRS only provides estimates of colors in quiescence, so to transform V-band data in outburst to g-band, we assume typical CV colors in quiescence ($B-V = 0.1$; Bruch 1984) and typical color changes during outburst ($\Delta(B-V) = -0.1$ for DNe and $\Delta(B-V) = 0.13$ for CNe; Warner 1995). These rough color estimates were converted from B and V to g and r using equation 2.3 and additional filter transformations from Kostov & Bonev (2018). This implies

[3] `http://casjobs.sdss.org/CasJobs`

an intrinsic color of $g-r = -0.29$ for DNe and -0.08 for CNe. We then use the measured Pan-STARRS colors to estimate the reddening and ultimately the observed $g - r$ color in outburst.

For objects without color information in Pan-STARRS, we have to make additional assumptions. For DNe, we assume $g_{P1}-r_{P1} = 0$ in quiescence, but for CNe we assume a $g_{P1}-r_{P1} = 1$, as most CNe are more distant and closer to the Galactic plane, and therefore reddened by dust. Although all of these color estimates and assumptions are very crude, this transformation only changes the flux of a typical object by a fraction of a magnitude. However, for some CNe with high reddening, the transformation applied can exceed a magnitude. If the reddening is substantially underestimated, the error in the magnitude shift could be as high as a magnitude, making the source appear brighter than it actually was in quiescence.

G_{BP} observations of CNe in quiescence were corrected as

$$g - G_{BP} = -0.318 + 0.932x - 0.932x^2 + 0.507x^3 - 0.107x^4 + 0.007x^5 \tag{2.4}$$

where x = $G_{BP} - G_{RP}$ using a polynomial we fit to sources with colors ranging from $G_{BP} - G_{BP} = 0.6$ to $G_{BP} - G_{BP} = 3.4$ in both *Gaia* and SDSS. This correction is typically a fraction of a magnitude, reaching up to $\sim$1 magnitude for the most highly reddened objects. We assume any differences between the ASAS-SN g filter, the Pan-STARRS g filter, and the SDSS g filter are negligible.

2.6.2 Quiescent Magnitude Measurements

The Pan-STARRS 3π Steradian Survey (Chambers et al., 2016) covers the sky north of declination $\delta = -30^\circ$, and the stacked catalog has a median 5σ depth of $g_{P1} \simeq 23.3$ mag. Quiescent magnitude measurements were made using the g_{P1} passband, as this filter is the most similar to the g-band measurements made by ASAS-SN and avoids the need for any extinction correction to the outburst amplitude.

The Pan-STARRS 3π catalog reaches its full depth and astrometric accuracy by combining 12 exposures taken between 2009 Jun 2 and 2014 Mar 31 (Chambers et al., 2016). This is a potential issue for estimating the quiescent magnitude of DNe, because a substantial fraction of them have multiple outbursts over this time frame. Therefore, it is possible, and in many cases highly probable, that the flux of a DNe listed in the stack or mean catalog is contaminated by outbursts and does not accurately reflect the quiescent brightness of the source. To minimize the possibility of this issue, flux measurements were obtained from the `ForcedWarpMeasurement` table from Pan-STARRS Data Release 2. This table contains single epoch forced photometry measurements at the position of objects detected in the stacked images (Flewelling et al., 2016). For each source, the quiescent magnitude was estimated from the median flux from the faintest 50% of g_{P1} observations. This increases the chance that observations contaminated by outbursts were excluded, and we only measure the quiescent brightness for objects where the median absolute deviation of the apparent magnitude measurements is less than 0.9 mag to avoid estimates that are still likely contaminated.

If no source is present in the Pan-STARRS catalog (details of cross matching in Section 2.6.3), an upper limit was placed on the brightness based on the g_{P1} magnitude corresponding to the 98% completeness of the field obtained from the `StackDetEffMeta` table.

The limiting magnitudes are estimated from the number of fake sources recovered for each skycell in the 3π stacked survey (Munari et al., 2011).

We estimate the quiescent magnitude of the CNe in the same way for those in the observing field of Pan-STARRS. Since the CNe in our sample only outburst once, we are able to supplement the Pan-STARRS photometry with *Gaia* DR2 photometry for CNe that erupted after *Gaia* DR2 observations Gaia Collaboration et al. (2018b), for objects outside of the observing field of Pan-STARRS. Quiescent magnitudes for CNe estimated using *Gaia* were made using the G_{BP} filter, as it is the most similar to ASAS-SN g-band, and transformed to g as describe in §2.6.1.

2.6.3 Astrometry and Catalog Matching

When matching sources from different catalogs, the possibility exists that two different sources with similar sky positions can be mistaken as the same object; this largely depends on the astrometric accuracy of the surveys involved. Yaron et al. (2019b,a) investigated the astrometric accuracy of various surveys, including ASAS-SN, by comparing the positions of objects reported by an individual survey to those independently reported by the *Gaia* Alerts Project[4]. They estimated the positional accuracy of various surveys and found that 95% of discoveries by ASAS-SN have astrometric errors < 3.4 arcseconds. Since many of the objects in our sample are discovered by ASAS-SN, we use a positional offset threshold of four arcseconds when considering matches between the DNe in our sample and objects in Pan-STARRS. This is a generous search radius, as the typical error on the discovery position is $\sim$1 arcsecond (Jayasinghe et al., 2018a). For CNe, we assume the discoveries are followed up at higher angular resolution, and therefore place a stricter bound on the astrometric

[4] `http://gsaweb.ast.cam.ac.uk/alerts/home`

uncertainty of one arcsecond.

We use CN and DN coordinates as listed in the VSX catalog. When transients discovered by ASAS-SN and other surveys are entered into VSX, their positions are updated using *Gaia* DR2 (taking epoch and equinox J2000.0) if there is an object within a fraction of an arcsecond from the reported transient position. If no object exists within ∼1 arcsecond, other optical surveys with similar limits like Pan-STARRS, SDSS (York et al., 2000), and the Guide Star Catalog (GSC2.3; Lasker et al. 2008) are checked for matches within a fraction of an arcsecond. If there are no matches in surveys with reliable astrometry, the position is derived from the discovery report or follow-up astrometry.

For each DN in our sample, we estimate the probability that it is coincident by chance with a different, nearby object in the Pan-STARRS catalog. A positional offset was defined for each source as the angle between the DN's VSX position and the closest object in the Pan-STARRS stack catalog. We then search the Pan-STARRS catalog at random positions on a circle of one degree around the source and compute the frequency of having a Pan-STARRS source closer than the measured positional offset. Only sources that had random matches less than 5% of the time were considered secure matches. The maximum positional offset that results in a secure match is roughly 2 arcseconds.

For CNe, we only consider a Pan-STARRS object within 1 arcsecond of the VSX position to be a secure match. DNe with a Pan-STARRS source within 4 arcseconds and CNe with a source within 2 arcseconds where random matches were found >5% of the time are considered ambiguous matches, and we do not attempt to estimate their outburst amplitudes. If no source exists in the Pan-STARRS catalog within 4 arcseconds for DNe and 2 arcseconds for CNe of the VSX position, we consider the quiescent counterpart definitively not detected in the Pan-STARRS 3π stack catalog, and place an upper limit on the quiescent brightness.

We successfully estimate or place a limit on the quiescent brightness for ∼90% of DNe in the Pan-STARRS observing field.

For CNe south of $\delta = -30$ degrees, we consider *Gaia* DR2 sources within one arcsecond to be secure matches. If no *Gaia* DR2 source appears to be within two arcseconds of the CNe position, we place an upper limit on the brightness of the source. The magnitude that corresponds to 98% completeness in *Gaia* is not currently available and likely spatially variable, but we assume this will roughly be the magnitude that corresponds to a magnitude error of 0.1 mag. We find that this value is on average $G_{BP} \approx 19.7$ mag, and therefore use this as an upper limit on the magnitude for CNe with no *Gaia* DR2 source within two arcseconds. By using Pan-STARRS and *Gaia* observations we are able to measure or place a limit on ∼80% of CN outbursts.

2.6.4 Sensitivity/Contamination

We injected fake transients into our data and attempted to recover them in order to estimate the ranges of peak magnitudes and decline times to which our analysis is sensitive, given the cadence of ASAS-SN. We generated linearly declining (in magnitude versus time) outbursts with peak apparent magnitudes ranging from 18 to 10 mag. and t_2 values ranging from an hour to a year. These outbursts were injected into the ASAS-SN light curves obtained for our CV sample with random outburst epochs. We sampled the mock-outburst evolution with the cadence and sensitivity of observed ASAS-SN light curves. The same analysis that was run on the real CV sample was run on the fake transients, in order to estimate how frequently we could successfully measure or place limits on t_2. The results are shown in Figure 2.9 and are compared to the measured values from our CV sample.

The top panel in Figure 2.9 shows the distributions of real CV decline times as a blue

histogram, and the relative frequency with which fake transient decline times could be estimated (red line). This shows that our analysis is best at detecting transients with $t_2 \approx 30$ days, although we most frequently find DN outbursts that decline by two magnitudes from maximum in roughly 10 days. Also, the sensitivity of our analysis as a function of decline time drops off much more slowly than the distribution of real decline times. Though we are certainly worse at detecting CV outbursts with extremely short decline times, the results are not significantly biased by our analysis and observing cadence.

The bottom panel of Figure 2.9 shows the distribution of peak magnitude versus t_2 for the real DN outbursts (shown in blue) and contours of the probability that the fake transients were recovered (shown in red). Even the brightest and slowest transients are not always recovered successfully, and this is largely due to an outburst happening while Sun constrained. The completeness is not strongly dependent on the peak magnitude of the source unless it is near the limiting magnitude of ASAS-SN.

As discussed in the main text, there is a chance that the quiescent magnitude measured from Pan-STARRS is contaminated by an outburst. To investigate the likelihood for this to occur, we measure the outburst duty cycle, defined as the fraction of time a CV spends in outburst. We estimate this as the number of days the object is detected by ASAS-SN divided by the total number of days the field is observed. Since image subtraction light curves were used to study the DN outbursts in our sample, the assumption that each detection is during an outburst is a safe one, but it can break down when contamination from a nearby bright star occurs. Due to this, we only estimate the duty cycle for objects with no $g < 14$ mag stars within an 8 ASAS-SN pixel (64 arcseconds) radius.

As shown in Figure 2.10, it does appear to be the case that DNe with larger duty cycles have smaller outburst amplitudes. Though this is consistent with the nature of DNe

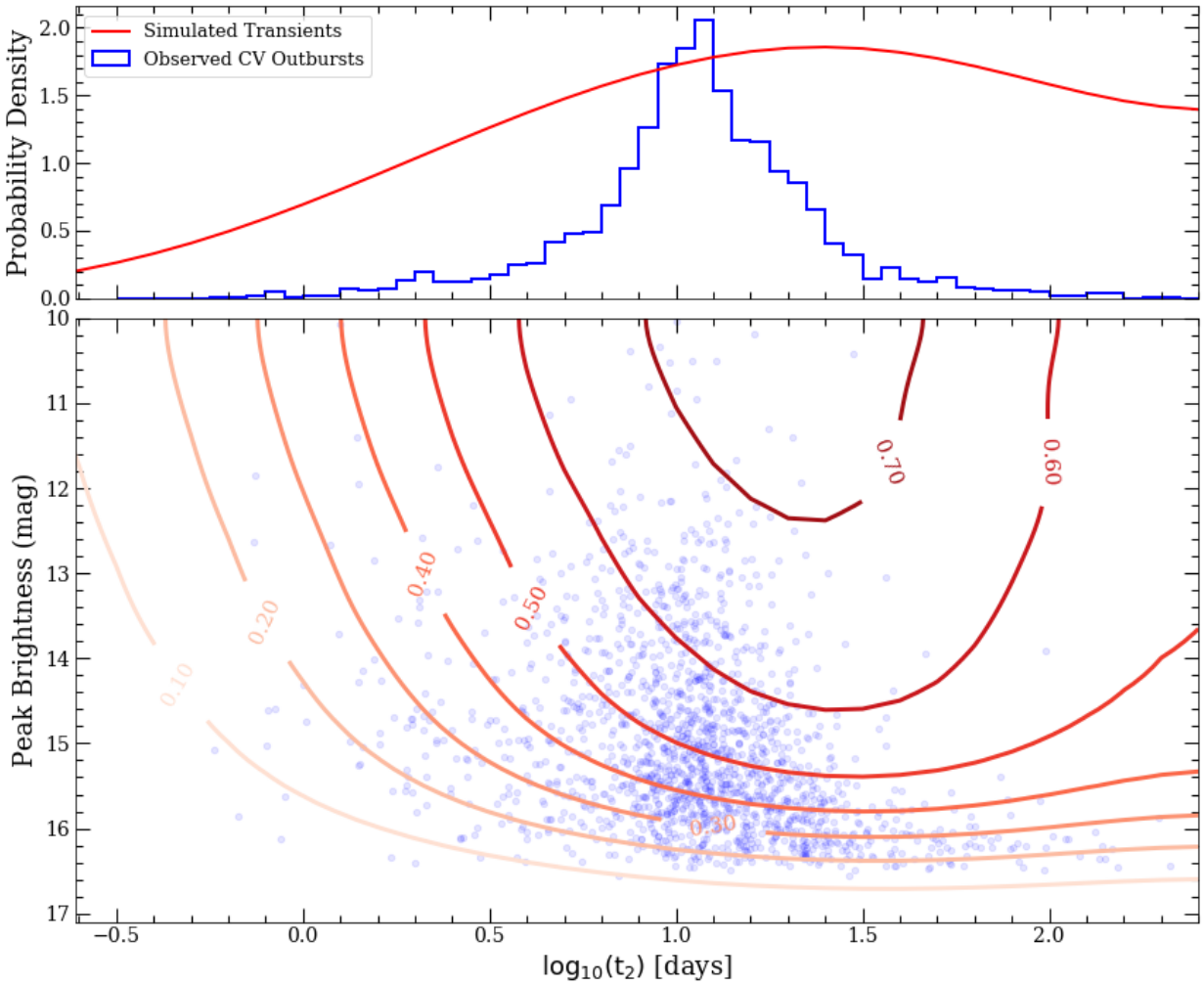

Figure 2.9 Top: Distribution of observed time to decline by two magnitudes for detected DN outbursts in blue and the probability distribution for measuring the decline as a function of t_2 in red. Both distributions are normalized so that the area under the curve is unity, but the red curve is then multiplied by a factor of four for visualization purposes. Bottom: Peak g magnitudes of DN outbursts vs. measurements and limits of the time to decline by two magnitudes from maximum. Real DN outbursts are shown as blue circles. The red contours show the fraction of time the decline time of fake transients could be successfully measured or constrained with an upper limit in our analysis.

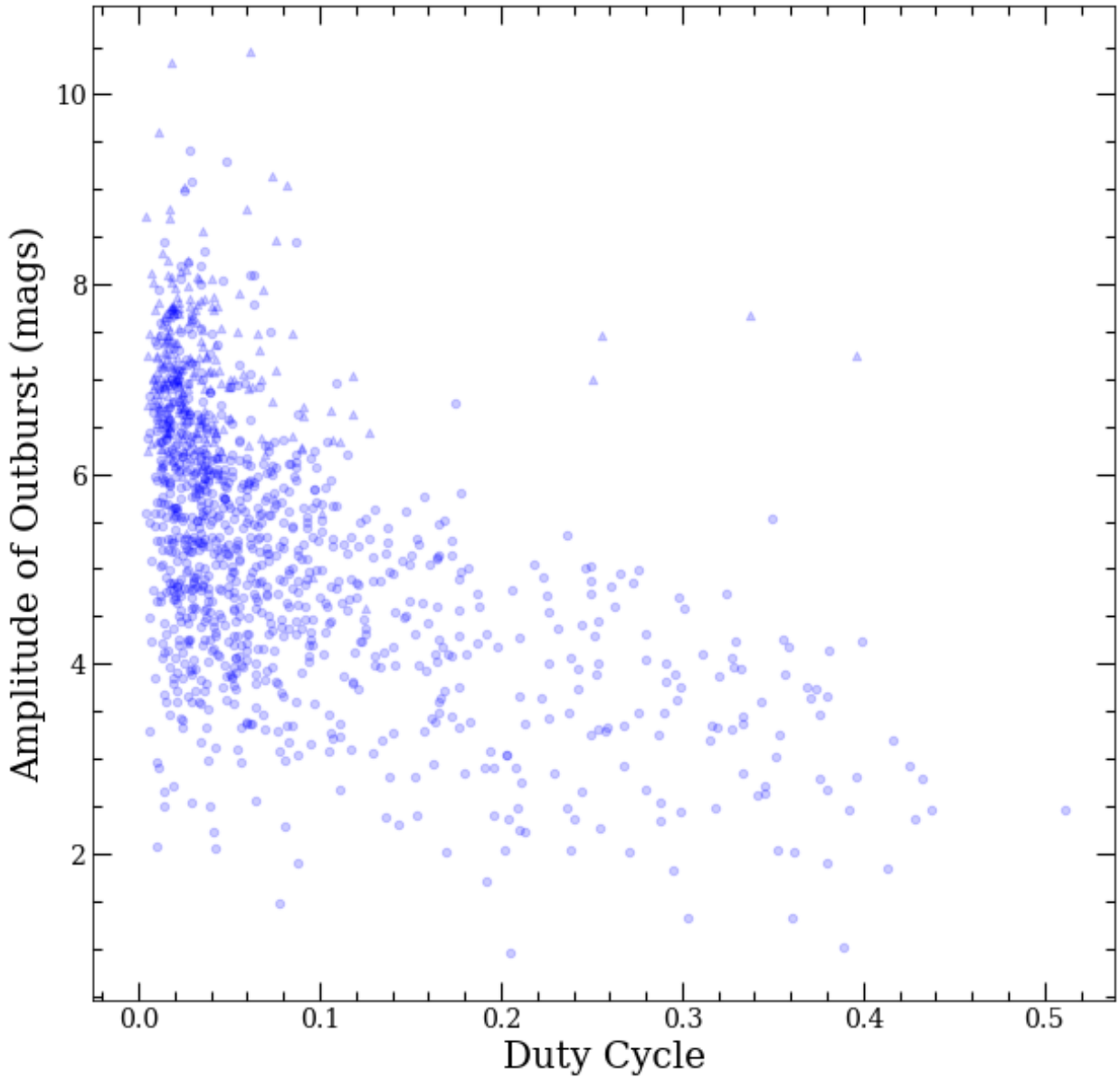

Figure 2.10 Outburst amplitude for the dwarf novae as a function of duty cycle.

(Coppejans et al., 2016), our analysis may significantly underestimate the outburst amplitude for an object with a high duty cycle. Objects that spend more time in outburst have a higher probability of being observed by Pan-STARRS in outburst, and thus will result in an underestimate in the outburst amplitude estimated in this work. This should not significantly alter the distribution of the outburst amplitude, but we encourage the use of caution when quoting the outburst amplitude of an individual object,

Contamination in the ASAS-SN light curve from a nearby, bright star could result in a false positive of a DN outburst. Careful inspection and flagging of the light curves was performed to mitigate these artifacts, though the possibility still remains.

2.6.5 Classical and Reccurent Nova Outburst Properties

Here, we provide the outburst properties of the classical novae and recurrent novae in our sample in Table 2.3. This table is available electronically in a machine readable format. The data used to measure these properties for four classical novae are shown as light curves in Figure 2.11.

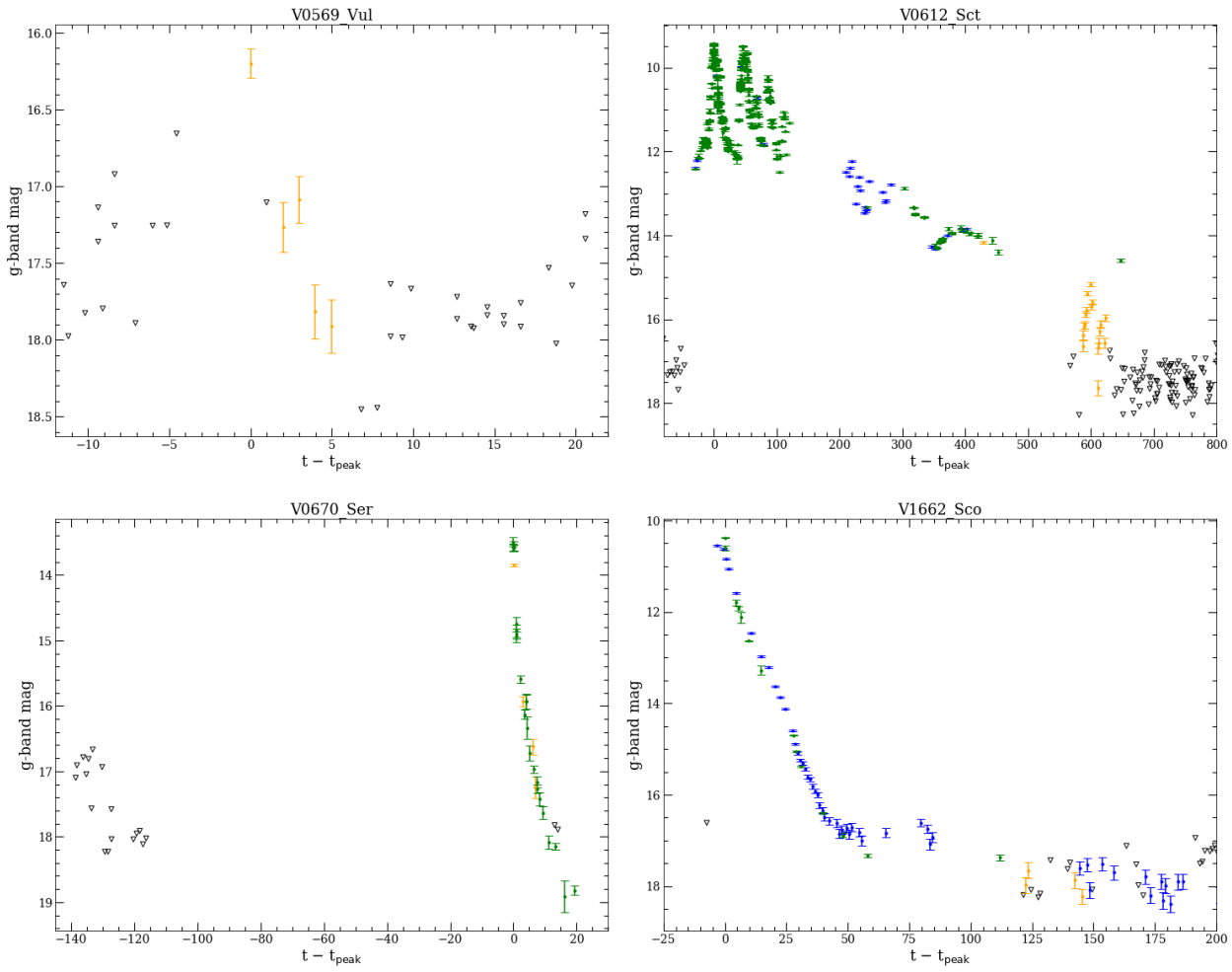

Figure 2.11 Light curves of four classical novae analyzed in this work. The ≥5-sigma detections for ASAS-SN g-band, ASAS-SN V-band and AAVSO V-band observations are shown in orange, blue, and green respectively after converting to brightness in g-band. The black triangles denote 5-sigma upper limits from non-detections These show examples of faint outbursts (top left), flares causing multiple peaks (top right), outbursts during solar conjunction (bottom left), and smooth declines (bottom right).

Table 2.3. Outburst Properties of Classical and Recurrent Novae

Name	RAJ2000 h m s	DEJ2000 ° ′ ″	Peak mag	Amp. mag	Amp. Flag boolean	t_2 days
V0392 Per	4:43:21.37	47:21:25.9	7.0	10.5	1	3.0
V0339 Del	20:23:30.68	20:46:03.8	4.6	13.2	1	11.8
V2659 Cyg	20:21:42.32	31:03:29.4	9.9	11.7	1	115.5
V0569 Vul	19:52:08.25	27:42:20.9	16.2	6.0	0	6.0
V0962 Cep	20:54:23.75	60:17:06.9	11.6	11.1	0	32.5
V0435 CMa	7:13:45.84	−21:12:31.3	10.4	11.5	1	53.4
V2860 Ori	6:09:57.45	12:12:25.2	10.6	9.6	1	9.4
V5668 Sgr	18:36:56.83	−28:55:40.0	4.4	11.9	1	75.3
V5855 Sgr	18:10:28.29	−27:29:59.3	8.4	11.9	1	12.7
V5856 Sgr	18:20:52.25	−28:22:12.1	6.5	14.4	1	7.2
V1707 Sco	17:37:09.54	−35:10:23.2	12.9	6.8	1	4.5
V1659 Sco	17:42:57.68	−33:25:42.9	13.6	6.1	1	22.0
V3661 Oph	17:35:50.41	−29:34:23.8	12.3	7.9	0	3.8
V5669 Sgr	18:03:32.77	−28:16:05.3	9.5	9.5	1	33.6
V5853 Sgr	18:01:07.78	−26:31:43.4	12.9	8.2	1	36.7
V5667 Sgr	18:14:25.15	−25:54:34.7	10.0	10.0	1	54.5
V3662 Oph	17:39:46.10	−24:57:55.8	14.7	7.6	0	43.7
V3890 Sgr	18:30:43.29	−24:01:08.9	8.1	12.9	1	4.1
V5666 Sgr	18:25:08.76	−22:36:02.6	10.1	8.6	1	12.7
V0612 Sct	18:31:45.86	−14:18:55.5	9.4	10.6	1	13.9
V0613 Sct	18:29:22.93	−14:30:44.2	11.6	9.5	0	36.8

Table 2.3 (cont'd)

Name	RAJ2000 h m s	DEJ2000 ° ′ ″	Peak mag	Amp. mag	Amp. Flag boolean	t_2 days
V3665 Oph	17:14:02.53	−28:49:23.3	10.0	11.6	0	34.8
V3666 Oph	17:42:24.11	−20:53:08.6	9.4	12.7	0	21.6
V2944 Oph	17:29:13.42	−18:46:13.8	9.6	10.4	1	16.2
V5857 Sgr	18:04:09.45	−18:03:55.8	11.7	10.6	0	16.9
V0670 Ser	18:10:42.29	−15:34:18.0	13.5	8.7	0	118.3[a]
V0659 Sct	18:39:59.70	−10:25:41.9	8.9	13.0	0	7.6
V1830 Aql	19:02:33.38	3:15:19.0	16.8	5.8	0	20.6
V1831 Aql	19:21:50.15	15:09:24.8	15.8	7.0	0	17.8
V0906 Car	10:36:15.42	−59:35:53.7	6.5	13.1	1	43.7
V0549 Vel	8:50:29.62	−47:45:28.3	9.7	8.2	1	90.1
FM Cir	13:53:27.59	−67:25:00.9	6.7	10.6	1	82.3
V1405 Cen	13:20:55.35	−63:42:19.1	11.3	8.2	1	108.4
V1655 Sco	17:38:19.31	−37:25:08.7	12.0	8.0	1	28.9
V1662 Sco	16:48:49.62	−44:57:03.2	10.4	9.3	1	8.1
V1657 Sco	16:52:18.87	−37:54:18.9	13.3	6.4	1	38.7
V1656 Sco	17:22:51.46	−31:58:37.1	12.0	7.7	1	9.0
V1661 Sco	17:18:06.37	−32:04:27.7	11.3	8.4	1	10.7
V0408 Lup	15:38:43.86	−47:44:42.1	10.4	9.7	1	59.4
V0407 Lup	15:29:01.79	−44:49:39.5	7.4	12.3	1	5.5

[a]The eruption likely occurred during solar constraint and $t_{2,up}$ is the time from before solar constraint to once the light curve dropped below the apparent two magnitude threshold.

Note. — Names, positions, peak apparent brightness, amplitude of outburst, and time it takes to decline to decline two magnitudes from maximum brightness of classical and recurrent novae in our sample. The Amp. Flag column equals one when we are able to make a measurement of the outburst amplitude and zero when we are able to place a lower limit. The t_2 Flag column equals one when were are able to detect the object below the two magnitude threshold and is zero when there is only a non-detection below this threshold or when the eruption appeared to occur during solar constraint. The $t_{2,low}$ column gives the time until last detection brighter than the two magnitude threshold and the $t_{2,up}$ column gives the time until the first detection or non-detection fainter this threshold. These last two columns are lower and upper limits on t_2, respectively.

Chapter 3

Galactic Extinction: How Many Novae Does it Hide and How Does it Affect the Galactic Nova Rate?

Abstract

There is a longstanding discrepancy between the observed Galactic classical nova rate of ~ 10 yr^{-1} and the predicted rate from Galactic models of ~ 30–50 yr^{-1}. One explanation for this discrepancy is that many novae are hidden by interstellar extinction, but the degree to which dust can obscure novae is poorly constrained. We use newly available all-sky three-dimensional dust maps to compare the brightness and spatial distribution of known novae to that predicted from relatively simple models in which novae trace Galactic stellar mass. We find that only half (53%) of novae are expected to be easily detectable ($g \lesssim 15$) with current all-sky optical surveys such as the All-Sky Automated Survey for Supernovae (ASAS-SN). This fraction is much lower than previously estimated, showing that dust does substantially affect nova detection in the optical. By comparing complementary survey results from the ASAS-SN, OGLE-IV, and the Palomar Gattini IR surveys using our modeling, we find a tentative Galactic nova rate of ~ 30 yr^{-1}, though this could be as high as ~ 40 yr^{-1}

depending on the assumed distribution of novae within the Galaxy. These preliminary estimates will be improved in future work through more sophisticated modeling of nova detection in ASAS-SN and other surveys.

3.1 Introduction

A classical nova occurs in an interacting binary system with a white dwarf primary, referred to as cataclysmic variable (CV; see Warner 1995). The white dwarf accretes material from the secondary, usually a low-mass main sequence star, until a critical pressure and temperature are reached, leading to a thermonuclear runaway at the bottom of the hydrogen-rich shell accreted by the white dwarf (see Bode & Evans 2008 for a review). Expulsion of the accreted envelope occurs, causing the system to brighten significantly, by 5 to >19 mag (Kawash et al., 2021b). Studies of classical novae in M31 have constrained the peak luminosities to range from $M_V \approx -4$ to -10 mag (Shafter, 2017).

Historically, amateur astronomers have been the driving force in finding classical novae, with discoveries dating back thousands of years (Patterson et al., 2013; Shara et al., 2017b). Novae began to be more systematically discovered in the mid 20th century, when on average ∼3 per year were visually discovered. When film photography became commonly used in the 1980s and 1990s, there were ∼4 discovered novae per year and then ∼8 per year in the 2000s and 2010s when digital cameras became widely available. Then, in 2017, the All-Sky Automated Survey for SuperNovae (ASAS-SN) became the first survey to systematically observe the entire night sky with nearly daily cadence down to $g \approx 18.5$ mag (Shappee et al., 2014), significantly deeper than most amateur observations. Since 2017, there have been roughly 10 classical novae discovered per year on average.

The first prediction for the total frequency of Galactic nova eruptions was by Lundmark (1935), who estimated there should be about 50 novae per year (see Della Valle & Izzo 2020 for a review of Galactic nova rate predictions). Estimates from the early 1990s predicted much lower rates ranging from 11 to 20 per year, derived from observations of other galaxies (Ciardullo et al., 1990; van den Bergh, 1991a; della Valle & Livio, 1994a). More recent surveys of M31 have increased these predictions for the Milky Way rate to 34^{+15}_{-12} yr^{-1} (Darnley et al., 2006) and as high as ~ 50 to ~ 70 yr^{-1} when accounting for incompleteness for faint and fast novae (Shafter, 2017). Recent work modeling novae in our Galaxy predict rates of 50^{+31}_{-23} yr^{-1} from a sample of bright novae (Shafter, 2017) and $43.7^{+19.5}_{-8.7}$ yr^{-1} from a sample of novae detected in IR observations (De et al., 2021). If these recent, higher estimates are correct, novae could be key contributors to various isotopes present in the Galaxy (José et al., 2006) like ^{26}Al (José & Hernanz, 1998; Bennett et al., 2013) and ^{7}Li (Starrfield et al., 1978b; Hernanz et al., 1996), but there must be a reason the majority of novae go undetected.

So, what is the cause of the discrepancy between the predicted and the observed rate? One idea put forward is that the majority of observable classical nova events go undetected due to insufficient sky coverage of observations. However, the emergence of large sky surveys, including ASAS-SN, should solve this issue. The most common Galactic transient ASAS-SN discovers is a dwarf nova outburst, and Kawash et al. (2021b) explored the possibility that some classical novae were being mistaken for dwarf novae. Though it is possible a small number of novae can be mis-classified, there are too few to significantly alter the discovery rate of classical novae.

Another possibility is that interstellar dust obscures a majority of classical novae that erupt in the Galaxy. This prospect is supported by the recently discovered sample of highly

reddened, and optically missed, novae discovered by the Palomar Gattini IR-survey (PGIR; De et al. 2020b; De et al. 2021). These results suggest that dust could cause a substantial fraction of Galactic nova events to go undetected by optical observations, but how many remains an open question.

Shafter (2017) used an exponential disk to model extinction in the Galaxy, with 1 mag of extinction per kpc in the mid-plane in V-band. This predicts that over 90% of all Galactic novae should get brighter than $V = 18$ mag, inconsistent with the results of De et al. (2021). The primary goal of this work is to investigate how utilizing a more robust Galactic extinction model changes these conclusions, and the availability of three-dimensional Galactic extinction maps now make it possible to explore this exact question.

Recent large photometric surveys combined with models of stellar spectral energy distributions have resulted in several three dimensional extinction models of the Galaxy. Green et al. (2019) used a combination of *Gaia*, Pan-STARRS, and 2MASS observations to model the extinction north of $\delta = -30°$, and Marshall et al. (2006) used 2MASS data to model extinction in the inner Galactic plane. Neither of these maps cover the entire sky, but Bovy et al. (2016) combined these maps along with analytic models from Drimmel et al. (2003) to build an all-sky three dimensional model of extinction in the Galaxy.

The Green et al. (2019) 3D dust map was used in De et al. (2021) to build a model of Galactic novae in the PGIR field of view ($\delta > -28.9°$). This model was then compared to the PGIR sample of novae discovered at J band and optically discovered novae. De et al. (2021) found that the amount of extinction predicted by the model was much more consistent with PGIR sample of novae, implying that IR observations are sensitive to a significant fraction of novae that optical observations are not, but this analysis did not cover a large portion of the bulge and inner disk. Here, we extrapolate to the entire sky using the Bovy et al. (2016)

all-sky dust map to build upon these recent findings.

The goal of this work is to model the distribution of novae and dust within the Galaxy, and explore how that combination affects how bright novae are when observed in the optical. In Section 3.2, we discuss the implementation and assumptions of the model, including the resulting apparent magnitude distribution of novae, how many optically missed novae we should expect, and where to find them with IR observations or optical observations in redder bands. Then in Section 3.3, we use our model along with observational constraints from various surveys to estimate the global frequency of nova eruptions in the Galaxy. Lastly, in Section 3.4, we explore how sensitive our results are to our model assumptions.

3.2 Nova Model/Results

Here we discuss the components and assumptions that go into our Galactic nova model, the resulting Galactic apparent magnitude distribution of novae, and the spatial distribution of optically observable versus unobservable novae.

3.2.1 Stellar Density Profile

To analyze the effects of extinction on novae, we first must assume some distribution of novae within the Galaxy. For our primary model, we simply assume that the distribution of novae follows the distribution of stellar mass, but in Section 3.4.3 we also consider additional models with a higher rate of nova production per unit mass in the bulge (as compared with the disk). The stellar mass distribution is inferred by implementing a version of the Besançon Galactic mass model with a two component bulge from Simion et al. (2017) and a thin disk, thick disk, and a halo component from Robin et al. (2003). An explanation of the stellar

density model, including the model parameters assumed can be found in Section 3.6.1. The distribution of mass is calculated on a three-dimensional Cartesian grid with size (x,y,z) = (30,30,30) kpc and a resolution of 0.1 kpc. The total mass of each component is calculated and shown in Table 3.6.1. In Section 3.4.2, we also distribute novae based on the Contracted Halo version of the mass profile presented in Cautun et al. (2020) to investigate how our results depend on the assumed distribution of novae, and this does slightly affect the resulting apparent magnitude distribution.

3.2.2 Extinction Model

To date, there is no single three-dimensional dust map that models Galactic extinction across the entire sky. However, the maps of Green et al. (2015), Marshall et al. (2006), and Drimmel et al. (2003) were combined and made publicly available at `http://github.com/jobovy/mwdust` to provide a stitched together map over the entire sky (Bovy et al., 2016). This model, hereafter referred to as `mwdust`, can use several different map combinations, and here we use the `combined19` version. This uses the updated map of the sky north of declination $\delta = -30^\circ$ from Green et al. (2019), the Marshall et al. (2006) maps covering the sky around the Galactic center $-100^\circ \leq l \leq 100^\circ$ and $-10^\circ \leq b \leq 10^\circ$, and the Drimmel et al. (2003) map for the rest of the sky not covered by the first two. The Marshall et al. (2006) map takes precedence over the Green et al. (2019) map where they overlap, because the former relies more heavily on near-infrared data it is able to model extinction out to larger distances at low latitude. A detailed explanation of the default model can be found in the Appendix of Bovy et al. (2016).

`mwdust` can estimate the extinction in a wide array of observing bands by assuming an extinction law with $A_V/A_{K_s} = 8.65$. However, Nataf et al. (2016) argue that toward the

inner Galaxy the extinction law varies, and they find a median value of $A_V/A_{K_s} = 13.44$, 55% larger than the default `mwdust` value. This roughly corresponds to a 25% increase in the extinction in the ASAS-SN g-band filter, A_g, so we also explore how our results change from this steeper extinction curve. This change introduces additional systematic uncertainties in the model, because extinction in the various maps that make up `mwdust` are measured in different filters and with different techniques. In addition, not all novae in our model are in the inner Galaxy. Nonetheless, this alternate model roughly captures the effects of a different Galactic extinction curve on our ability to find novae.

3.2.3 Positions and Distances

We ran Monte Carlo simulations of 1000 Galactic novae by probabilistically distributing them following the stellar mass of the Besançon Galactic model from Robin et al. (2003). The resulting distribution of novae in Galactic cylindrical coordinates for the primary model and a secondary stellar density model from Cautun et al. (2020) are shown in Figure 3.1. In Figure 3.2, these positions are transformed to sky coordinates in the reference frame of the Sun at $R_\odot = 8.122$ kpc (Gravity Collaboration et al., 2018; Cautun et al., 2020) in the top panel, and a face-on view of the Galaxy is shown in the bottom panel. As expected, novae hug the disk plane, and there is a large increase in density toward the Galactic center.

The distances to Galactic novae are often hard to constrain even with *Gaia* parallaxes (Schaefer, 2018). Figure 3.3 shows the expected distribution of distances based on our primary model. We expect the median distance to a nova to be 8.7 kpc, 68% of novae to have distances between 6 and 13 kpc, and 95% of novae are expected to be within 16 kpc of the Sun. Also shown in Figure 3.3 is the distribution of distances from a magnitude limited sample of novae that we expect to more closely resemble the sample of optically

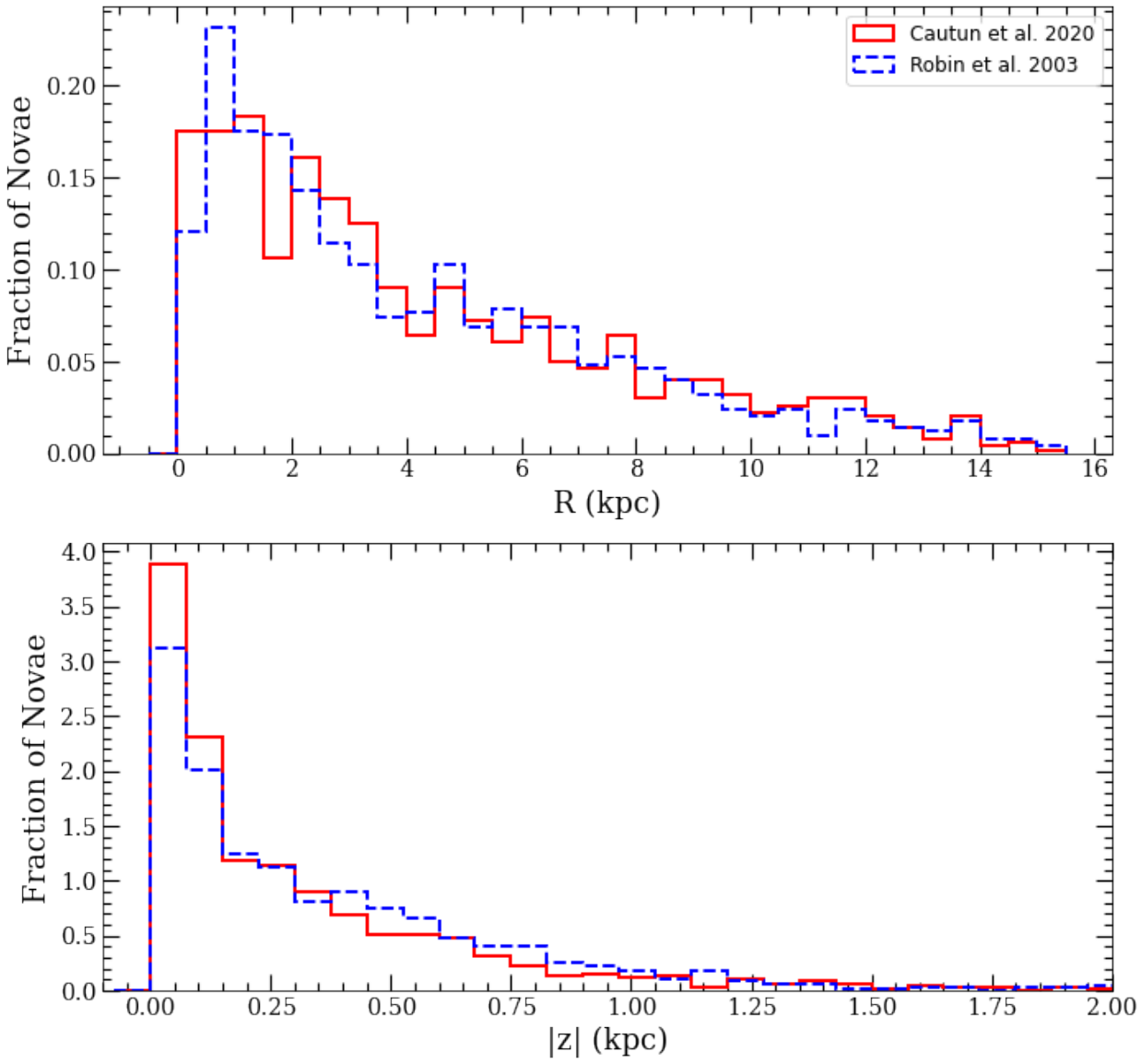

Figure 3.1 Distributions of Galactic positions in cylindrical radii (top) and height above the disk (bottom) for 1000 randomly sample novae distributed by randomly sampling from the Robin et al. (2003) shown as the blue dashed line and from the Cautun et al. (2020) model shown as the red solid line.

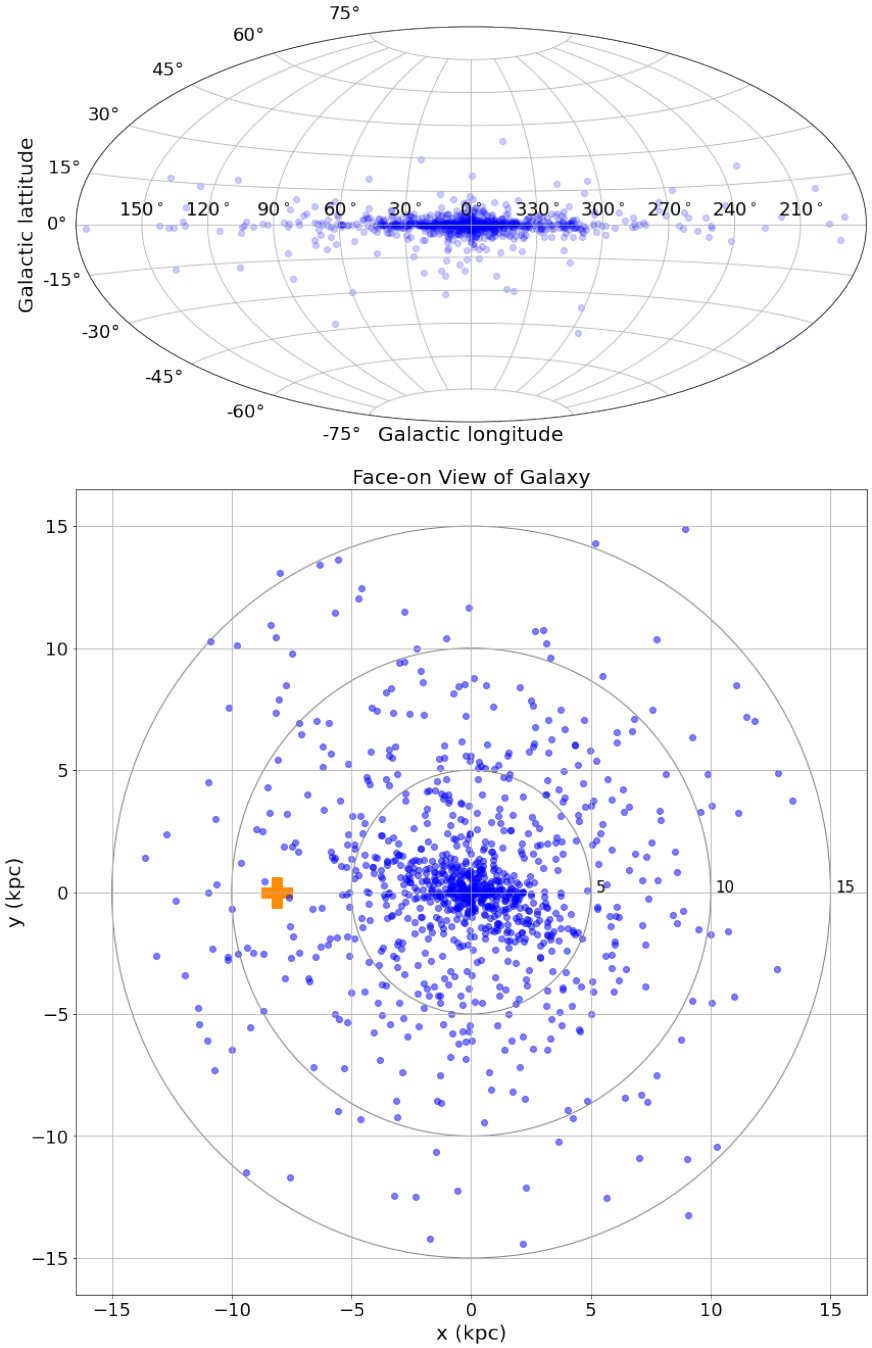

Figure 3.2 Top: positions of N = 1000 simulated novae in Galactic coordinates, distributed by randomly sampling the Robin et al. (2003) stellar density model. Bottom: same as top but in an external face-on view of our Galaxy. Novae are plotted in blue, and the position of the Sun is as an orange cross.

discovered novae. The median distance of this distribution is 7.9 kpc, very similar to the global population, and we expect 95% of this magnitude limited sample to be within 13 kpc. Overall, the distribution of distances for a magnitude limited sample is not significantly different than the global population, suggesting that distance alone is not the determining factor for missed novae.

3.2.4 Brightness Distribution

The peak absolute magnitude of each nova is randomly sampled from a normal distribution with a mean and standard deviation of $\mu = -7.2$ mag and $\sigma = 0.8$ mag, respectively (Shafter, 2017). This distribution was derived for M31 novae in the V-band, and we assume there is no magnitude difference between this and Milky Way novae at g-band peak (van den Bergh & Younger, 1987a; Miroshnichenko, 1988; Hachisu & Kato, 2014). In deriving Galactic nova rates, both Shafter (2017) and De et al. (2021) explored altering the luminosity function for the bulge and disk novae together and separately. We only assume the above luminosity function for all of the novae in our model, as De et al. (2021) found it was not a significant factor for their results; however, we plan to investigate the effects of the luminosity function in Kawash et al. 2022 (in preparation). After a Galactic position was randomly assigned to the nova, the accompanying extinction for that line of sight and distance was estimated using the `mwdust` package. These values were combined with the distance and randomly assigned absolute magnitude to estimate the peak apparent magnitude for each nova.

The cumulative distribution of peak apparent magnitudes of Galactic novae is shown in blue and red for an assumed extinction curve of $A_V/A_{K_s} = 8.65$ and 13.44, respectively in Figure 3.4, and compared to a distribution excluding dust and a distribution implementing the disk extinction model of Shafter (2017). It is clear that the disk model of extinction

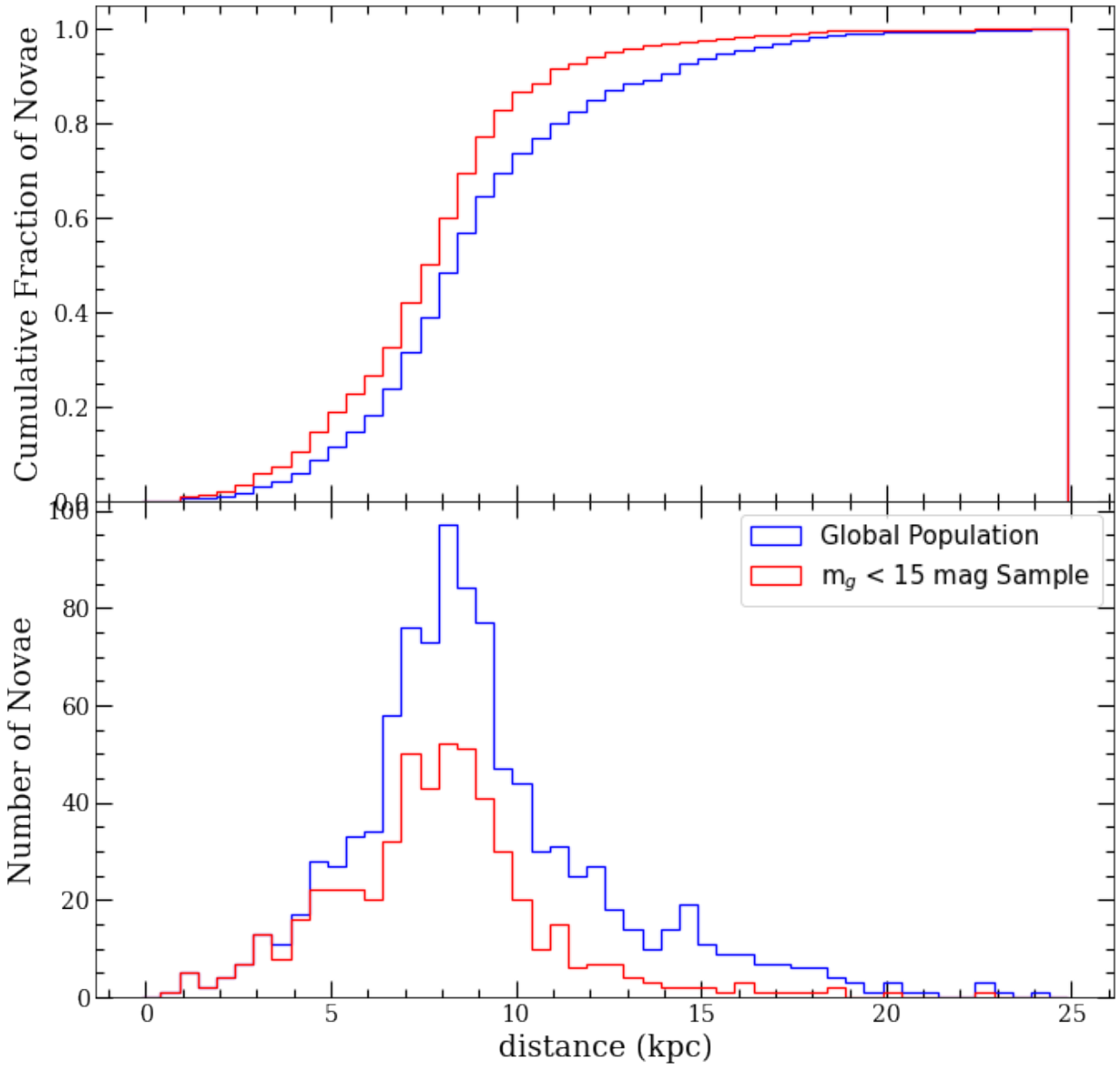

Figure 3.3 Distribution of distances from the Sun for N = 1000 simulated novae. The top panel shows a cumulative distribution, and the bottom panel is a normalized histogram.

utilized in Shafter (2017) vastly underestimates the effects of dust relative to the estimates from three-dimensional dust maps. Specifically, the extinction from the three-dimensional dust maps predicts that only 53%, to as low as 46% for the steeper extinction curve, of novae in the Galaxy will get brighter than $g = 15$ mag, while Shafter (2017) predicted that 82% of novae will be brighter than $g = 15$ mag. This could explain why ASAS-SN observations have not resulted in a significant increase in the nova discovery rate, and it is consistent with the scenario that a large fraction of nova eruptions are too faint to be detected in blue optical bands but are detectable in the IR, like the recently discovered PGIR sample (De et al., 2021). Also, this likely means the deeper observations of the Vera C. Rubin Observatory Legacy Survey of Space and Time (LSST; Tyson 2002) will discover many more Galactic novae than previously thought if the bulge and plane are observed at a moderate cadence. Also shown in Figure 3.4 is the distribution of peak apparent magnitudes for nova discovered since the year 2000. As expected, observations are heavily biased towards detection of the brightest novae, so most faint, and highly extinguished, novae are undetectable by optical observations.

The accuracy of this model distribution relies heavily on the ability of the 3D dust maps to estimate high extinctions at low latitudes out to large distances. A majority of the novae (94%) are in the area of the sky that the Marshall et al. (2006) map covers, and for regions at high column densities, this map only has information out to $\sim$7 kiloparsecs. Only 5% of novae fall within the Green et al. (2019) region, and this model only extends to a few kiloparsecs. The remaining few novae lie in the Drimmel et al. (2003) region, where the analytic model extends out to a galactocentric radius of $R = 15$ kpc, or the entire size of the grid. So, a large fraction of the novae in our model could have underestimated extinction values, but we suspect this is only for the severely extinguished novae, and thus they are

already unobservable in the optical but not necessarily in the IR. For example, in the inner Galactic plane ($|l| < 30^\circ$ and $|b| < 2^\circ$) out to 7 kpc the `mwdust` map predicts on average $A_g \sim 10$ mags of extinction in the g-band but only $A_J \sim 2$ mags of extinction in the J-band. So, a nova with a luminosity of $M = -7.2$ mag would peak at $m_g = 17$ mag in the ASAS-SN g-band filter but as bright as bright as $m_J = 9$ mag in the PGIR J-band filter Therefore, we do not expect that our prediction that only 46% to 53% of novae in the Galaxy get brighter than $g = 15$ mag would change if the extinction model was complete for the entire Galaxy, although it would change predictions for IR surveys and observations carried out in redder bands.

3.2.5 Reddened Novae

Figure 3.5 shows the positions of our model novae in Galactic coordinates around the Galactic center, distinguished by whether the peak apparent magnitude reached $g = 15$ mag. As expected, almost all of the heavily obscured, and therefore faint, novae lie within a couple degrees of the Galactic plane. This implies that optical observations will struggle to discover novae in regions within a couple degrees of the plane and especially towards the Galactic center.

To explore how our model predictions compare to the known sample of optically discovered novae, we have compiled a list of known novae by combining the sources from the CBAT list of novae in the Milky Way[1] and Koji's List of Recent Galactic Novae[2]. The CBAT list consists of objects from 1612 to 2010, and we only include objects with eruptions after 1900. A literature search was then performed on the entire list to investigate if any contaminating

[1] `http://www.cbat.eps.harvard.edu/nova_list.html`

[2] `https://asd.gsfc.nasa.gov/Koji.Mukai/novae/novae.html`

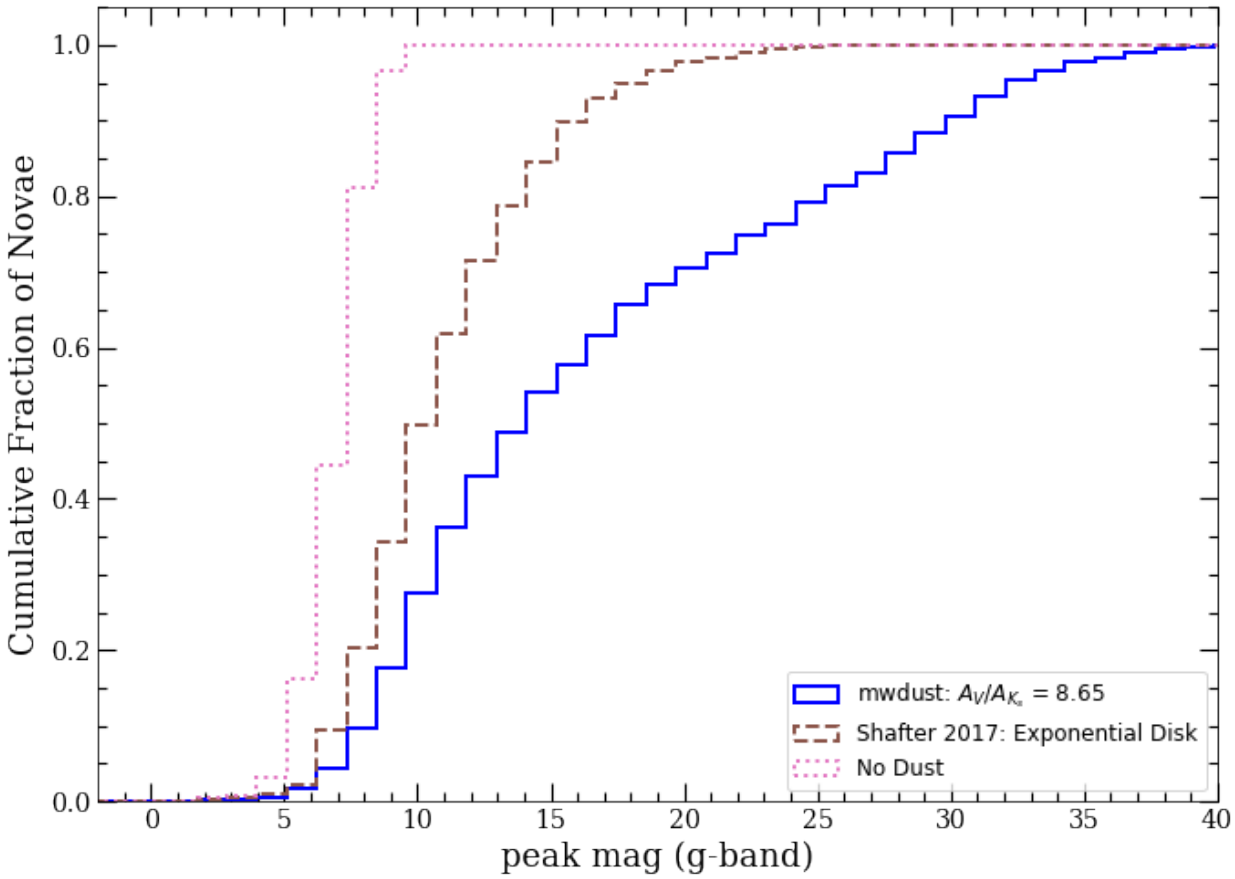

Figure 3.4 Cumulative distributions of peak apparent magnitudes of N = 1000 simulated novae compared to the distribution of observed novae discovered since 2000 (orange dash dotted line)

. Note: this observed distribution of peak brightness is measured in various observing bands and no color correction has been made. Four models are shown: one that includes no dust (pink dotted line), one with an exponential disk as implemented in Shafter (2017) (brown dashed line), and the `mwdust` model using the default reddening law (blue solid line) and a higher value of $A_V/A_{K_s} = 13.44$ (red dotted line). The different models yield significantly different distributions, highlighting the importance of accurately modeling dust to estimate the nova rate.

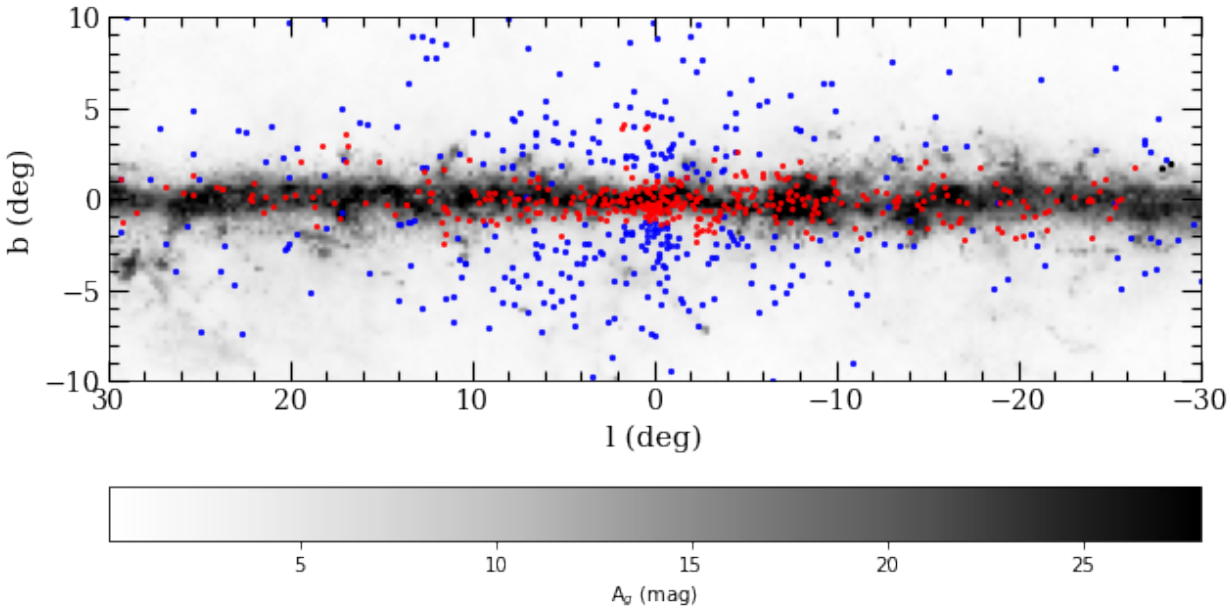

Figure 3.5 Galactic coordinate positions of N = 1000 simulated novae around the Galactic center. The blue points indicate novae that reach a peak brightness of g = 15 mag or brighter, and would likely be discovered by optical observations. The red points indicate novae that never reach g = 15 mag and have a much lower chance to be discovered by optical observations. The amount of extinction integrated out to 15 kpc from the `mwdust` model is shown as a grey scale color map. The resolution of the map is 0.25 degrees with a maximum extinction value of 28 mag for visualization purposes.

sources were present and how many objects have been spectroscopically confirmed as novae. We found that 10 objects from the CBAT list are not classical novae and removed them from our list. 351 of the objects have spectroscopic or photometric observations suggesting they are indeed classical novae, but we found no information about the remaining 47 objects. We assume that these objects are classical novae, but the possibility of contamination by other sources still remains.

Figure 3.6 shows the positions of optically discovered novae from our list in Galactic coordinates towards the Galactic center. Consistent with predictions from our model, there appears to be a significant lack of novae near the Galactic plane where most of the obscuring dust resides ($|b| \lesssim 2^\circ$). However, there also appears to be a bias against discovery of novae at lower declination. This is likely due to a historic lack of observations in the Southern Hemisphere, although this issue has been recently addressed by ASAS-SN's Southern Hemisphere facilities and increasing numbers of amateur observers in Australia and Brazil (e.g., the Brazilian Transient Search, BraTS).

Also shown in Figure 3.6 are nova candidates discovered by The Vista Variables in the Via Lactea (VVV; Minniti et al. 2010) and the Optical Gravitational Lensing Experiment (OGLE; Udalski et al. 2015a). The VVV deep near-IR observations and the OGLE I-band observations of the Galactic bulge and nearby disk are better suited than most optical observations to discover novae in dustier fields at low Galactic latitudes, although the cadence of OGLE observations is much lower in high extinction regions at low lattitude (Udalski et al., 2015b). The 20 candidates from VVV (Saito et al., 2012, 2013a; Beamin et al., 2013; Saito et al., 2013b, 2014; Montenegro et al., 2015; Saito et al., 2015; Contreras Pena et al., 2016; Gutierrez et al., 2016; Saito et al., 2016, 2017) and 19 from OGLE (Kozlowski et al., 2012; Wyrzykowski et al., 2014a,b; Mroz & Udalski, 2014, 2016) were either discovered in the

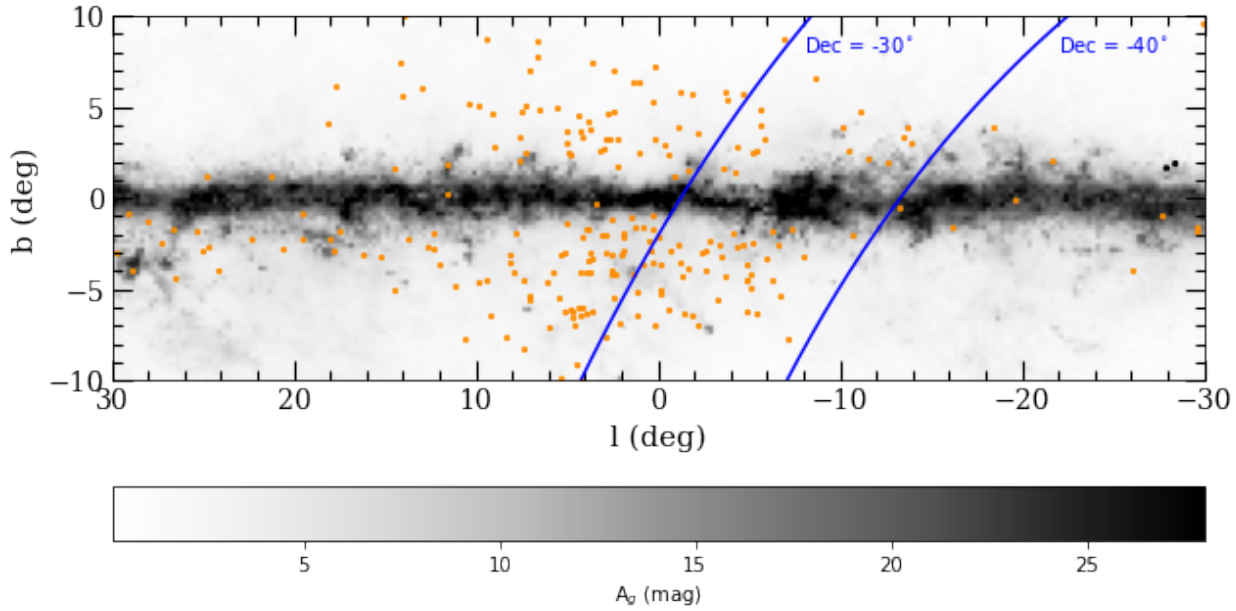

Figure 3.6 Positions of known, optically discovered novae in Galactic coordinates around the Galactic center as orange dots. Nova candidates reported by VVV and OGLE observations are shown as red stars. VVV and OGLE should be better suited for finding reddened novae in the plane than bluer optical observations, but OGLE has a lower cadence in these highest extinction regions. The dust map is the same as Figure 3.5. Lines of constant declination are shown in blue to highlight the lack of optically discovered novae at the most southern declinations.

data after eruption or were not followed up spectroscopically. Many are likely classical nova eruptions, though the sample could be contaminated by a few dwarf novae and young stellar objects. As seen in Figure 3.6, it does appear to be the case that there are more VVV and OGLE nova candidates closer to the plane, but there are still regions where few to no novae or nova candidates have been discovered.

For example, there has never been a nova or nova candidate discovered in the 20 $\deg^2$ patch of sky with a Galactic longitude and latitude of $-10^\circ < l < 0^\circ$ and $-1^\circ < b < 1^\circ$, respectively. Our model predicts that $\sim 10\%$ of Galactic novae should be in this region, but the average extinction for this region is $A_g = 23$ according to the Marshall et al. (2006) dust map. This is a region that OGLE observed less frequently than other bulge fields (Udalski et al., 2015b), but ASAS-SN has observed this region at a high cadence.

The absence of novae at low Galactic latitude is perhaps shown more clearly in Figure 3.7, which compares the Galactic latitude distribution of simulated novae with known optically discovered novae. Our model predicts that $\sim 60\%$ of novae erupt within $|b| < 2^\circ$; however, only $\sim 20\%$ of the optically discovered sample resides within this region. Also shown in Figure 3.7 is the distribution of a model magnitude-limited ($g < 15$ mag) sample of novae. This distribution peaks at a Galactic latitude of 2 degrees, similar to the observed distribution, consistent with a historic magnitude-limited sample with dust as the determining factor.

3.3 Global Nova Rate Estimates

Next, we discuss how our nova model, described in Section 3.2, can be used to explore what fraction of simulated novae would be observable for various surveys and what that implies for the global Galactic nova rate.

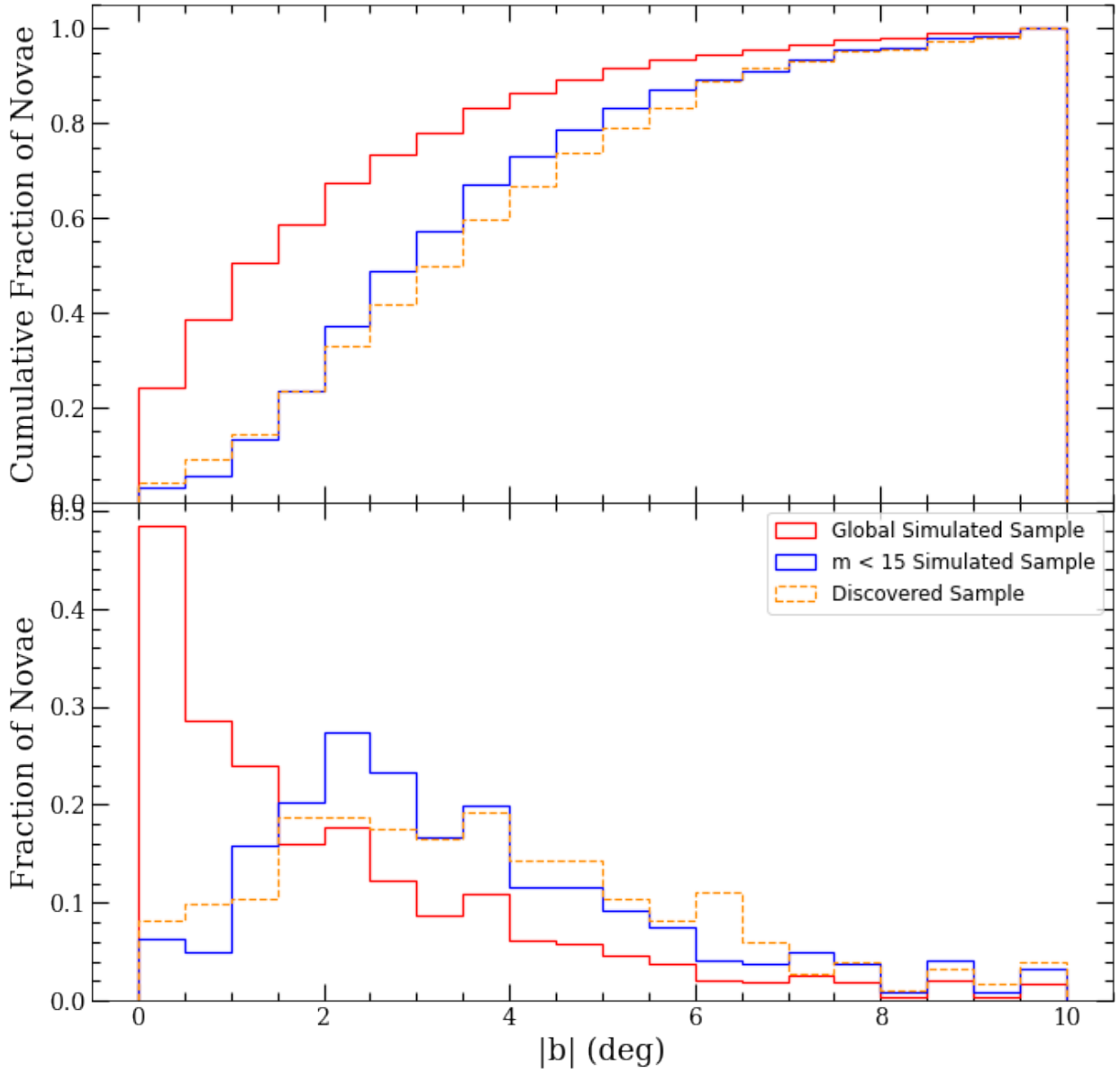

Figure 3.7 Normalized cumulative distribution (top) and normalized histogram (bottom) of novae as a function of Galactic latitude. All simulated novae are plotted in red, while simulated novae that reach a brightness of $g = 15$ mag are shown in blue. Optically discovered novae are plotted as an orange dashed line. The discovered sample more closely resembles the bright m ¡ 15 mag model, suggesting a bias against discovering novae in regions of heavy extinction and a severe historic lack of novae discovered at low Galactic latitude.

The all-sky and nearly one day cadence observations of ASAS-SN provide an unprecedented opportunity to better constrain the Galactic nova rate. Even though the limiting magnitude of ASAS-SN is as deep as $g \sim 18$ mag, nova searches have some unique challenges and we believe the current infrastructure of the transient candidate pipeline is best suited to discover novae brighter than g $\sim$ 15 mag for various reasons. First, ASAS-SN usually flags portions of the sky known to contain variable stars, and avoids searching for transients in these regions—but classical novae often have variable hosts. To address this issue, a special "ASAS-SN Nova Alert" email is generated for essentially all transients $g \lesssim 15$ mag, regardless of previous variability, and is immediately sent to alert several of the co-authors upon detection. Second, confusion from neighboring sources—many of which are variable—is a much larger issue in the Galactic plane, and essentially translates to a shallower detection limit. Additionally, the candidate pipeline dedicated to discovering novae has a cutoff at this threshold. And finally, the number of contaminants greatly increases closer to the detection limit, so candidates fainter than $g = 15$ mag are not always checked. ASAS-SN can, and does, find Galactic transients fainter than this threshold, but the detection efficiency likely falls off quickly at $g > 15$ mag. This detection threshold is bright, especially when compared to the number of fainter CV candidates and extragalactic supernova candidates discovered by the survey[3], and the detection efficiency of crowded fields at deeper thresholds will be explored in future work.

Currently, the detection efficiency of Galactic transients brighter than $g \approx 15$ mag is not known for ASAS-SN. For extragalactic SNe, Holoien et al. (2019) found that ASAS-SN is essentially complete down to $m = 16.2$ mag, but we do not expect the completeness to be as deep in the plane where almost all novae reside. To estimate this value, a fake transient

[3]http://www.astronomy.ohio-state.edu/asassn/transients.html

recovery analysis performed on ASAS-SN data is needed, but it is beyond the scope of this work. Even with perfect recovery in observable fields, an optical transient survey is limited to detection rates $\lesssim 80\%$ due to Solar conjunction (Mróz et al., 2015b), and preliminary estimates of detecting fainter, but longer lived, Type Ia supernovae in ASAS-SN suggest detection capabilities between 70% and 80% (Desai et al. 2021, in prep). A fake transient recovery analysis was performed on PGIR data in De et al. (2021), and they estimated that 36% of all Galactic novae that reach $J = 14$ mag in their field of view could be detected ($\delta > -28.9^\circ$ at a cadence of ≈ 2 nights). This lower detection fraction is largely due to crowding/blending from an 8" pixel scale, contamination from nearby bright stars, and the Galactic center being unobservable for a large fraction of the year from PGIR's Mt. Palomar location. We expect the first two issues to be present in ASAS-SN data since the two surveys have the same pixel scale and a majority of novae should be found within a couple degrees of the crowded plane, but the last issue does not affect ASAS-SN because it has facilities in both the Northern and Southern Hemisphere. Taking all of the above information, we estimate ASAS-SN can detect 60% of Galactic novae that reach $g = 15$ mag. To be clear, this estimated detection efficiency is only applicable to Galactic novae, and the detection efficiency is known to be higher for extragalactic transients in less crowded fields off of the plane.

Between 2018–2020, there were 31 known Galactic novae that peaked brighter than $g = 15$ mag. A majority of these were clearly detected and flagged as transients in ASAS-SN data, but there are at least a few examples of novae that were not detected or flagged as nova candidates. V3731 Oph (De et al., 2020c) was detected as a transient candidate in the ASAS-SN pipeline but was confused with a coincident variable within a pixel of the nova. V6567 Sgr (De et al., 2020d) was detected on the rise in ASAS-SN data and initially reported

as a CV candidate. And though V1709 Sco (Kawash et al., 2020) was detected as bright as $V = 12.7$ mag by other observers, it was never detected brighter than $g = 15$ mag in ASAS-SN data likely due to facilities being shutdown for a large portion of 2020 due to the pandemic. It is likely that more observable nova events were missed by all transient surveys and observers and even more due to Solar conjunction, so this is consistent with our 60% detection efficiency estimate for this time period. This estimation is very crude, and it will be one of the major goals of Kawash et al. (2022 in preparation) to better understand and constrain it.

We use our model to distribute N = 1000 novae in a mock galaxy, estimate what fraction would be detectable by ASAS-SN by assuming detections of 60±6% that reach g < 15 mag, and extrapolate to a global rate from an annual discovery rate of $R = 10.3 \pm 1.9$. This analysis is carried out for 1000 iterations, each time randomly distributing novae according to the stellar density model and sampling a normal distribution with a mean and standard deviation equal to the estimated value and uncertainty, respectively, for the discovery rate, detection efficiency, and the luminosity function of novae in order to evaluate the most likely Galactic nova rate based on ASAS-SN observations.

Because this is the first nova rate estimate from ASAS-SN, and because the detection efficiency is not well constrained, we compare our results to those derived from other transient surveys. First, it was estimated that between 2010–2013 OGLE-IV observations discovered up to 80% of novae brighter than $I = 17$ mag in the most frequently visited fields in their field of view ($-10^\circ < l < 10^\circ$ and $-7^\circ < b < 5^\circ$, with a cadence varying from 20 minutes to a few days; Mróz et al. 2015b). The OGLE discovery rate was $R = 4.8 \pm 1.1$ yr^{-1} over this time period. We carry out the same analysis as we did for ASAS-SN to derive a Galactic nova rate from OGLE-IV observations using a detection efficiency as a function of

sky position estimated from Figure 9 of Mróz et al. (2015b), but we ignore novae directly in the plane ($|b| < 1^\circ$) and fields with a detection efficiency less than 25% to account for the different extinction model used in our analysis. We believe this is a safe assumption as only one nova from Table 1 of Mróz et al. (2015b) lies within this ignored region. OGLE-IV observations have a much lower cadence in the highest extinction regions in the plane Udalski et al. (2015b), so a large fraction of novae are likely undetected despite the better pixel scale and redder filter compared to ASAS-SN. However, roughly $40 - 50\%$ of these novae are too highly extinguished to be detectable even with improved monitoring of the field.

Another survey with a published rate of nova discovery is the PGIR survey (De et al., 2021). Over the first 17 months of observations, they discovered 7.8 novae per year and estimated they could detect 36% of all novae brighter than $J \sim 14$ mag in their field of view ($\delta > -28.9^\circ$ at a cadence of ≈ 2 nights). We run our analysis on a PGIR detection rate of $r = 7.8 \pm 2.3$ yr^{-1} and detection efficiency of $36 \pm 3.6\%$ in the field of view.

Lastly, Shafter (2017) derived a Galactic nova rate with a bright, nearby sample of novae. Between 1900 and 2020, there have been only 7 novae that reached an apparent magnitude of $m = 2$. We carry out our analysis assuming that 90% of all novae that reached this brightness were discovered.

The distributions of nova rates derived from these various observational constraints are shown in Figure 3.8. All of these distributions except for the $m < 2$ mag constraint are well fit by a normal distribution, and for those we derive the mean and standard deviation (listed in Table 3.3). The ASAS-SN (32.5 ± 7.3 yr^{-1}), OGLE (35.6 ± 8.8 yr^{-1}), and PGIR (44.2 ± 14.7 yr^{-1}) derived rates are all consistent at the 1σ level. The PGIR rate has a higher variance because of the limited field of view and because they are unable to observe the Galactic center for a large portion of the year. The bright nova constraint ($m < 2$ mag) results in

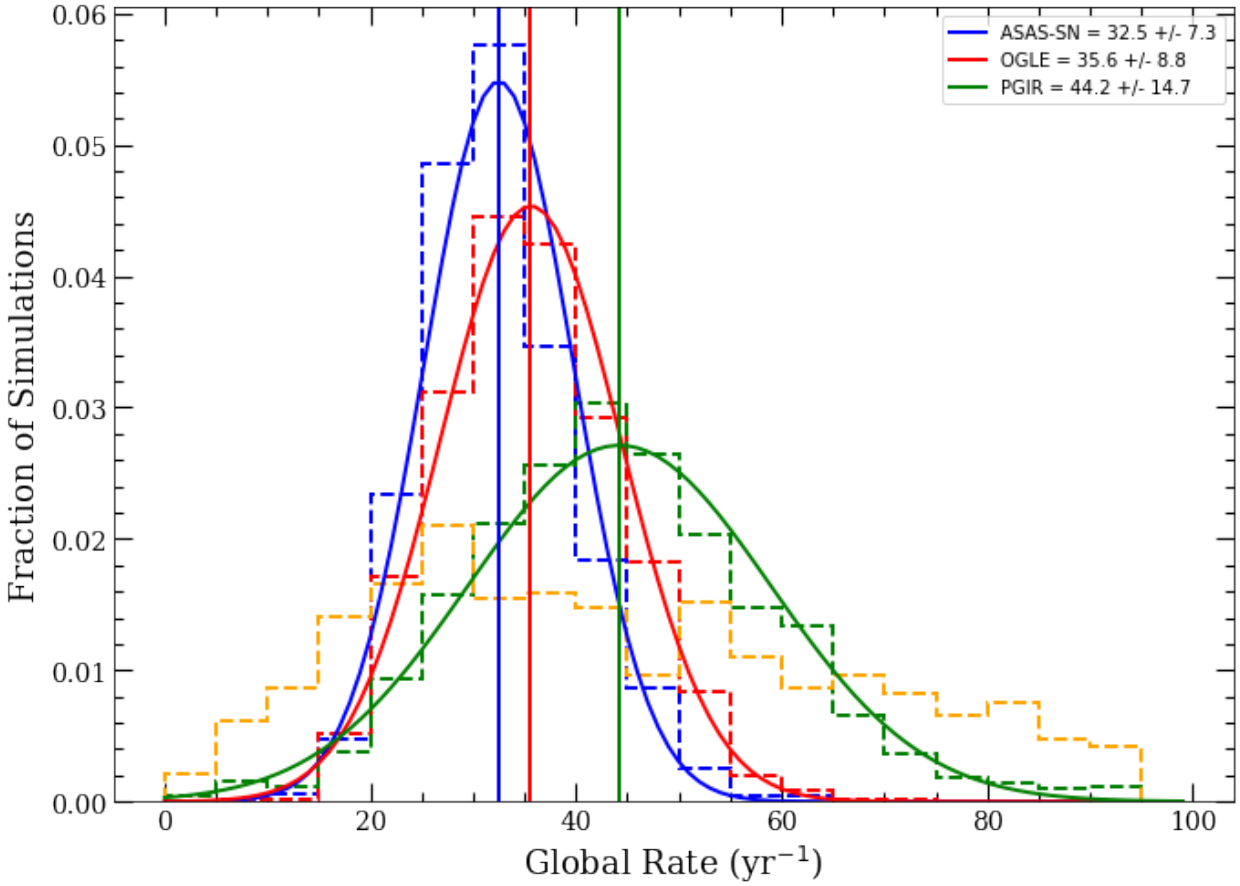

Figure 3.8 Distribution of the Galactic nova rate from 1000 iterations of our primary model based on observational constraints from ASAS-SN (blue), OGLE (red), PGIR (green), and historic bright novae (orange) shown as dashed histograms. The results from ASAS-SN, OGLE, and PGIR observations are well fit by a normal distribution, and this is shown for each respective survey along with the mean value.

Table 3.1. Galactic Nova Rates For Various Parameters

θ	Dust Model	Mass Model	N_d/N_b	ASAS-SN	OGLE	PGIR	Average ($\bar{\chi}$)
1.0	mwdust: 8.65	Besancon	1.7	33 ± 7	36 ± 9	44 ± 15	35
1.0	mwdust: 8.65	Cautun	5.0	38 ± 8	52 ± 13	45 ± 15	43
1.0	exponential disk	Besancon	1.7	24 ± 5	36 ± 9	43 ± 14	28
0.4	mwdust: 8.65	Besancon	0.7	31 ± 6	27 ± 6	43 ± 14	31
0.4	mwdust: 8.65	Cautun	1.7	38 ± 8	41 ± 10	44 ± 15	40
1.0	mwdust: 13.44	Besancon	1.7	38 ± 9	36 ± 9	55 ± 19	40
1.0	mwdust: 13.44	Cautun	5.0	44 ± 10	54 ± 13	44 ± 15	47

Note. — Model parameters and derived Galactic nova rates based on ASAS-SN, OGLE, and PGIR detections of novae. The default extinction curve for the `mwdust` model is $A_V/A_{K_s} = 8.65$, but the last two rows show results for a steeper value. θ is the ratio of disk to bulge novae per unit mass and N_d/N_b is the resulting disk to bulge ratio of novae for a given mass model. $\bar{\chi}$ is the weighted average of the Galactic nova rate from the three surveys.

a distribution with high variance due to a low observed rate (7 novae over 120 years). The ASAS-SN derived distribution results in the distribution with the lowest variance, but this distribution is derived with only a rough estimate of the detection efficiency of novae. Once this value is better constrained, and more observations are accumulated, ASAS-SN could provide the best constraint on the Galactic nova rate to date.

The observational constraints from these various surveys are almost completely independent. The OGLE rate is derived from OGLE-IV observations, occurring between 2010–2013. The ASAS-SN discoveries occur between 2018–2020, overlapping with the PGIR discoveries from July 2019 − November 2020. There have been no m = 2 mag novae that have erupted since any of these surveys started observing. A simple weighted average of ASAS-SN, OGLE, and PGIR derived rates results in a Galactic nova rate of $R \approx 35$ yr^{-1}.

3.4 How Sensitive Are The Results to our Assumptions?

Here we explore how our results change as we vary certain assumptions in our model. In Section 3.4.1, we change the extinction model from the 3D dust maps to the simple exponential used in Shafter (2017) and also explore implementing a different reddening law. Then in Section 3.4.2, we see how our results depend on the mass model of the Galaxy. Finally, we briefly explore how assuming different populations of bulge and disk novae affects our results in Section 3.4.3. The derived rates for various sets of parameters are shown in Table 3.3.

3.4.1 Extinction Models

The dust maps of Green et al. (2019), Marshall et al. (2006), and Drimmel et al. (2003)—stitched together by Bovy et al. (2016)—form the best all-sky three dimensional dust map to date. It is almost certainly superior to simply assuming a disk of dust (i.e., as in Shafter 2017), but it is only able to model extinction out to a few to $\sim$ 10 kpc depending on the direction. For this reason, we investigate how the rates change if we implement the exponential disk model of extinction used in Shafter (2017). The results are shown in the top right panel of Figure 3.9.

As expected, the rate estimated from the g-band observations of ASAS-SN is extremely sensitive to the dust model used. The exponential model of extinction underestimates the amount of dust in the plane relative to the `mwdust` model, therefore yielding a higher detection fraction and ultimately a much lower rate. The OGLE derived rate is not sensitive to the dust model since we assume they do not detect novae in the fields with the highest extinction, and the IR observations of PGIR are also not sensitive to the dust model. The

rates derived from the three surveys are no longer consistent at the 1σ level when using this dust model, and it is clear that an under- or over-estimation of Galactic extinction will cause a significant error in the derived nova rate from ASAS-SN observations. This conclusion is consistent with predictions for observing the next Galactic supernova. Adams et al. (2013) found that different dust models yield different likelihoods of observing a Galactic supernova in the optical but were less important for near-IR observations.

`mwdust` assumes an extinction ratio of $A_V/A_{K_s} = 8.65$ across the entire sky, but this is not a safe assumption along all lines of sight, especially toward the inner Galaxy (Nataf et al., 2016). Therefore, we also investigate how our results change assuming a extinction ratio of $A_V/A_{K_s} = 13.44$, causing extinction in g-band to be 25% higher than the default `mwdust` value. As expected, the g-band observations of ASAS-SN are sensitive to variations in the extinction curve, with steeper reddening laws leading to a higher inferred rates of nova production (see last two rows of Table 3.3). However, not all novae in the model are in the inner Galaxy, and therefore the extinction is likely overestimated for a fraction of the lines of sight. Hence this alternate model should be considered closer to a limit on the effects of a different extinction law on the Galactic nova rate, rather than a best estimate of the effect.

3.4.2 Mass Model

The Robin et al. (2003) stellar density model is just one of many widely used Galactic mass models, so we explored if our results change if we implement another model. A stellar density model inferred from *Gaia* DR2 data was recently presented in Cautun et al. (2020), and we implement the bulge, thin disk, and thick disk components from the Contracted Halo version of this model. The grid was calculated using the same resolution and boundaries as our primary model, and the mass of each component was found to be consistent with the

derived mass in Table 2 of Cautun et al. (2020).

The Besançon model of the Galaxy has a more massive, bar-like bulge component, while Cautun et al. (2020) assume an axisymmetric bulge for simplicity and state that they are unable to constrain the bulge mass or its radial profile. However, by implementing the Cautun et al. (2020) stellar density model, we are able to see how the derived nova rate changes with a different assumed distribution of novae in the model galaxy. As seen in Figure 3.1, the Cautun et al. (2020) model places fewer novae at smaller Galactic radii but more novae at lower Galactic height from the plane. So, the Cautun et al. (2020) model results in fewer bulge novae but more in the highest extinction regions in the plane. As seen in Figure 3.9, this predicts a slightly higher rate from ASAS-SN observations and a significantly higher rate from OGLE observations. The PGIR rate does not appear to be sensitive to the stellar distribution model. Overall, using the Cautun et al. (2020) model results in a higher prediction of the Galactic nova rate. but it is still consistent at the 1σ level with using the Robin et al. (2003) model.

3.4.3 Differing Bulge and Disk Populations

It has been posited that novae that erupt in the bulge have different properties than those that erupt in the disk because of different progenitor populations hailing from differing star formation histories (Della Valle & Izzo, 2020). Darnley et al. (2006) found that the favoured model of novae in M31 supported separate disc and bulge populations that erupted at different rates per unit r-band flux. They found that, per unit r-band flux, the ratio of disk novae to bulge novae was 0.18. Shafter & Irby (2001) also studied the spatial distribution of novae in M31, and estimated this ratio to be 0.4. In a similar fashion, we define θ as the ratio of disk novae to bulge novae per unit mass in our model. So far, we have assumed one

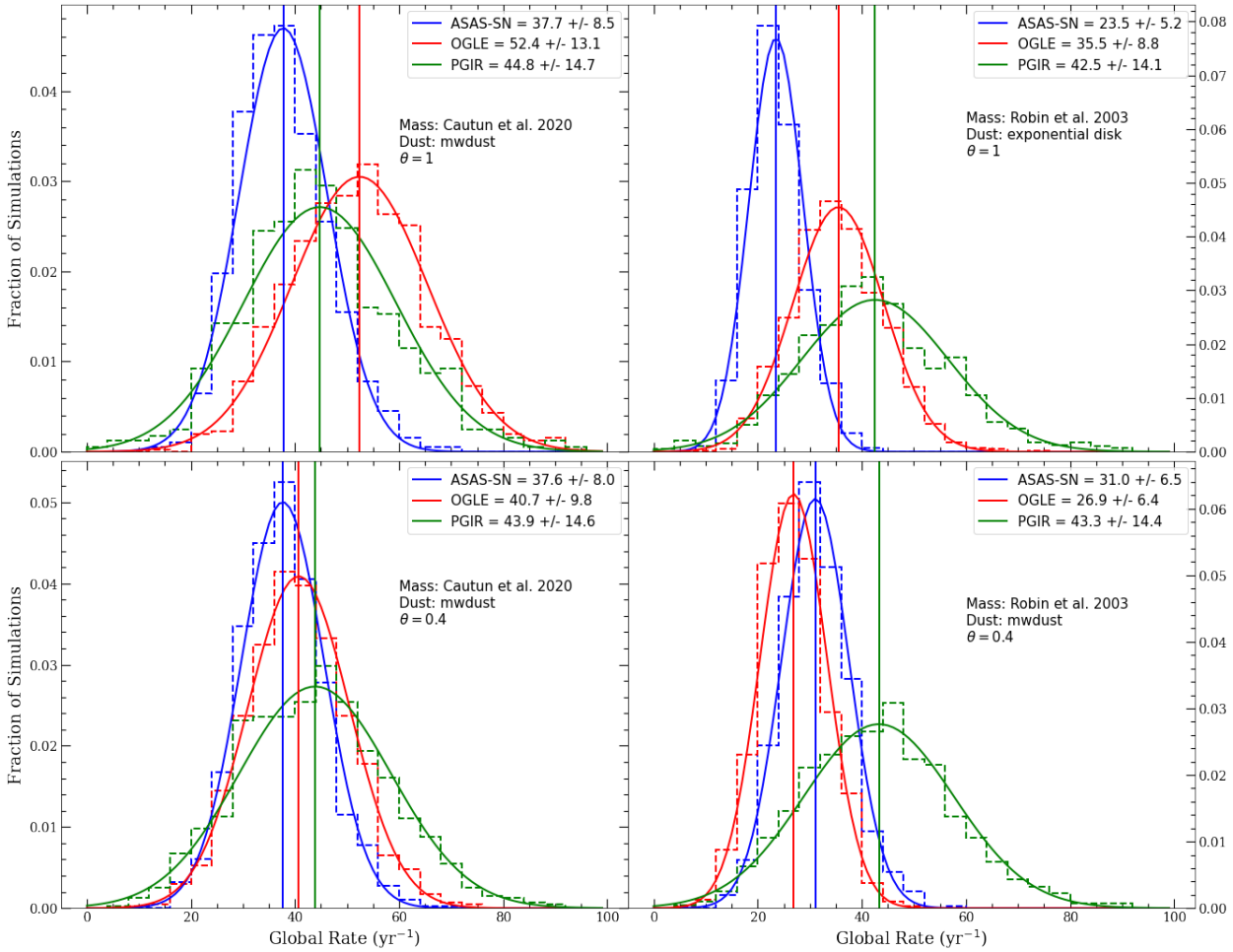

Figure 3.9 Same as Figure 3.8 for various combinations of stellar density models, extinction models, and ratio of disk to bulge novae per unit mass (θ). Top Left: Galactic nova rate distributions resulting from using the Cautun et al. (2020) mass model. Top Right: Galactic nova rate distributions resulting from changing the `mwdust` model to an exponential disk; this results in rate estimates inconsistent at the one-sgima level. Bottom Left: Galactic nova rate distributions from an elevated rate of nova production in the bulge using the Cautun et al. (2020) mass model. Bottom Right: same as bottom left but for the Robin et al. (2003) model Overall, the ASAS-SN and OGLE derived rates are sensitive to the model assumptions but the PGIR rate is not.

population of novae that traced the overall stellar mass of the Galaxy ($\theta = 1$), resulting in a ratio of disk-to-bulge novae of $N_{\rm disk}/N_{\rm bulge} \approx 5$ for the Cautun et al. (2020) mass model and $N_{\rm disk}/N_{\rm bulge} \approx 1.7$ for the Robin et al. (2003) mass model.

Does the Milky Way Galaxy produce more novae per unit mass in the bulge than in the disk? Because distances are often hard to constrain, this is not an easy question to answer, but to first order, the higher the nova rate in the bulge, the more novae we should expect to find near $l = 0^\circ$. From our model where novae simply trace the stellar mass of the Galaxy ($\theta = 1$), we expect 40% of bright ($g < 15$ mag) novae to be located within $|l| \leq 10^\circ$. Of all the known Galactic novae from our list, 45% have erupted within $|l| \leq 10^\circ$. This could support the idea of bulge enhancement, or the bulge producing more novae per unit mass relative to the disk, especially since the observed sample of novae is likely biased towards nearby disk novae.

For this reason, we explore how our results changed when using an elevated bulge rate of $\theta = 0.4$. This model predicts that 49% of bright ($g < 15$ mag) novae are within $|l| \leq 10^\circ$ based on the Cautun et al. (2020) mass model and 67% for the Robin et al. (2003) model. The value of θ is difficult to constrain due to the unknown number of foreground disk novae, but the number of known novae around the Galactic Center suggests it is larger than $\theta = 0.4$. The nova rate results for this elevated bulge distribution of novae are shown in the bottom panels of Figure 3.9 for both the Cautun et al. (2020) and Robin et al. (2003) mass models.

If the production of novae in the bulge is elevated relative to the disk per unit mass, the global rate based on OGLE-IV observations decreases. This is expected, as OGLE observations are heavily biased towards finding bulge novae. ASAS-SN and PGIR observations are less sensitive to the ratio of disk to bulge novae, as the field of view of these surveys are less biased towards the bulge or disk.

3.5 Conclusions

We have used an all-sky three dimensional dust map to explore the effects of Galactic extinction on the discovered nova rate. This model predicts that roughly half of nova eruptions will be too faint for current ASAS-SN discovery abilities, much higher than previous estimates that used a simpler dust model, and likely explaining much of the discrepancy between observed and predicted rates. Many of the highly extinguished, reddened novae lie within two degrees of the plane. Our model predicts that $\sim 60\%$ of all novae should erupt within two degrees of the plane, compared to only $\sim 20\%$ of the discovered sample being found in this region. This further highlights the necessity of optical surveys to observe in redder bands and IR transient surveys like PGIR to detect these highly reddened novae in the plane, although these fields have lower recovery rates for surveys with large pixel scales.

For the first time, we have estimated a Galactic nova rate based on an all-sky survey with nightly cadence. ASAS-SN observations between 2018 and 2020 suggest a Galactic nova rate of 33 ± 7 yr^{-1}. This derived rate relies heavily on the detection efficiency (assumed to be 60% in this work for novae brighter than $g < 15$ mag), a value that will need to be better understood in the future. However, the derived rate from ASAS-SN is consistent with rates derived from OGLE observations (R $= 36 \pm 9$ yr^{-1}) and PGIR observations (R $= 44 \pm 15$ yr^{-1}). Our results are consistent with the recent higher rates derived in De et al. (2021) and Shafter (2017), though we can not rule out lower rates at this time due to the large uncertainties in the model parameters.

The derived rate from ASAS-SN's blue g-band filter is sensitive to the extinction model implemented, so a precise nova rate estimation will depend on how accurately dust is modeled close to the plane. Similarly, the OGLE rate is sensitive to the level of bulge enhancement

and along with the ASAS-SN rate is sensitive to the model used to place novae within the mock Galaxy. The PGIR rate does not appear to be sensitive to altering any of the assumptions of our model. For any combination of stellar density model, extinction model, and level of bulge enhancement, the observations of ASAS-SN, OGLE, and PGIR suggest a Galactic nova rate of ~ 30 to ~ 40 per year.

Overall, this work makes significant progress in constraining the Galactic nova rate, but it can still be greatly improved. In Kawash et al. (2022, in preparation), we plan to estimate the detection efficiency of ASAS-SN through fake transient recovery and incorporating various decline rates to our simulated sample of novae. Knowing this, along with continued observations from ASAS-SN and PGIR will allow us to further constrain the rate of novae in the Galaxy. We can further quantify the effects of Solar constraint on nova discovery rates and make predictions for next generation transient facilities like LSST.

Acknowledgments

We thank P. Mroz for providing data contributing to this work. We also thank Jo Bovy, D. J. Marshall, A. C. Robin, I. T. Simion for helpful discussions and the referee for suggestions that substantially improved the paper. AK, LC, EA, and KVS acknowledge financial support of NSF award AST-1751874 and a Cottrell fellowship of the Research Corporation. JS acknowledges support from the Packard Foundation. BJS, CSK, and KZS are supported by NSF grant AST-1907570. CSK and KZS are supported by NSF grant AST-181440.

We thank the Las Cumbres Observatory and its staff for its continuing support of the ASAS-SN project. ASAS-SN is supported by the Gordon and Betty Moore Foundation through grant GBMF5490 to the Ohio State University, and NSF grants AST-1515927 and

AST-1908570. Development of ASAS-SN has been supported by NSF grant AST-0908816, the Mt. Cuba Astronomical Foundation, the Center for Cosmology and AstroParticle Physics at the Ohio State University, the Chinese Academy of Sciences South America Center for Astronomy (CAS- SACA), and the Villum Foundation.

The analysis for this work was performed primarily in `ipython` (Perez & Granger, 2007) using `numpy` (Oliphant, 2006; Van Der Walt et al., 2011), `Astropy` (Price-Whelan et al., 2018), `Matplotlib` (Hunter, 2007), and `scipy` (Virtanen et al., 2020).

3.6 Appendix

3.6.1 Besancon Mass Model

Here we discuss the form of each component of the Besancon Mass model used to distribute novae for our primary model. The total mass and normalization of each component is shown in Table 3.6.1.

We use a Cartesian grid with resolution 0.1 kpc, R = $\sqrt{x^2 + y^2}$ is the radial distance from the Galactic center, and z is the distance perpendicular to the Galactic plane. The assumed Solar radius from Robin et al. (2003) is $R_\odot = 8.5$ kpc.

3.6.1.1 Thin Disk

The form of the thin disk density is from Robin et al. (2003)

$$\rho = \rho_0 \times \left\{ \exp\left[-\left(0.5^2 + \frac{a^2}{h_{R+}^2} \right) \right] - \exp\left[-\left(0.5^2 + \frac{a^2}{h_{R-}^2} \right) \right] \right\} \tag{3.1}$$

Table 3.2. Mass and Normalization values for the various components of the Galactic model

Component	Normalization $M_\odot$ pc^{-3}	Total Mass 10^9 $M_\odot$
Thin Disk	1.45	35.0
Thick Disk	0.002[a]	4.67
Bulge (Model S)	2.37	22.1
Bulge (Model E)	1.17	1.20
Halo	0.00005	0.55

[a]Density at the solar position, where the other normalization values refer to the density at the Galactic center

Note. — Normalization values and the total mass of the various components of the Galactic model utilized in this work. We set the normalization values to achieve a consistent total mass with that derived in Robin et al. (2003), Simion et al. (2017), or Bland-Hawthorn & Gerhard (2016)

where $a^2 = R^2 + (z/\epsilon)^2$, $h_{R_+} = 2.5$ kpc is the scale length of the disk, $h_{R_+} = 0.9$ kpc is the scale length of the hole, and ϵ=0.0791.

3.6.1.2 Thick Disk

A piece-wise thick disk density distribution is utilized from Robin et al. (2003)

$$\rho = \begin{cases} \rho_0 \exp\left(-\frac{R-R_\odot}{h_R}\right) \times \left(1 - \frac{z^2/h_z}{\xi \times (2+\xi/h_z)}\right) & \text{if z} \leq \xi \\ \rho_0 \exp\left(-\frac{R-R_\odot}{h_R}\right) \times \exp\left(-\frac{|z-z_\odot|}{h_z}\right) \times \frac{2\exp(\xi/h_z)}{2+\xi/h_z} & \text{if z} > \xi \end{cases} \tag{3.2}$$

where $h_R = 2.5$ kpc is the radial scale length, $h_z = 0.8$ kpc is the vertical scale length, and $\xi = 0.4$ kpc. The local density $\rho_0 = 0.002$ $M_\odot$ pc^{-3} is set to be four percent of the local thin disk density (Bland-Hawthorn & Gerhard, 2016).

3.6.1.3 Bulge/Bar

For the bulge, we use an updated fit to VVV data from Simion et al. (2017). The best fit model combines a hyperbolic secant density distribution

$$\rho = \rho_0 \operatorname{sech}^2(r_s) \quad \text{(model S)} \tag{3.3}$$

and an exponential distribution

$$\rho = \rho_0 \exp(-0.5 r_s^n) \quad \text{(model E)} \tag{3.4}$$

where,

$$r_s = \left\{ \left[\left(\frac{x}{x_0}\right)^{c_\perp} + \left(\frac{y}{y_0}\right)^{c_\perp} \right]^{\frac{c_\parallel}{c_\perp}} + \left(\frac{z}{z_0}\right)^{c_\parallel} \right\}^{1/c_\parallel}. \tag{3.5}$$

$c_{\parallel}$ and $c_{\perp}$ controls the face-on and edge-on shape of the bulge, respectively, and x_0, y_0, and z_0 are the scale lengths in each respective direction. We use the best fit parameters using the Besancon discs presented in Simion et al. (2017). For the sech component (model S) the best fit parameters are $c_{\parallel} = 2.89$, $c_{\perp} = 1.49$, and (x_0, y_0, z_0) = (1.65,0.71,0.50) kpc, and for the exponential component, the best fit parameters are $c_{\parallel} = 3.64$, $c_{\perp} = 3.54$, and (x_0, y_0, z_0) = (1.52,0.24,0.27) kpc, and n = 2.87. The elongated direction of the bar is offset from the Sun-Galactic Center line by 21.1° and 2.1° for the hyperbolic secant and exponential component, respectively. The bulge density has a cutoff Radius $R_c = 6.96$ kpc implemented by multiplying the bulge density ρ by the function

$$\begin{aligned} f(R) &= 1 & R < R_c \\ f(R) &= \exp\left[-2\left(R - R_c\right)^2\right] & R > R_c. \end{aligned} \tag{3.6}$$

3.6.1.4 Stellar Halo

We use a power law form of the halo similar to the one presented in Robin et al. (2003)

$$\rho = \begin{cases} \rho_0 \left(a_c / R_\odot\right)^n & a < a_c \\ \rho_0 \left(a / R_\odot\right)^n & a > a_c \end{cases} \tag{3.7}$$

where $a = \sqrt{x^2 + y^2 + (z/\epsilon)^2}$, $a_c = 0.5$ kpc is the cutoff radius, and $n = -2.44$.

Chapter 4

The Galactic Nova Rate: Estimates from the ASAS-SN and *Gaia* Surveys

Abstract

We present the first estimate of the Galactic nova rate based on optical transient surveys covering the entire sky. Using data from the All-Sky Automated Survey for Supernovae (ASAS-SN) and *Gaia*—the only two all-sky surveys to report classical nova candidates—we find 39 confirmed Galactic novae and 7 additional unconfirmed candidates discovered from 2019–2021, yielding a nova discovery rate of ≈ 14 yr^{-1}. Using accurate Galactic stellar mass models, three-dimensional dust maps, and incorporating realistic nova light curves, we have built a sophisticated Galactic nova model that allows an estimate of the recovery fraction of Galactic novae from these surveys over this time period. The observing capabilities of each survey are distinct: the high cadence of ASAS-SN makes it sensitive to fast novae, while the broad observing filter and high spatial resolution of *Gaia* make it more sensitive to highly reddened novae across the entire Galactic plane and bulge. Despite these differences, we find that ASAS-SN and *Gaia* give consistent Galactic nova rates, with a final joint nova rate of 26 ± 5 yr^{-1}. This inferred nova rate is substantially lower than found by many other recent studies. Critically assessing the systematic uncertainties in the Galactic nova rate, we argue that the role of faint fast-fading novae has likely been overestimated, but that subtle

details in the operation of transient alert pipelines can have large, sometimes unappreciated effects on transient recovery efficiency. Our predicted nova rate can be directly tested with forthcoming red/near-infrared transient surveys in the southern hemisphere.

4.1 Introduction

A classical nova eruption is the result of a thermonuclear runaway of accreted hydrogen rich material on the surface of a white dwarf (see Bode & Evans 2008; Chomiuk et al. 2021a for reviews). At peak brightness, novae are relatively luminous, with absolute magnitudes between $M_V \approx -4$ to -10 mag (Shafter, 2017), allowing them to be discovered out to the largest Galactic distances and in nearby galaxies. Discoveries of Galactic novae date back thousands of years (Patterson et al., 2013; Shara et al., 2017b), and estimates of the total frequency with which the Milky Way produces novae date back nearly a century (Lundmark, 1935). The nova rate has broad implications in a range of areas, including Galactic nucleosyntheis, binary evolution, and the origin of Type Ia supernovae.

Found in both the Galactic disk and bulge, novae have long been thought to be significant contributors to the Galactic abundance of specific isotopes, including by-products of the CNO cycle (^{13}C, ^{15}N, and ^{17}O) and those that radioactively decay (^{7}Be, ^{22}Na, and ^{26}Al; José & Hernanz 1998). To quantify these contributions we need to not only understand how these isotopes are created and how much of them are ejected in individual eruptions, but also to have a solid estimate of the Galactic nova rate. Take, for example, ^{7}Be—the creation of which has been suggested in nova explosions for decades (Arnould & Norgaard, 1975; Starrfield et al., 1978a). However, predictions for the amount of ^{7}Be created in a typical nova were uncertain (José & Hernanz, 1998). ^{7}Be was recently detected in the ejecta of V339

Del and V5668 Sgr, placing yields on more solid ground (Tajitsu et al., 2015; Izzo et al., 2015). ^{7}Be decays to ^{7}Li with a half-life of 53.22 days, so nova eruptions could be responsible for a significant amount of the present day Galactic abundance of lithium (Romano et al., 2001; Prantzos, 2012; Rukeya et al., 2017; Starrfield et al., 2020).

Another radioactive isotope created during a nova eruption is ^{26}Al (José & Hernanz, 1998). This isotope, observed via its MeV γ-ray line emission, is also produced in supernovae, and has been used as a tracer of the Galactic supernova rate and star formation rate (Diehl et al., 2006). However, the recent study of Vasini et al. (2022) shows that novae are likely to be significant contributors to the Galactic ^{26}Al budget, perhaps accounting for the majority of the ^{26}Al mass (see also Bennett et al. 2013). The uncertainty in the nova rate makes determining such nucleosynthetic contributions difficult.

In addition to being an important input to chemical evolution models, the Galactic nova rate is also a constraint on binary population synthesis models (Chen et al., 2016; Kemp et al., 2021). It has recently been realized that nova eruptions may be an important mechanism of angular momentum loss from interacting close binary systems (Schenker et al., 1998; Schreiber et al., 2016; Pala et al., 2022) affecting their evolutionary outcome (Nelemans et al., 2016; Sparks & Sion, 2021; Metzger et al., 2021). In addition, some novae could be the progenitors to Type Ia supernovae (e.g., Patat et al., 2011; Dilday et al., 2012; Darnley et al., 2015), depending on the degree to which white dwarfs can retain accreted mass over the course of a nova eruption (Toonen et al., 2014; Starrfield et al., 2020). Binary models can now reproduce the zoo of accreting white dwarf binaries (Kalomeni et al., 2016), and, in the future, a comparison of nova rates with other white dwarf binary populations can shed light on how and when white dwarfs manage to grow in mass.

Determining the nova rate of the Milky Way is also important for understanding which—

and how many—novae are currently missing from our samples of discovered Galactic novae. Galactic novae are the eruptions we can study in great detail, bringing to bear observations from radio to γ-ray wavelengths and revealing the physics that drives these eruptions (Chomiuk et al., 2021a). However, it is unclear whether the targets of these detailed studies are a representative sample, or if particular kinds of novae are missing from our current Galactic samples.

For these reasons, constraining the Galactic nova rate is important, but it has proven to be a tricky feat. Below we summarize the efforts of the community in discovering Galactic classical novae and the published predictions of the frequency with which the Milky Way produces this class of stellar eruption.

4.1.1 History of Nova Discoveries

Though discoveries of Galactic novae date back millennia, the systematic monitoring of the sky by photographic means for novae began around the turn of the 20th century (Duerbeck, 2008). During the first half of the 20th century, $\sim$2 novae were discovered per year visually and using photographic plates. With the wide-spread use of astronomical photography (Pickering, 1893, 1895) and the advent of objective prism surveys (Duerbeck, 2008), the rate of discoveries increased to $\sim$3 per year in the mid-20th century. In the 1980s and 1990s, film photography became commonly used by amateur astronomers, and the discovery rate increased to $\sim$4 per year.

In the 2000s and 2010s, more sensitive large-format CCD and CMOS-based digital cameras became widely available to amateur astronomers, increasing the annual nova discovery rate to $\sim$8 yr^{-1} (see Figure 4.1). It was thought that discoveries were largely incomplete (Liller & Mayer, 1987), but the degree to which novae were missed due to a shallow magni-

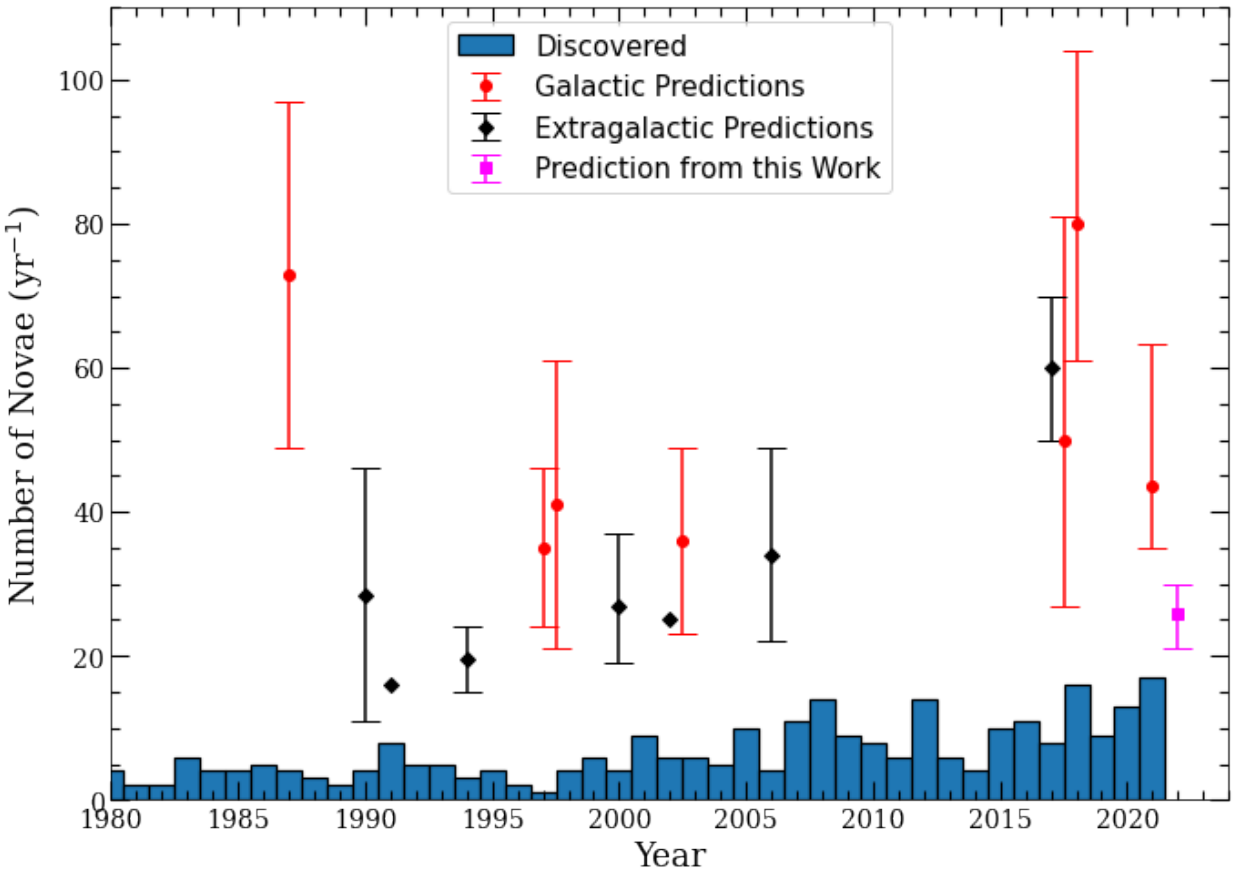

Figure 4.1 Galactic nova rate predictions as a function of the year published, compared with the number of novae confirmed each year since 1980. The rate predictions made using the Galactic or direct method are shown as red circles and using the extragalactic or indirect method are shown as black diamonds, along with error bars if the uncertainty was estimated. The prediction from this work is shown as the magenta square. The number of discovered and confirmed Galactic novae each year is plotted as a blue histogram, and was derived using Koji Mukai's List of Galactic Novae, Bill Gray's Database of Galactic Novae, and AAVSO's VSX. Citations for published rates from left to right: Liller & Mayer (1987); Ciardullo et al. (1990); van den Bergh (1991a); della Valle & Livio (1994a); Shafter (1997); Hatano et al. (1997); Shafter et al. (2000); Shafter (2002); Darnley et al. (2006); Shafter (2017); Özdönmez et al. (2018); De et al. (2021).

tude limit, low cadence of observations, or lack of sky coverage was unknown. Therefore, it was unclear if professional surveys with systematic observations would have a large increase on the discovery rate.

The All Sky Automated Survey (ASAS-3 Pojmański, 2001) was one of the first CCD surveys imaging the entire sky reachable from its observing site and contributed to nova discoveries in the early 2000s. Many surveys at the time were focused on searching for supernovae, asteroids, or transiting exoplanets, so observations of transients in the Galactic plane were lacking, but surveys like ASAS-3 inspired the next generation of wide-field nova searches.

In the 2010s, large sky surveys began to contribute significantly to the discovery of Galactic novae. The Fourth Phase of the Optical Gravitational Lensing Experiment (OGLE-IV; Udalski et al. 2015b) began in 2010, with high cadence I-band observations of the central bulge discovering a large number of candidate bulge novae (Mróz et al., 2015b). The New Milky Way Survey (NMW; Sokolovsky et al. 2014) began searching for transients in the Northern Hemisphere Galactic plane at high cadence down to $V \approx 13.5$ mag in 2011. The All-Sky Automated Survey for SuperNovae (ASAS-SN; Shappee et al. 2014) started searching for transients in 2013, and then in 2017 became the first survey to systematically observe the entire night sky, including the Galactic plane, with nearly daily cadence down to $g \approx 18.5$ mag (Kochanek et al., 2017). These high-cadence and systematic observations allowed for fast-declining novae to be discovered anywhere on the sky. The Palomar Gattini-IR survey (PGIR; De et al. 2020b) began surveying the northern hemisphere Galactic plane in 2019 down to $J \approx 15.3$ AB mag. As a near-IR survey, PGIR can discover highly extinguished novae not discovered in previous years (De et al., 2021). These surveys were designed to discover transients, but the astrometrically focused *Gaia* (Gaia Collaboration et al., 2016)

has been a surprising contributor to the discovery of Galactic novae. The broad observing filter, high angular resolution, and all-sky coverage allow *Gaia* to detect highly reddened novae anywhere on the sky, including the southern Galactic plane (Hodgkin, S. T. et al., 2021). These surveys have helped to increase the average discovery rate to 10.5 yr^{-1} since 2010, with 17 spectroscopically confirmed novae in 2021, the highest number on record (see Figure 4.1). A higher discovery rate allows for better estimates of the global Galactic nova rate, as there is less sensitivity to model assumptions.

4.1.2 Galactic nova rate predictions

Two methods have been used to estimate the total rate of classical nova production in the Galaxy. The first method extrapolates a sample of discovered Galactic novae based on the estimated completeness (commonly referred to as the Galactic or direct method). The second method estimates the rate in a nearby galaxy and infers the Milky Way rate by scaling on the relative luminosity of the two galaxies (referred to as the extragalactic or indirect method).

The direct method was used to make the first prediction for the total frequency of Galactic nova eruptions. It was estimated there should be at least, but probably much higher than, $R = 50$ novae per year (Lundmark, 1935). Two decades later, Allen (1954) used a sample of 19 novae to estimate a Galactic rate of R $\sim$ 100 per year. Kopylov (1955) used 23 novae thought to be within 1500 pc of the Sun observed over a 60 year period, arriving at a rate of $R = 50$ Galactic novae per year. In another two decades, Sharov (1972) extrapolated from a sample of eight novae in the Solar neighborhood to estimate a nova rate of $R = 259$ per year for the entire Galaxy. In a similar fashion, Liller & Mayer (1987) extrapolated from a sample of 17 novae thought to be within a 60° slice of the Galaxy to a total rate of $R = 73 \pm 24$ yr^{-1}. Then, Hatano et al. (1997) assumed that novae in the Galaxy are disk

dominated and arrived at an annual rate of $R = 41 \pm 21$ yr^{-1}.

In the 1990s, estimates began to be derived from extragalactic samples of novae using the indirect method. Ciardullo et al. (1990) estimated the nova rate of NGC 5128 to infer the nova rate in our own Galaxy to be between $R = 11 - 46$ per year. van den Bergh (1991b) considered the nova rates in M31 and M33 and the globular cluster population ratios to deduce a Galactic nova rate of $R \sim 16$ yr^{-1}. della Valle & Livio (1994b) derived a Galactic rate of $R = 24$ per year by measuring the rates in 5 other galaxies and assuming the rates were proportional to the galaxy luminosity. Finally, Darnley et al. (2006) used a survey of M31 to infer a Galactic nova rate of $R = 34^{+15}_{-12}$ yr^{-1}.

Shafter (1997) is the first in a series of papers that extensively looked at the Galactic nova rate, and by extrapolating samples of novae of varying sector size, limiting magnitude, and time period estimated that the Galactic nova rate is 35 ± 11 yr^{-1}. Then, Shafter et al. (2000) estimated the nova rates in M51, M87, and M101 to indirectly estimate a Galactic nova rate of $R = 27^{+10}_{-8}$ yr^{-1}. A couple years later, Shafter (2002) assumed that the discovered sample of $m_V < 2$ mag novae are complete, extrapolated to a global rate of $R = 36 \pm 13$ yr^{-1} and also derived a rate of $R \sim 25$ per year by comparing the K-band luminosity and nova rate of M31 to the Milky Way. In the most recent paper of this series, Shafter (2017) assumed that the $m_V < 2$ mag novae are 90% complete and estimated that the most likely nova rate is $R = 50^{+31}_{-23}$ yr^{-1}. An even higher rate was predicted a year later when Özdönmez et al. (2018) estimated the local density of nova eruptions to predict an average estimate of the disk nova rate of $R = 67^{+21}_{-17}$ yr^{-1}, and by combining this with a bulge rate estimate of $R = 13.8 \pm 2.6$ yr^{-1} (Mróz et al., 2015b), predicted a Galactic nova rate of $R \sim 80$ yr^{-1}.

These predictions from the past 40 years, along with the history of the nova discovery rate, are summarized in Figure 4.1. One noticeable feature is that rate estimates made in the

1990s and early 2000s, dominated by extragalactic predictions, estimated much lower rates than the recent predictions from Galactic data. The *Hubble Space Telescope* (*HST*) survey of M87 novae (Shara et al., 2016) derived a nova rate for M87 over three times larger than that estimated by Shafter et al. (2000). The authors argue that *HST* is more sensitive to faint and fast novae and that previous extragalactic nova surveys had underestimated nova rates because they neglected this harder-to-discover class of novae. Assuming this to be the case, the Galactic rate derived from the M31 sample in Darnley et al. (2006) was increased to between ~ 50 and ~ 70 per year (Shafter, 2017).

Accounting for faint and fast novae could finally make the predictions from both the direct and indirect methods consistent, but it also appears at odds with the only modest increase in the discovery rate after the advent of large sky surveys: the implication would be that we are still discovering fewer than a quarter of the Galaxy's novae. With these new surveys, it is less plausible that time sampling is the main reason that novae are being missed, so another explanation is needed. A reasonable possibility is dust—that many novae are being hidden from optical surveys by foreground extinction. Kawash et al. (2021c) quantified the contribution of interstellar dust extinction to the optical discovery rate of Galactic novae and found that dust can hide $\sim 50\%$ of the Galactic population from being discovered by observers using V- or g-band filters. This helps explain some—but not all—of the discrepancy between the discovered and predicted rates.

Luckily, the well defined observing patterns of large time-domain surveys now make it possible to make systematic predictions of the Galactic nova rate by calculating the expected completeness in the survey data. This new era of Galactic nova rate estimates from large sky surveys began with a prediction using data from the Palomar Gattini-IR survey, where a sample of 11 highly reddened novae was used to derive a rate of $R = 44^{+20}_{-9}$ yr^{-1} (De et al.,

2021). This is consistent with the higher rates that have been published recently, and more predictions from other large sky surveys could help bolster these higher frequency estimates.

For the first time, in this paper we use data from multiple all-sky surveys to estimate the nova rate of the Milky Way. The use of all-sky surveys reduces the sensitivity of our results to possible differences in nova behavior between the disk and bulge (see, e.g., Della Valle & Izzo 2020)

To date, there are only two all-sky surveys that have reported a nova candidate. First, ASAS-SN became able to scan the entire night sky at a one day cadence in 2017. This high cadence was unprecedented, allowing for the discovery of fast novae anywhere on the sky.

Gaia is the only other all-sky survey that reports nova candidates. *Gaia* is designed to repeatedly scan the whole sky to make astrometric measurements, and its observing pattern allows for the discovery of many transients, including novae. Usually, a pair of observations are taken 106.5 minutes apart and followed up 2–4 weeks later if the field is not Sun constrained. Though the cadence is much lower than ASAS-SN observations, the high angular resolution ($0.06'' \times 0.18''$), the broad G-band observing filter, and the limiting magnitude ($G < 19$ mag.), make *Gaia* sensitive to certain novae in the plane that no other survey can detect (Hodgkin, S. T. et al., 2021). So, these two surveys are sensitive to different types of hard to detect novae: ASAS-SN to fast novae and *Gaia* to highly reddened novae in crowded fields. Making a rate estimation using both surveys allows us to better predict the Galactic nova rate, capitalizing on both surveys' distinct strengths.

In Section 4.2, we discuss the sample of novae detected by the surveys and the assumptions we make to calculate the discovery rates. In Section 4.3, we explain how we modeled the population of Galactic novae using a Monte Carlo simulation to estimate the Galactic nova rate. Then, in Section 4.4 we show the results and compare the simulated detections to the

real sample. In Section 4.5, we compare our results to previous estimates and explore how different model assumptions can change the results. Finally, in Section 4.6, we summarize our results and the broader implications.

4.2 Discovered Samples

The direct method of predicting the Galactic nova rate corrects the observed rate for the incompleteness, typically quantified as the recovery efficiency. All spectroscopically confirmed Galactic novae discovered from 2019 to 2021 are listed in Table 4.1. The names and positions of the novae are taken from an online Galactic nova catalog maintained by one of us (K.M.)[1]. Although both ASAS-SN and *Gaia* had been discovering nova candidates before 2019, the observing strategies and pipelines were less stable and hence more difficult to model.

If the nova was detected by ASAS-SN or *Gaia*, we list the date of first detection and the peak detected brightness for each respective survey. The peak brightness does not always occur on the date of first detection, and the peak brightness detected by a survey can be significantly fainter than the true peak brightness if a nova was first detected after a seasonal gap. To be as complete as possible we also list reported transients that were never followed up spectroscopically and could have been classical novae in Table 4.2 (individual objects are discussed in Sections 4.2.1 and 4.2.2).

[1] "Koji's List of Recent Galactic Novae"; `https://asd.gsfc.nasa.gov/Koji.Mukai/novae/novae.html`

Table 4.1. Confirmed Galactic Classical Novae 2019–2021

Name	RAJ2000 h m s	DEJ2000 ° ′ ″	ASAS-SN t_0 yyyy-mm-dd	peak g mag	*Gaia* t_0 yyyy-mm-dd	peak G mag
AT 2021abud	15:27:31.61	−55:06:23.8			2021-10-06	13.9
AT 2021abxa	17:54:14.14	−24:12:23.5			2021-09-20	13.8
AT 2021aaav	17:32:21.96	−33:01:41.5			2021-09-19	18.2
AT 2021aadi	18:00:44.88	−21:39:40.5			2021-09-20	16.2
ASASSN-21pa	17:26:19.38	−33:27:10.7	2021-07-30	17.5	2021-08-22	14.
AT 2021wkq	16:44:50.21	−45:15:48.1			2021-08-18	16.3
RS Oph	17:50:13.17	−06:42:28.6	2021-08-10	5.8		
V0606 Vul	20:21:07.70	+29:14:09.1	2021-07-16	10.6		
V1711 Sco	17:39:44.74	−36:16:40.6	2021-06-22	12.8	2021-09-18	15.5
V1674 Her	18:57:30.98	+16:53:39.6	2021-06-12	9.4		
AT 2021nwn	19:12:38.61	+12:41:34.4			2021-05-12	15.7
V2030 Aql	19:07:58.62	+08:43:45.8			2021-05-13	17.3
V1710 Sco	17:09:08.11	−37:30:40.9	2021-04-12	9.7		
V6595 Sgr	17:58:16.09	−29:14:56.6	2021-04-05	9.0		
V6594 Sgr	18:49:05.07	−19:02:04.2	2021-03-25	10.1		
V1405 Cas	23:24:47.73	+61:11:14.8	2021-12-16	10.2	2021-03-30	6.5
V3732 Oph	17:33:14.83	−27:43:11.0			2021-02-15	15.7
V1112 Per	04:29:18.85	+43:54:23.0	2020-11-26	8.9	2021-02-16	14.1
V6593 Sgr	17:55:00.00	−21:22:40.1	2020-09-29	11.3		
V1708 Sco	17:23:41.94	−31:03:07.6	2020-09-08	14.4		
V1391 Cas	00:11:42.96	+66:11:20.8	2020-07-28	11.7	2020-08-31	11.6

Table 4.1 (cont'd)

Name	RAJ2000 h m s	DEJ2000 ° ′ ″	ASAS-SN t_0 yyyy-mm-dd	peak g mag	*Gaia* t_0 yyyy-mm-dd	peak G mag
V6568 Sgr	17:58:08.48	−30:05:35.9	2020-07-15	10.6	2020-08-14	16.9
YZ Ret	03:58:29.55	−54:46:41.2	2020-07-08	6.5	2020-08-19	7.2
V2029 Aql	19:14:26.30	+14:44:40.2			2020-08-25	14.0
AT 2020oju	15:25:50.94	−55:10:29.7			2020-07-09	15.9
V6567 Sgr	18:22:45.32	−19:36:02.2	2020-06-02	13.5	2020-08-18	12.8
V2000 Aql	18:43:53.33	+00:03:49.4				
V1709 Sco	17:12:00.18	−40:17:56.7	2020-05-10	16.1		
V0670 Ser	18:10:42.28	−15:34:18.5	2020-02-23	13.9	2020-02-23	11.5
V6566 Sgr	17:56:14.04	−29:42:58.2	2020-02-15	12.3	2020-02-20	11.2
V0659 Sct	18:39:59.70	−10:25:41.9	2019-10-30	9.7		
V2891 Cyg	21:09:25.53	+48:10:52.2	2019-10-21	15.6	2019-10-07	12.7
V1707 Sco	17:37:09.54	−35:10:23.2	2019-09-14	13.2	2019-09-15	10.1
V3730 Oph	17:38:31.82	−29:03:47.1	2019-09-12	16.6^X	2019-09-14	12.3
V3890 Sgr	18:30:43.29	−24:01:08.9	2019-08-27	8.5	2019-09-11	10.5
V0569 Vul	19:52:08.25	+27:42:20.9			2019-08-24	13.5
V2860 Ori	06:09:57.45	+12:12:25.2	2019-08-18	12.9	2019-08-19	11.6
V3731 Oph	17:38:34.83	−25:19:04.8	2019-07-12	13.4		
V1706 Sco	17:07:34.17	−36:08:23.2	2019-05-13	13.1		
N Aql 2019	19:03:14.95	+01:20:28.2			2019-04-06	16.2

Note. — List of all spectroscopically confirmed Galactic novae discovered between 2019 and 2021. The names and positions are taken from Koji's List of Recent Galactic Novae and AAVSO's VSX. For both ASAS-SN and *Gaia*, the date of first detection t_0 and the peak brightness are listed. If no values are listed, it was not detected by that survey. X: Though V3730 Oph was detected by ASAS-SN, it was not flagged and reported in the transient pipeline (likely because it was faint), so it is not included in the ASAS-SN discovery rate.

4.2.1 Gaia Discovery Rate

Gaia transients are reported publicly to the *Gaia* science alerts (GSA) website[2], but only 25% of GSA transients have been classified spectroscopically. The vast majority of confirmed candidates are extragalactic supernovae (Hodgkin, S. T. et al., 2021), and as seen in Figure 14 of Hodgkin, S. T. et al. (2021), there are a large number of Galactic plane transients that are not classified. Therefore, the number of confirmed classical novae reported by GSA is certainly lower than the actual number detected. To quantify this, we have searched the

[2]http://gsaweb.ast.cam.ac.uk/alerts

Table 4.2. Unconfirmed Classical Nova Candidates 2019–2021

Name	RAJ2000 h m s	DEJ2000 ° ′ ″	ASAS-SN t_0 yyyy-mm-dd	ASAS-SN peak g mag	*Gaia* t_0 yyyy-mm-dd	*Gaia* peak G mag
Gaia21axf	17:34:38.07	−31:08:00.1			2021-02-16	18.2
Gaia20dfc	15:22:33.52	−55:59:40.4			2020-07-09	14.9
Gaia20btn	17:50:19.43	−31:07:37.9			2020-04-11	18.7
ASASSN-19pw	18:31:05.75	−14:47:52.6	2019-06-22	15.5		
ASASSN-19nf	14:19:35.09	−59:58:24.0	2019-05-13	16.1		
ASASSN-19fd	17:03:19.29	−29:52:23.3	2019-03-05	13.6		
ASASSN-19am	09:30:39.31	−54:47:04.3	2019-01-08	16.3		

Note. — The same columns as Table 4.1 for reported transients from between 2019 and 2021 that could have been novae but have no spectroscopic detections. All of these transients are near the Galactic plane, so they could be luminous enough to be novae at a reasonable distance with moderate extinction. The *Gaia* candidates all appear reddened in their BP/RP spectra, but no color information is available for the ASAS-SN transients. These candidates are given 50% weight compared to the spectroscopically confirmed novae when calculating the discovery rate.

entire archive of GSA transients for missed Galactic nova events.

In September 2021, we performed a retroactive nova search on the $\sim 17,500$ transients in the GSA website. Those at high Galactic latitude (b$> 4^\circ$) or those with small measured outburst amplitudes (amp. < 5 mag) are unlikely to be missed Galactic novae (Kawash et al., 2021b). If the quiescent or historic magnitude is too faint to be detected by *Gaia*, we do not make a cut on the amplitude. We eliminated those at high latitude and those with small amplitudes, and the number of candidates decreased to 435. The bright candidates ($G < 14$ mag) have all been classified, with the vast majority being classical novae plus a few high amplitude dwarf nova outbursts. The faint candidates ($G > 14$ mag) also include confirmed, and highly reddened, classical novae, but there are also many unclassified transients. In the absence of extinction, an intrinsically faint nova with peak absolute magnitude $M_G = -5$ mag at a large Galactic distance of 20 kpc would peak at an apparent magnitude of $m_G = 11.5$, so the faint ($G > 14$ mag) nova candidates will all be heavily extinguished and appear

red. Most reported transients also include a low resolution (R $\sim$ 100) and uncalibrated (in wavelength and flux) BP/RP spectrum, a tool that has proven to be crucial in identifying highly reddened nova candidates. We examined the spectra of the remaining unclassified candidates to identify any transient with a majority of its flux in the red RP filter or with strong emission lines. This identified five highly reddened Galactic plane transients detected between 2019 and 2021 with no spectroscopic followup.

We obtained spectra of these candidates using the Goodman spectrograph (Clemens et al., 2004) on the 4.1 m Southern Astrophysical Research (SOAR) telescope to look for evidence of past nova eruptions. We detected spectral features in Gaia20dfb and Gaia21dwe consistent with past nova eruptions (Kawash et al., 2021a) and list them as confirmed novae in Table 4.1. Because the followup observations were taken months to years after the eruption and the sources are likely highly extinguished, we did not detect flux from Gaia21axf, Gaia20btn, and Gaia20dfc, but we still consider these transients as Galactic nova candidates and list them in Table 4.2 because their positions, colors, spectral features, and lightcurves are all consistent with other classified classical novae. Their colors rule out the most common type of classical nova contamination (dwarf novae; Kawash et al. 2021b), but the chance of contamination from microlensing events, young stellar objects, and Be star outbursts remains. Given the rate of confirmation of other candidates, and in lieu of a more complex contamination model, we assign each of these candidates a 50% probability of being a nova for our Monte Carlo simulations described in Section 4.3.

As seen in Table 4.1, *Gaia* reported 7, 8, and 12 confirmed novae in 2019, 2020, and 2021, respectively, with an additional 3 unconfirmed candidates listed in Table 4.2. Assuming Poisson uncertainty for this sample of $\sim$ 28.5 novae yields a mean and standard deviation of the discovery rate of 9.5 and 1.8 yr^{-1}, respectively when running the Monte Carlo simulation

over the years 2019 to 2021. The dates listed as "*Gaia* t_0" in Table 4.1 are the epoch of *Gaia*'s first detection, which can lag the start of the eruption by weeks to months because of *Gaia*'s non-uniform scanning law.

4.2.2 ASAS-SN Discovery Rate

The ambitious goal of ASAS-SN to observe the entire night sky daily has provided unprecedented cadence for Galactic observations of transients. ASAS-SN transients are reported publicly to https://www.astronomy.ohio-state.edu/asassn/transients.html. In 2018, ASAS-SN switched from observing in V-band to exclusively observing in g-band. To allow time for deep g band reference images to be built, we only calculate the discovery rate between 2019−2021. Over this time period we inspected all the ASAS-SN data of confirmed Galactic novae, and found that 26 novae were detected in the transient pipeline. If there is no ASAS-SN value for t_0 or peak brightness listed in Table 4.1, the nova was too highly reddened, and therefore too faint ($g \lesssim 18.5$ mag) to be detected by ASAS-SN. V3730 Oph was detected at $g = 16.6$ mag but was never flagged in the pipeline as a transient (fainter transients have a smaller chance of being reported relative to brighter ones). We therefore do not include it as a nova in the ASAS-SN discovery rate. Kawash et al. (2021b) found that there were four more reported CV candidates in 2019 that could be luminous enough to be novae if they are distant enough to be significantly obscured by dust extinction. As for the *Gaia* candidates, we make the simple assumption that these four candidates, listed in Table 4.2, have a 50% probability of being classical novae. So, over the three years considered here, there were 26 confirmed and 4 unconfirmed novae, for a total population of 28 novae. Assuming Poisson statistics yields a mean and standard deviation of the ASAS-SN discovery rate of 9.3 and 1.8 yr^{-1}, respectively.

4.2.3 The joint ASAS-SN and Gaia Discovery Rate

If we combine both surveys and account for overlapping discoveries, there were a total of 39 confirmed classical novae and 7 additional candidates detected between 2019–2021. This yields a mean and standard deviation of the discovery rate of 14.2 and 2.3 yr^{-1}, respectively. While this observed nova rate is still far below most predictions, it is still the highest *observed* rate ever used to infer the total nova rate.

4.3 Monte Carlo Simulations

Our work attempts to repeatedly answer this basic question: if a nova erupted at a specific time and location in the Galaxy, would it be detected and reported as a transient by ASAS-SN and/or *Gaia*? This idea is expanded to a large sample of simulated novae to estimate what fraction of the Galaxy's novae these surveys detect. By implementing a Monte Carlo analysis, we derive the most likely Galactic nova rate and accompanying uncertainty based off of ASAS-SN and *Gaia* observations and the uncertainty in the model parameters.

4.3.1 Positions

The positions of the model novae in the Galaxy are derived by assuming that they trace the stellar mass density of the Galaxy. The stellar density model is outlined in the appendix of Kawash et al. (2021c) and includes a thin disk, thick disk, and halo component as described in Robin et al. (2003) and a two component, elongated, triaxially symmetric bulge from Simion et al. (2017). The ratio of the disk mass to the bulge mass, and therefore the ratio of disk to bulge novae assuming equal production per stellar mass, is 1.7. For each run of the Monte Carlo simulation, we randomly pick 1,000 nova positions from a possible 10,000

positions. Because this study requires lightcurves to be generated in each survey at every position, we limit the total number of possible positions to 10,000. In Kawash et al. (2021c), we explored how sensitive the derived nova rate is to the stellar density model, where it was found to change results by $\sim$ 15% for the ASAS-SN rate, subdominant to other uncertainties in our calculation.

4.3.2 Peak Apparent Magnitude

The peak absolute magnitude of each nova is assigned by randomly sampling a normal distribution, described with a mean and standard deviation of $M_{g,G} = -7.2 \pm 0.8$ mag (Shafter, 2017). This distribution was measured from M31 novae, and we assume the Milky Way has an identical distribution.

The extinction along the line of sight to each nova position is calculated from the `mwdust` package (Bovy et al., 2016). We use the `combined19` version of this extinction model, which is built by combining the Marshall et al. (2006) map of the inner Galactic plane, the Green et al. (2019) map of the Northern Hemisphere, and the Drimmel et al. (2003) map of the Southern Hemisphere. The various maps take precedence over each other where they overlap in the order they were listed above. The vast majority of the model novae (95%) lie in the Marshall et al. (2006) map region of the sky. For ASAS-SN, we query the extinction in the SDSS g-band, as it is the most similar to ASAS-SN's g-band filter. Extinction in the broad *Gaia* G-band filter is not directly accessible in `mwdust`, so we estimate this value by first querying the extinction in the SDSS g- and SDSS i-bands. The relationship between these SDSS filters and *Gaia's* G-band filter were fit to a third order polynomial with the form

$$G - g = -0.1064 - 0.4964x - 0.09339x^2 + 0.004444x^3 \tag{4.1}$$

where $x = g - i$ (Gaia Collaboration et al., 2021).

An additional concern when estimating the extinction for a model of Galactic novae is that the 3D dust maps that comprise the `mwdust` package only estimate the extinction out to distances where the colors of stars can be measured, and therefore do not extend to the largest Galactic distances and the highest extinction regions. If a model nova is beyond the largest distance bin of `mwdust`, we add extinction by fitting the amplitude of the extinction along a line of sight and assuming the dust is described with an underlying double exponential distribution that is a function of Galactic radius and height from the plane. We use $(r_0, z_0) = (3.0, 0.134)$ kpc for the scale length and height, respectively (Li et al., 2018). The amount of extinction is fit out to the distance where `mwdust` has information, then we use the results to extrapolate to the nova distance. For 55% of simulated novae, `mwdust` extends to the distance of the nova, so no extinction is added. For those remaining novae beyond the 3D dust maps, the mean extinction added in the g- and G-bands is 0.9 and 0.6 mag, respectively. The distributions of estimated extinction before and after this correction are shown in Figure 4.2. The median nova will experience ~ 10 mag of extinction in g-band and ~ 6 mag of extinction in G-band.

With the peak luminosity, the distance, and the extinction in g- and G-bands estimated, the peak apparent magnitude of each model nova can be calculated using the distance modulus. The results are shown for 10,000 model novae in Figure 4.3. The differences between the *Gaia* and ASAS-SN peak apparent magnitude distributions are entirely due to the different observing filters used; the bluer ASAS-SN g-band is more vulnerable to extinction from interstellar dust compared to the broader *Gaia* G-band. This figure shows that extinction is the largest factor in determining the apparent brightness of a Galactic nova. The dashed black distribution ignores extinction, and therefore its variance is caused by variations in

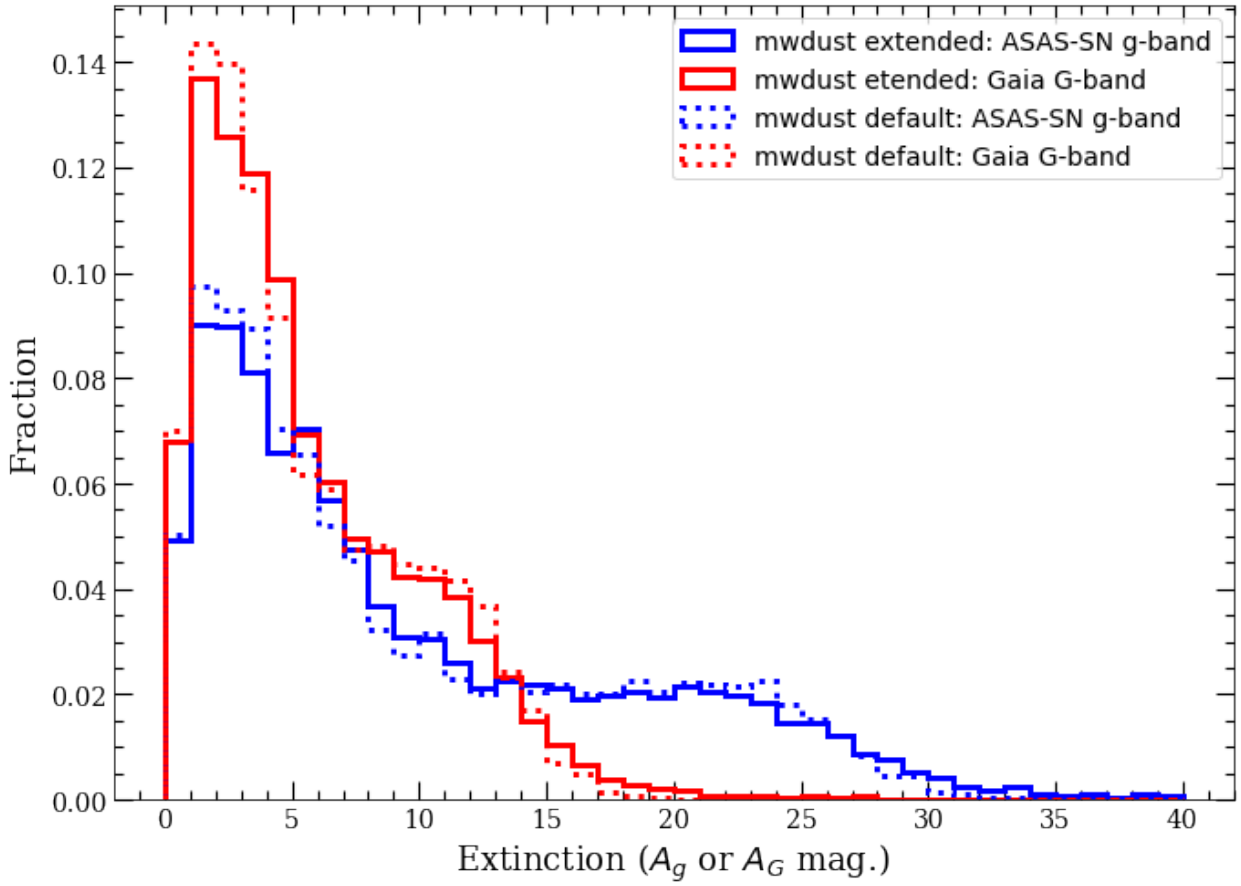

Figure 4.2 The normalized extinction distributions of 10,000 simulated novae in the ASAS-SN g-band filter (blue) and *Gaia* G-band filter (red). These distributions are estimated from the `mwdust` package (default values shown as dotted lines), and we add additional extinction if the line of sight is not complete out to the distance of the nova (solid line).

the luminosity and distance of a nova; in this case, the median absolute deviation in the peak apparent brightness is only 1.1 mag. However, when considering extinction, the median absolute deviation of the peak brightness seen in *Gaia*'s G-band filter is 4.2 mag, and in ASAS-SN's g-band filter, the median absolute deviation is 7.2 mag. Based only on the peak brightness, $\sim 90\%$ percent of Galactic novae are bright enough to be detected by *Gaia* ($G < 19$ mag), compared to the only $\sim 60\%$ percent detectable by ASAS-SN ($g < 18.5$ mag.).

Some studies have suggested that Milky Way novae are more luminous than M31 novae (Shafter et al., 2009; Özdönmez et al., 2018), but we do not explore different luminosity functions as it is clear that extinction is a much larger factor than the absolute magnitude for determining the brightness of a nova in the optical.

4.3.3 Lightcurves

The modeling work to derive the apparent magnitude distribution of Galactic novae was largely laid out in Kawash et al. (2021c), but the detection efficiency in the survey data was only broadly estimated. Here, we incorporate the model into each survey's data to more accurately estimate the detection efficiency. Each simulated nova is given a random eruption date between January 1, 2019 and December 31, 2021. While in principle novae first discovered at the start of our survey period (2019 January) could have exploded in 2018, and hence outside of our simulation, the predicted and observed number of novae in the first half of January is so low that this potential issue does not have a meaningful ($\lesssim 1\%$) affect on our results. Though not entirely symmetric, this effect is also diminished by novae that erupt near the end of the simulation in late 2021 that would be discovered in 2022, after the end of the simulation.

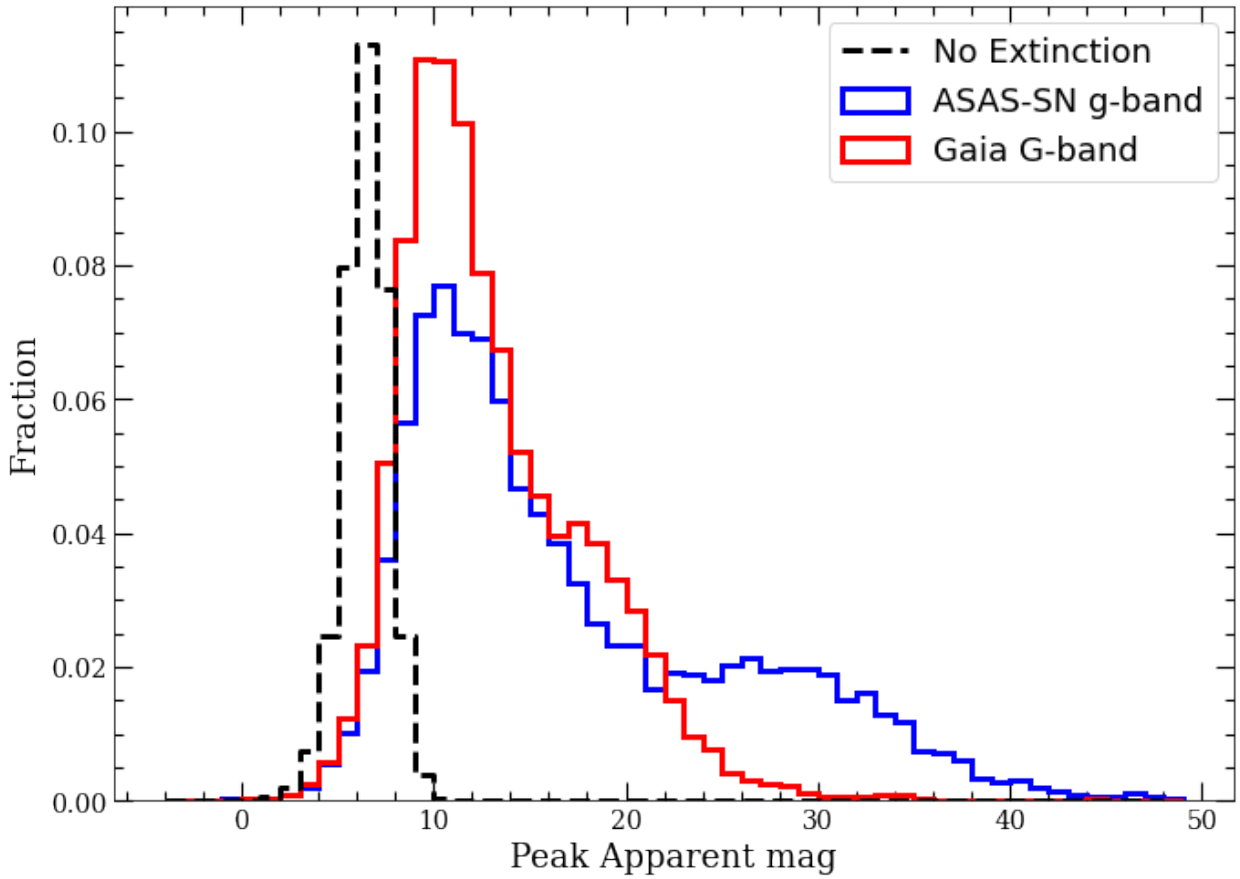

Figure 4.3 The normalized distributions of peak apparent magnitude of 10,000 simulated novae in the g-band filter (blue) and G-band filter (red). Also shown is the distribution with zero extinction with the peak scaled to fit (black dashed line). This demonstrates that dust is a much larger factor than the luminosity or distance in determining the peak apparent magnitude of a nova.

The temporal evolution of the brightness is modeled by sampling a distribution of nova speeds and then constructing the full shape of the lightcurve from a sample of known nova lightcurves. We used 93 AAVSO V-band nova lightcurves from Strope et al. (2010) and 75 Stony Brook/SMARTS V-band lightcurves from Walter et al. (2012) as lightcurve templates. V-band was chosen because it was the most well-sampled filter from the two databases and also close to the g and G bands of ASAS-SN and *Gaia*. Motivated by the typical intrinsic colors of novae (e.g., van den Bergh & Younger 1987b), we assume a flat spectrum ($V_{\rm peak} = g_{\rm peak} = G_{\rm peak}$) when transforming these templates to g- and G-band.

Previous completeness studies have used several methods to estimate how long a nova is detectable, including defining a discrete number of observable days after eruption (Mróz et al., 2015b) and assuming a linearly declining lightcurve (De et al., 2021). By using real lightcurves as templates, we do not have to make simplifying assumptions about the shape of the lightcurves, which can be quite complex (Strope et al., 2010). However, we also carry out the analysis by using linearly declining lightcurves to explore how sensitive the results are to this property and discuss the results in Section 4.5.2.

We took additional steps to reduce errors in the light curve templates. A template should only include flux from the nova eruption and not from when the nova has returned to the quiescent state or from nearby background stars. Most of the quiescent magnitudes are listed in Table 1 of Strope et al. (2010) for the novae presented in that work, so we truncate the lightcurve once it declines to within 3 mags of this quiescent magnitude. Walter et al. (2012) notes that there are cases in the SMARTS sample of novae when the fading remnant becomes blended with a background star, and from inspecting these lightcurves, this does appear to be true in a few cases. We also cut off lightcurves within a magnitude of any prolonged plateaus many magnitudes below maximum to eliminate this contamination. If

the duration of the template lightcurve is shorter than the survey length, we extend the template by assuming it will decline linearly at the average pace of the lightcurve.

Each nova is randomly assigned a decline speed by sampling a log-normal distribution for t_2 (the time it takes a nova to decline two magnitudes from peak) with mean and standard deviation equal to 18.7 and 3.2 days, respectively, based on modeling of observed novae and accounting for selection effects (Kawash et al., 2021b).

There has been a large effort to establish novae as standard candles. The relationship between the luminosity and the speed of a nova, commonly referred to as the maximum magnitude vs. the rate of decline (MMRD) relation, was once thought to be tightly correlated (Capaccioli et al., 1989a; della Valle & Livio, 1995), but in recent years, many examples of novae that do not follow the published relationships have been found, especially those that are fainter and faster (Kasliwal et al., 2011; Shara et al., 2017a). These faint fast novae have been suggested to be a reason for a factor of three discrepancy in extragalactic nova rate estimates (Shara et al., 2016). In our primary model, we assume the luminosity of a nova simply sets an upper bound on the speed or t_2 value. Put another way, the luminous novae are restricted to having small t_2 values, but the fainter novae are allowed all values of t_2. The boundary between the forbidden and allowed values is shown as a blue dashed line in Figure 4.4 with the allowed values being below this line. Any model nova with a given luminosity that is assigned a forbidden t_2 value has this parameter resampled until an allowed value is found. This forbids luminous slow nova, as no such example has been found but allows for any number of faint fast novae.

The maximum magnitude versus rate of decline of 10,000 model novae are shown in Figure 4.4. The distribution of t_2 is discontinuous because of the discrete t_2 values of the template lightcurves. Also show on this plot is the MMRD correlation measured in

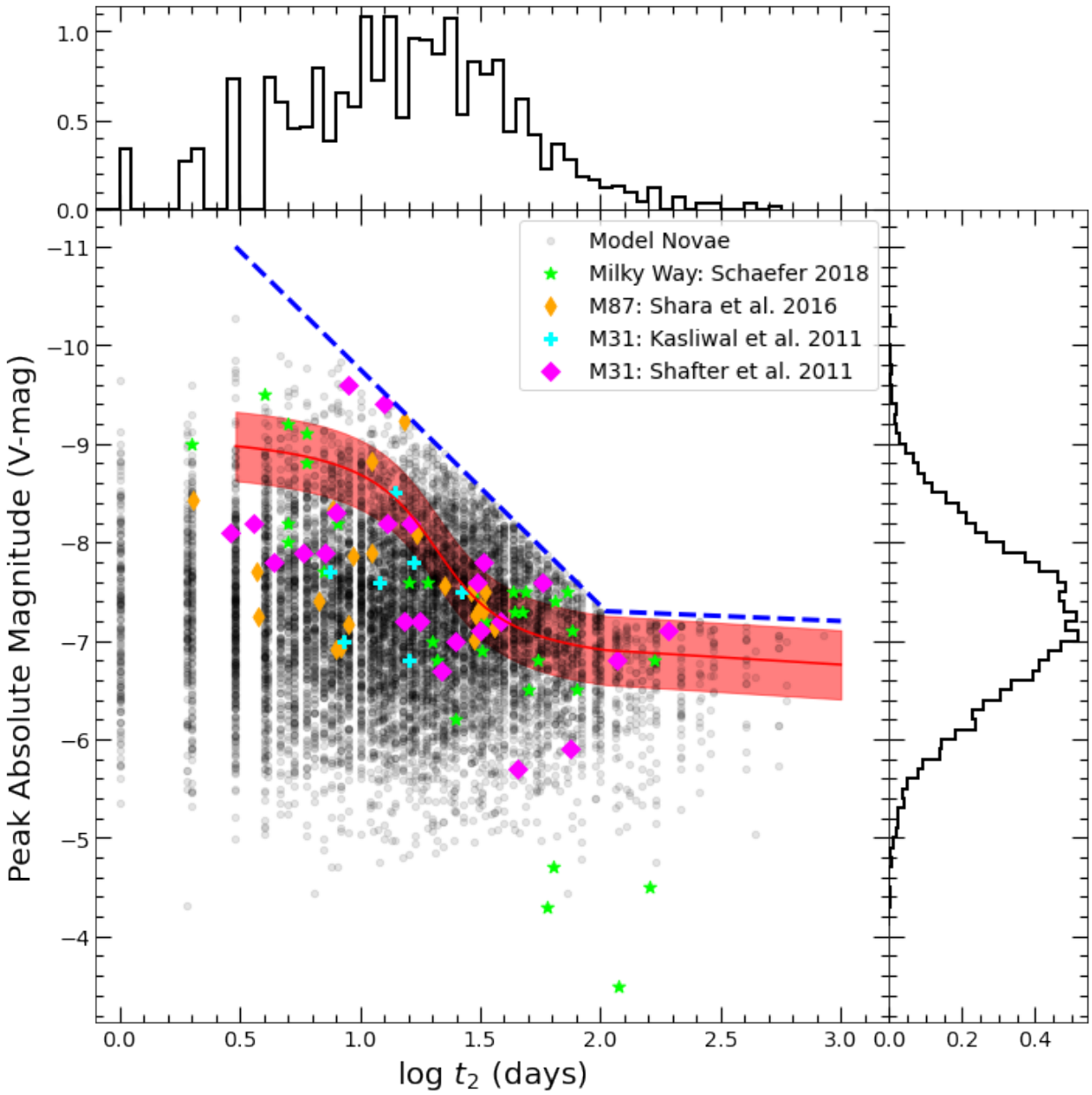

Figure 4.4 Distribution of the peak absolute magnitude versus time to decline by two magnitudes from maximum (t_2) for 10,000 model novae (black dots). The peak absolute magnitudes are sampled from a normal distribution, and the t_2 values are sampled from a log-normal distribution. The patchiness in the t_2 distribution is the result of a limited number of nova lightcurve templates. The allowed values in this parameter space are shown below the blue dashed line, and this is compared to real Galactic nova values estimated from *Gaia* distances (Schaefer 2018; denoted with green stars), extragalactic measurements (pink diamonds, cyan crosses, and orange diamonds; Shafter et al. 2011; Kasliwal et al. 2011; Shara et al. 2016), and the MMRD correlation derived in della Valle & Livio (1995) (shown as the red shaded region).

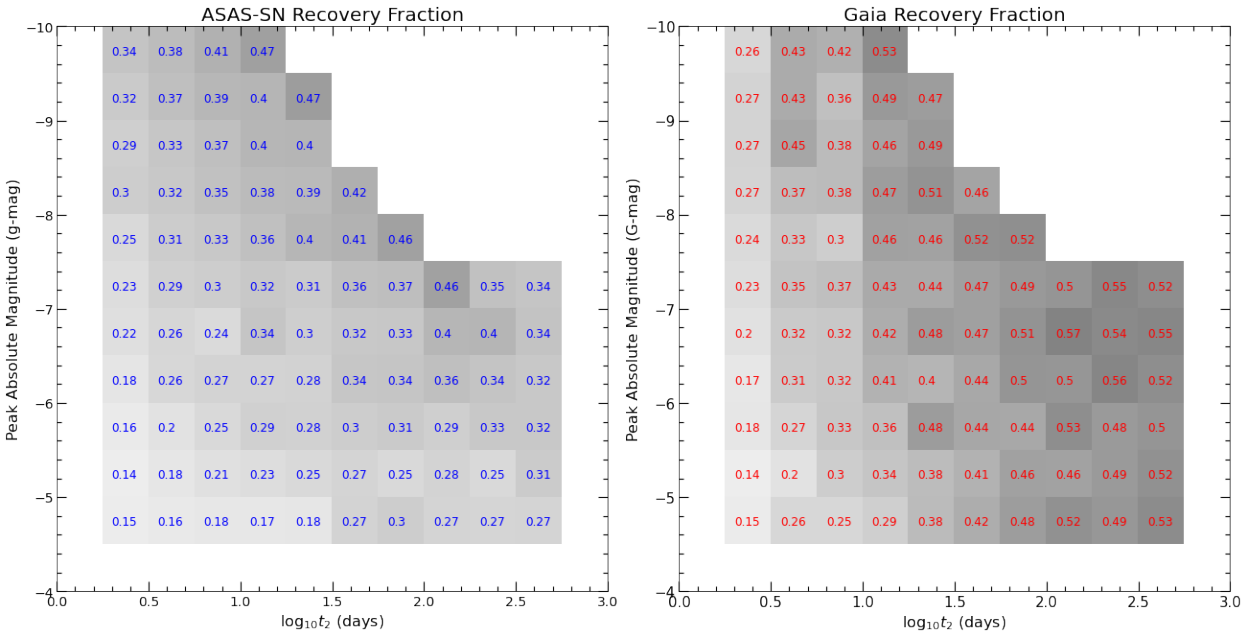

Figure 4.5 The recovery fraction of model novae in ASAS-SN and *Gaia* as a function of peak absolute magnitude and t_2. The recovery fraction values are calculated on a grid of 0.5 mag by 0.25 $\log_{10}(t_2)$ days, and are shown on each square, with darker grey-scale indicating a higher recovery fraction. While novae that adhere to the supposed MMRD relation are on average easier to detect, they are only recovered about twice as efficiently as faint fast novae, implying that all-sky surveys would have detected a substantial population of faint fast novae if they were present.

della Valle & Livio (1995) as the red shaded region, real Galactic nova values measured from "Gold" and "Silver" *Gaia* distances (denoted as the green stars; Schaefer 2018) , and various extragalactic novae (Shafter et al., 2011; Kasliwal et al., 2011; Shara et al., 2016). The faint, fast novae are arguably over represented in our model compared to observations, so we also rerun the analysis by treating MMRD as a strict correlation and discuss the results in Section 4.5.2. We explored the detection efficiency of each survey in this parameter space (see §4.3.4 and 4.3.5 for details on detection efficiency), and the results are shown in Figure 4.5. Though faint fast novae are clearly harder to detect in the model, the difference in the recovery fraction of faint fast novae compared to novae that adhere to the MMRD relation is no more than a factor of two. This means that it is unlikely a large population of faint fast novae exists in the Galaxy that has not been detected by all-sky surveys, unless such novae have a very different spatial distribution and are more embedded in dust than typical novae.

Once each model nova is given a decline rate, we assign a lightcurve template by finding the Strope et al. (2010) or Walter et al. (2012) lightcurve closest to the randomly assigned t_2 value. The template is then scaled so that the peak apparent magnitude matches the value calculated above. The model novae now have all of the information needed to inject them into the survey data, and below we discuss how that is performed for each survey.

4.3.4 Gaia Simulation

For each nova position we used the Gaia Observation Forecast Tool[3] to provide the epochs at which *Gaia* observed the location, and we assume a fixed detection threshold of $G < 19$ mag. We then sample the template lightcurve at the cadence of *Gaia*, and several examples

[3]https://gaia.esac.esa.int/gost/

are shown in the right-hand column of Figure 4.6. We draw the noise in the lightcurve from a normal distribution with standard deviation

$$\sigma = 3.43779 \text{ mag} - (\text{G}/1.13759\ ) + (G/3.44123\ )^2 - (G/6.51996\ )^3 + (G/11.45922\ )^4 \quad (4.2)$$

if $13 < G < 19$ mag and $\sigma = 0.02$ mag for $G < 13$ mag.

To determine if a model nova would be reported by GSA we start with three basic requirements (outlined in Hodgkin, S. T. et al. 2021). First, there need to be detections in both FOVs (fields of view; preceding or trailing) brighter than $G < 19$ mag within 40 days of each other. Second, the detected brightness needs to exceed that of all stars within a $1.5''$ radius in *Gaia* DR2, and last, there cannot be a $G < 12$ mag star within a $10''$ radius in *Gaia* DR2.

Even if a transient satisfies these three requirements, there are additional ways for it to be missed in the pipeline. For example, a single source can have: multiple source IDs, ambiguous matches in *Gaia* DR2, or multiple sources within the core region, etc. (Kostrzewa-Rutkowska et al., 2018). It is difficult to determine when this will happen in the simulation, so we make a statistical estimate by looking at the reporting efficiency of novae in Table 4.1. There are 20 novae reported by GSA that were also detected by other surveys (amateurs, ASAS-SN, PGIR, etc.); however, after further inspection of the *Gaia* database and the *Gaia* observation forecast tool, there are 7 additional novae (V0569 Sct, V1708 Sco, V5693 Sgr, V1710 Sco, V1674 Her, V0606 Vul, and RS Oph) that should have been reported based on the three major criteria listed above. So, GSA reported no more than $20/27 \approx 74\%$ of the novae that passed these criteria, and the true reporting efficiency is likely somewhat lower because of the

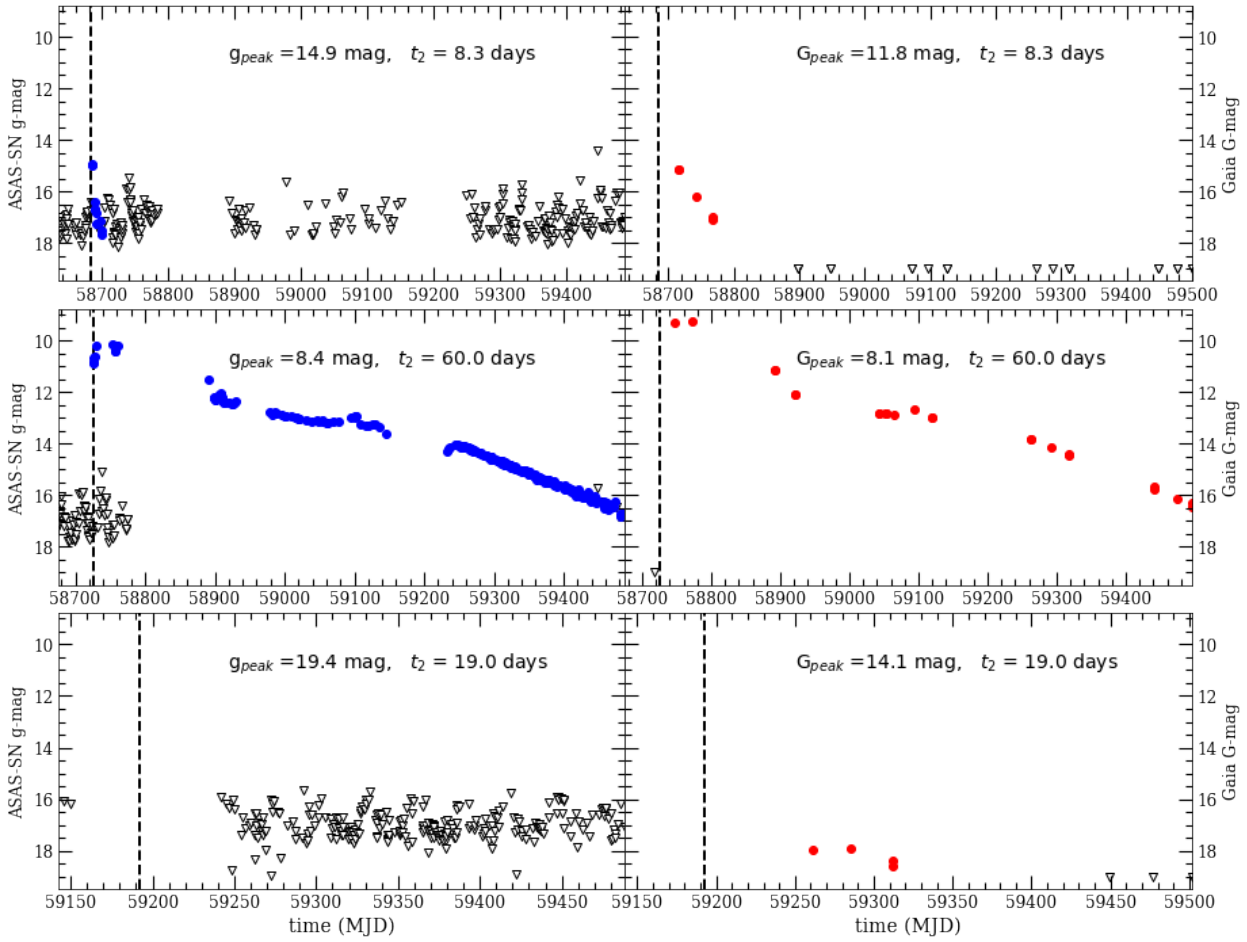

Figure 4.6 Three examples of simulated novae in ASAS-SN (left) and *Gaia* (right). The detections are shown in blue for ASAS-SN and red for *Gaia*, with non-detections shown as black triangles. The epoch of eruption is denoted by the vertical dashed line and the peak apparent magnitude and t_2 are listed in each panel. The top row shows a fast reddened nova, the middle row shows a nearby and slow nova (the non-detections shortly after the eruption indicate that the transient has saturated the ASAS-SN detectors), and the bottom row shows a reddened nova that was only detected by *Gaia*.

strong chance of additional candidates that were unreported by other observers. We treat this estimate as a 1σ upper limit with 10% uncertainty, so for each Monte Carlo trial, we assign *Gaia* a reporting probability for novae that pass all of the hard-coded requirements by sampling a normal distribution with mean $\mu = 0.67$ and standard deviation $\sigma = 0.067$. This is necessarily a crude model to summarize the complex process that leads to a candidate nova being reported and undoubtedly an important source of uncertainty in our simulations. Future observations of novae and *Gaia* alerts can help constrain this reporting efficiency.

4.3.5 ASAS-SN Simulation

The cadence and limiting magnitude of ASAS-SN observations were calculated by constructing image subtraction lightcurves without adding the reference flux from the ASAS-SN data over the 10,000 positions of the model novae. This automatically provides a sampling of the cadence, noise uncertainty (due to the lunar cycle and weather conditions), and contamination from bright, nearby stars. The formal photometric uncertainties reported in ASAS-SN lightcurves tend to underestimate the true uncertainties (Jayasinghe et al., 2018b), and this can particularly be true in the Galactic plane due to crowding, even with the benefits of image subtraction. We estimated a rescaling of the uncertainties for each light curve by looking at the distribution of the ratio f_i/σ_i where f_i is the flux and σ_i is the reported error in the flux of each camera at each position. If the error estimates are correct, then the standard deviation of this distribution should be unity. When it is larger, contamination is present, so we increase σ_i by the factor needed to make the distribution unity. For many of the random nova light curves, the rescaling is large enough to lead to a ~ 1 mag reduction in sensitivity on average. Because this work is looking at Galactic novae which tend to be located at crowded low Galactic latitudes, these affects are more severe than compared to

an extragalactic supernova study.

When injecting the model nova lightcurves into the ASAS-SN data, we assume that the nova would be detected if it is brighter than these rescaled 5σ upper limits on each particular epoch. Similar to the *Gaia* analysis, we fit a polynomial to photometric errors in ASAS-SN data, and we add noise to the lightcurve templates by sampling a normal distribution with a measured standard deviation of

$$\sigma = 0.08 \text{ mag} + 0.04(\text{g} - 13) - 0.04(\text{g} - 13)^2/\text{mag} + 0.02(g - 13)^3/\text{mag}^2 - 0.002(\text{g} - 13)^4/\text{mag}^3 \quad (4.3)$$

if $13 < g < 18.5$ mag, and $\sigma = 0.02$ mag for any $g < 13$ mag.

When a transient is reported by ASAS-SN, it is cross checked to catalogs like *Gaia* and the Panoramic Survey Telescope and Rapid Response System (Pan-STARRS; Chambers et al. 2016) to roughly estimate the outburst amplitude. This helps differentiate classical nova candidates from other CV outbursts, but the large pixel scale of ASAS-SN ($8''$ per pixel) can lead transients to have underestimated outburst amplitudes when their position is coincident with another star. To account for this, we also require detections to be 5 mags brighter (Kawash et al., 2021b) than the closest star in *Gaia* DR2 within half an ASAS-SN pixel, to assure the transient would be recognized as having a large outburst amplitude.

The goal of the ASAS-SN pipeline is to discover previously unknown transients and variable stars. To avoid continually looking at known variables, the ASAS-SN pipeline does not generate candidate images for flux changes detected within 5 pixels of known Mira, long-period, or semi-regular variables. A list of the positions, types, and magnitude range of known variables is acquired from VSX and OGLE and is maintained in the ASAS-SN

database. We inspect this same list in the simulation and require that the model novae also satisfy this condition. If a transient is near a different type of variable, a candidate image will be generated; however, if a new transient is found near a known one, it is possible for the new transient to be confused with a known repeater and consequently not reported. To incorporate this into the model, a transient has to be a magnitude brighter than the listed magnitude range of any known variable within half an ASAS-SN pixel of the simulated nova.

The last step for a transient that is detected by ASAS-SN to be reported is that a human needs to flag the source in the data as real and previously unreported. As mentioned above, the probability of this occurring scales with the SNR. The images of bright candidates ($g < 15$ mag) generate alert emails and are filtered into a pipeline dedicated to finding Galactic classical novae. Fainter Galactic transients are commonly reported by ASAS-SN but with lower completeness due to the number of false positives from artifacts increasing at fainter magnitudes. Generally, the closer a candidate is to the detection limit, the less likely the image is to be vetted by a human and reported as a transient. The probability for a single detection of an extragalactic supernova to be reported in ASAS-SN was studied by **Desai et al. (2022, in prep)** and found to be

$$\begin{cases} 0.65 & SNR >= 12 \\ (1 + (\mathrm{SNR} - 12)/7) \times 0.65 & SNR < 12 \end{cases} \tag{4.4}$$

where SNR is the signal-to-noise ratio of each detection. In the simulation, each detection that satisfies the above requirements has this probability of being flagged. This detection probability is per individual epoch, so the brighter and slower transients have a much higher likelihood of being reported than the faint and fast ones.

4.4 Global Nova Rate Estimates

The results of the Monte Carlo simulation show the probability distribution of the global Galactic nova rate based upon ASAS-SN and *Gaia* observations and reporting of Galactic novae between 2019 and 2021. We run the Monte Carlo 1,000 times, each time sampling different values for: (i) the nova positions, (ii) the lightcurves' speed and shape, (iii) eruption dates, (iv) peak luminosities, (v) the probability of detected transients being reported, and (vi) the discovery rates based on Poisson sampling. The Galactic nova rate is then calculated for each trial by dividing the discovered rate by the estimated recovery fraction for each respective sample. Each trial provides a different estimate of the Galactic nova rate, and we take the median rate as the most likely and 68.2% of the width as the 1σ uncertainty. The results of the Monte Carlo simulation are shown in Figure 4.7.

We simulate the *Gaia* and ASAS-SN surveys individually and as a joint search, providing three estimates of the Galactic nova rate. The joint estimate might appear to be redundant with the former two, but the fraction of novae discovered by neither, one, or both surveys provides additional information not captured in the prediction from a single survey since the surveys have different filters and cadences. The three rates are all consistent at the 1σ level: ASAS-SN, *Gaia*, and the combination of both surveys predict global Galactic nova rates of 28^{+6}_{-6} yr^{-1}, 22^{+5}_{-4} yr^{-1}, and 26^{+5}_{-4} yr^{-1}, respectively. This work estimates that the combined efforts of both all-sky surveys were able to detect $\sim$ 54% of the Milky Way's classical nova eruptions that occurred between 2019−2021, a much higher recovery fraction than recently estimated (Özdönmez et al., 2018; De et al., 2021). Individually we estimate that the recovery fraction of ASAS-SN is $\sim$ 33% and the recovery fraction of *Gaia* is $\sim$ 42%.

Breaking those estimates down further, for ASAS-SN, about 40% of novae are too faint

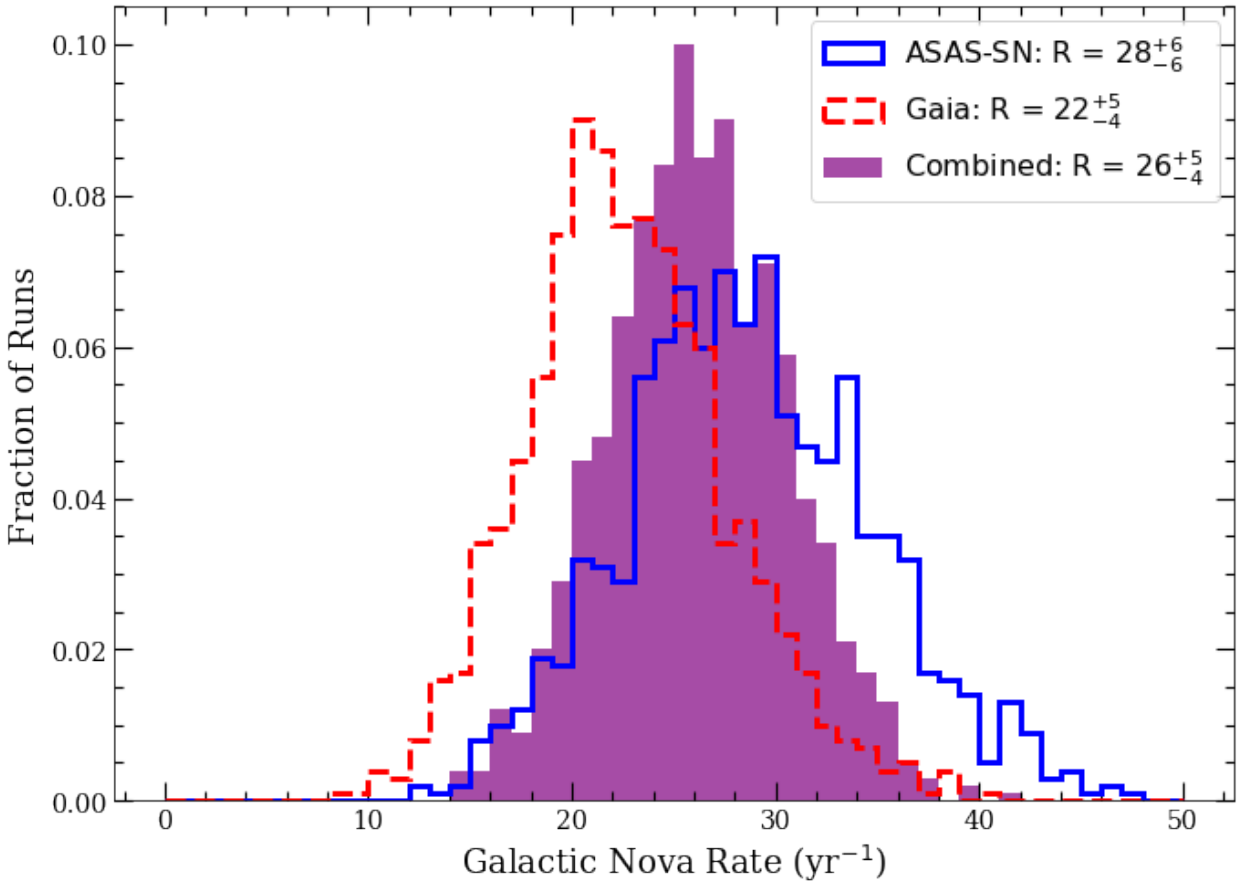

Figure 4.7 The predicted Galactic nova rate based on 1,000 Monte Carlo trials, from ASAS-SN (blue histogram), *Gaia* (red histogram), and a combination of both surveys (purple histogram). We give the median values of the distributions as the most likely Galactic nova rate, and include the 16% and 84% confidence regions. The redundancy of the three distributions is low, as the combined results are sensitive to when a nova is detected by both, just one, or neither surveys. The results are all consistent at the 1σ level, with the most likely rate from both surveys predicting a Galactic nova rate of $R = 26 \pm 5$ yr^{-1}.

for discovery because they are too highly extinguished, an additional $\sim 20\%$ are lost because there is not an observation while the nova is brighter than the average detection limit of $g < 17$ mag (largely from seasonal gaps), and the last $\sim 7\%$ are lost because of various pipeline features (low SNR, confusion, avoiding known variables, etc.). This is a lower fraction of novae lost because of cadence and the pipeline than the assumption of 40% used in Kawash et al. (2021c), so the nova rate derived in that work was overestimated.

For *Gaia*, only $\sim 14\%$ of novae are too faint because they are too highly extinguished, $\sim 12\%$ are lost because of lack of cadence, and $\sim 35\%$ are lost because of various pipeline features (requiring detections in both FOVs, source confusion, etc.). This is consistent with the analysis of extragalactic supernovae that found that the scanning law and the need to minimize the false alarm rate dominates the completeness of GSA (Hodgkin, S. T. et al., 2021). Surprisingly, the higher cadence of ASAS-SN loses more novae that peak bright enough for detection than *Gaia*, but this is again because of dust extinguishing novae so that the bluer ASAS-SN observations have a much shorter time for discovery and because ASAS-SN has a lower recovery rate at fainter magnitudes.

To assess the accuracy of the model, we compare the results of the simulation to the real novae in Table 4.1. Any significant conclusions should be taken with caution because of the small sample size of discovered novae, but this exercise can still shed light on the accuracy of the model. First we look at what fraction of the survey's discovery sample were also discovered by the other survey. In the simulation, about 60% of the ASAS-SN discovered novae were also discovered by *Gaia*, compared to the observed value of $14/26 \approx 54\% \pm 14\%$ (assuming Poisson uncertainty) of the ASAS-SN sample from Table 4.1 that were detected by *Gaia*. Roughly 50% of the simulated novae discovered by *Gaia* were also discovered by ASAS-SN, compared to the observed $14/30 \approx 47\% \pm 12\%$ of the real *Gaia* sample. The

overlap in discoveries in the simulation is consistent within uncertainties to the real novae.

The sky positions of the simulated and real samples of novae are shown in Figure 4.8. Again, the degree to which the positions agree is hard to assess because of low number statistics, but there is broad agreement between the distribution of simulated and observed novae. Notably, both the observed and simulated nova populations in the bulge region show more novae at Galactic longitude $l > 0^\circ$ than at $l < 0^\circ$. This is likely due to the elongated bulge ("bar") in this region of the Galaxy, which places typical novae at $l > 0^\circ$ at closer distances, and behind less dust, than those at $l < 0^\circ$.

The apparent exception to the agreement between model and data is in the southern region of the Galactic plane, where no novae were observed between an RA of 8 and 14 hours from 2019–2021. This could suggest a bias against discovering plane novae in the south compared to the north, which would not be expected given that both ASAS-SN and *Gaia* are all-sky surveys. This discrepancy could also primarily reflect small number statistics, since in 2017 and 2018, just before the timespan of this survey, several novae in this southern plane region were indeed discovered (V906 Car, V357 Mus, V549 Vel, V1405 Cen), which would tend to equalize the statistics.

In addition to comparing where novae are found, we also looked at when novae are discovered by the surveys. Although the simulated novae are given random eruption dates uniformly between 2019 and 2021, we do not expect them to be discovered uniformly throughout the year due to annual changes in observing conditions. When the novae are first detected by ASAS-SN and *Gaia* in our models are shown as histograms in Figure 4.9, along with the observed first detections of novae from Table 4.1 with 1σ Poisson errors. From November to January, the Galactic center region is behind the Sun, and therefore much of the Galaxy is not observable. In February, this field becomes observable again and the novae still bright

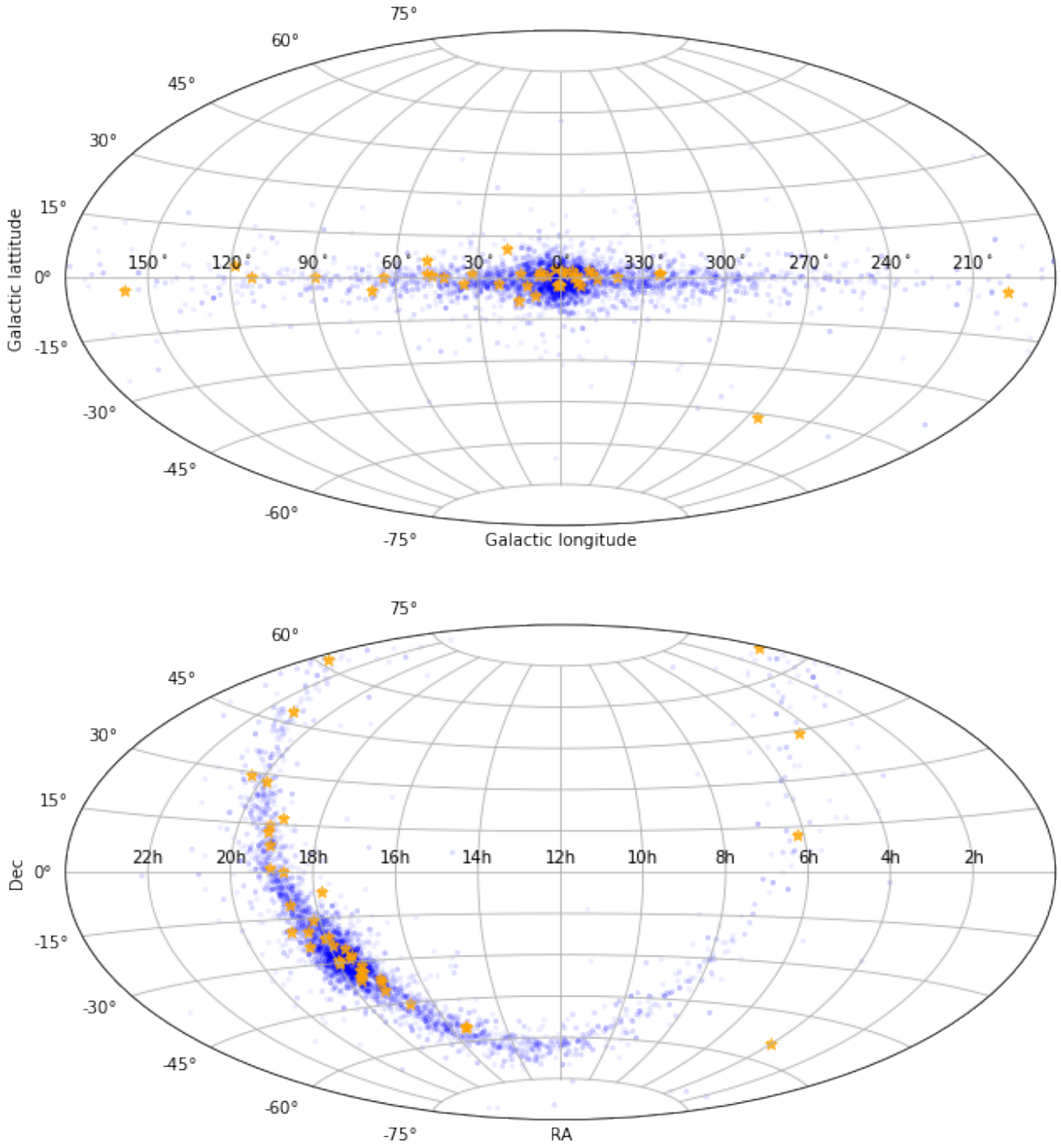

Figure 4.8 The positions of simulated novae that are discovered in our model (blue dots) compared to the real sample discovered between 2019 – 2021 (orange stars). The simulated positions are derived assuming novae trace the stellar density of the Galaxy. The elongated bulge, oriented at a roughly 20° angle from the Sun–Galactic center line, appears to place more recoverable bulge novae at $l > 0°$ compared to $l < 0°$.

enough for detection can be discovered, resulting in our model predicting this month to have the highest discovery rate for ASAS-SN and one of the highest for *Gaia*. These are the only pronounced patterns in the predicted annual discovery rate of ASAS-SN. The satellite observations of *Gaia* also have a second area of avoidance around Solar opposition (see Figures 4 and 5 of Gaia Collaboration et al. 2018a). This causes an annual pattern of two *Gaia* nova discovery seasons lasting roughly three months, with over half of first detections happening in February and August when the Galactic center comes out of the areas of avoidance. The ASAS-SN and *Gaia* detections track relatively well with the model predictions but with large uncertainty because of the small number of novae per monthly bin.

4.5 Comparisons to Previous Results

Our predicted rate of 26 ± 5 yr^{-1} is notably lower than most recent direct Galactic nova rate estimates (see Figure 4.1). It is perhaps consistent with the naked eye nova direct extrapolation rate of 50^{+31}_{-23} yr^{-1} (Shafter, 2017) but mostly due to the latter's large uncertainty. It is inconsistent with the rescaled (because of faint fast novae) M31 inferred Galactic rate of ~ 50 yr^{-1} to ~ 70 yr^{-1} performed in the same work.

4.5.1 Bulge vs. Disk Rates

In our primary model, we assume novae occur proportional to the stellar mass in both the bulge and disk. Because roughly 40% of the novae are in the bulge region ($R < 3$ kpc) compared to the 60% of novae that would be considered to be in the disk ($R > 3$ kpc), this predicts a bulge and disk rate of bulge $\approx 10 \pm 2$ yr^{-1} and disk $\approx 16 \pm 2$ yr^{-1}. There is an independent estimate of the bulge nova rate from the OGLE-IV survey, which is 13.8 ± 2.6

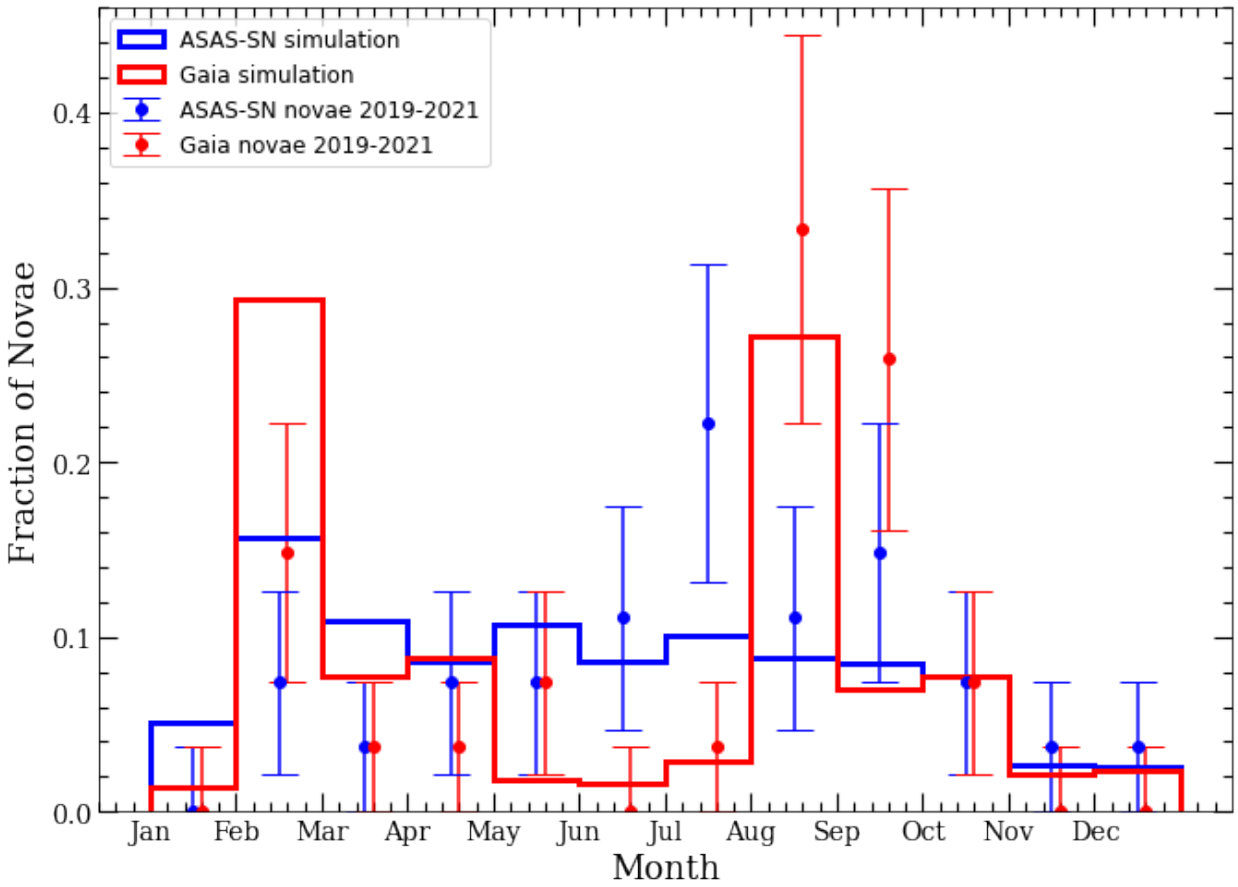

Figure 4.9 Comparison of the month of first detections of model novae (solid histograms) vs. discovered samples (scatter points with Poisson error bars). Both surveys have a seasonal gap while the Sun is in Sagittarius from November to January, and *Gaia* (shown in red) has an additional seasonal gap six months later because of the rotation direction of the satellite. When a field comes out of Solar constraint, the model predicts an excess of nova discoveries.

yr^{-1} (Mróz et al., 2015b), which is just over 1σ higher than our value.

We find little difference ($\lesssim 10\%$) in the detection efficiencies between the bulge and disk in our work, with ASAS-SN predicted to recover $\sim 37\%$ of disk novae and $\sim 28\%$ of bulge novae, and *Gaia* recovering $\sim 43\%$ of disk novae and $\sim 40\%$ of bulge novae. This means that our inferred total Galactic nova rate would not meaningfully change for reasonable differing assumptions about the bulge and disk populations of novae (Kawash et al., 2021c). As an example, Shafter & Irby (2001) estimated that in M31 the nova rate per unit luminosity of the disk was 0.4 that of the bulge. Assuming a similar ratio for the mass in our model yields rates of bulge ≈ 15 yr^{-1} and disk ≈ 11 yr^{-1}. So, even a mild enhancement of the bulge nova rate with respect to the disk nova rate could bring our results into full agreement with the OGLE-IV results, but as stated above the disagreement is small even with our standard model.

We do note that our inferred rate of disk novae is not consistent even at the 2σ level with the average disk rate estimate of 67^{+21}_{-17} yr^{-1} from Özdönmez et al. (2018). This rate was derived from an estimate of the local (within 1–2 kpc) nova population extrapolated to the entire disk. The origin of the disagreement is not immediately clear, but could potentially arise if the distances to some of the novae in their sample were underestimated.

4.5.2 Comparison to Palomar Gattini-IR

The rates derived in this work are perhaps most easily comparable to the PGIR estimate of 44^{+20}_{-9} yr^{-1} (De et al., 2021), the only other direct Galactic estimate made from a systematic large (though not all-sky) time domain survey. However, the PGIR rate is substantially higher than those derived here, with the overlap in the posterior distribution functions $< 20\%$. Here, we assess whether the discrepancy can be explained by different assumptions

between the two models.

Kawash et al. (2021c) explored the sensitivity of the ASAS-SN derived nova rates to various model assumptions and found that the rates are most sensitive to the assumed extinction law ($A_V/A_{K_s} = 13.44$ vs. $A_V/A_{K_s} = 8.65$; Nataf et al. 2016) and the stellar density model used to distribute the nova positions (Robin et al. 2003 vs. Cautun et al. 2020). Because a steeper reddening law increases the g-band extinction and the Cautun et al. (2020) model places more novae closer to the plane (see Figure 1 of Kawash et al. 2021c), the recovery fraction of novae in ASAS-SN decreases, resulting in a 33% increase in the derived rate. Assuming a similar increase for this work would increase the ASAS-SN derived Galactic nova rate to $R \approx 37$ yr^{-1}, still consistent with our primary model at the 2.2σ level and now consistent with the PGIR rate at the 1σ level. However, the *Gaia* rate is much less sensitive to these changes as it is better at finding extinguished novae in the plane, so a significant discrepancy between the *Gaia* and PGIR rates would remain.

As seen in Table 1 of Kawash et al. (2021c), the PGIR predicted rate is not sensitive to changes in the distribution of positions, extinction model, or bulge-to-disk ratios of novae. Those rates were derived assuming a detection efficiency of 17%, estimated from the completeness study of PGIR data (De et al., 2021).

Arguably the largest difference between the PGIR study and this work is the assumed shapes of nova lightcurves and the adherence to the MMRD relation. We assume that the distribution of speed classes is derived from the log-normal distribution of t_2 measured in Kawash et al. (2021b), then use a real nova lightcurve with the closest value of t_2 as a template to model the fading from maximum light. De et al. (2021) uses the peak luminosity to find the corresponding t_3 value using the MMRD relationship measured in Özdönmez et al. (2018) and then assumes the apparent magnitude will fade linearly in time. We rerun our

analysis, this time using the PGIR method to derive the lightcurve speed and shape, to see if this could explain the discrepancy in the results. If we do this, the derived rates marginally decrease, with the ASAS-SN, *Gaia*, and joint rates changing to 26 ± 5 yr^{-1}, 21 ± 5 yr^{-1}, and 24 ± 4 yr^{-1}, respectively. This minor decrease in the derived rate is because the MMRD relation measured in Özdönmez et al. (2018) maps the average nova luminosity of $M = -7.2$ mag to a relatively slow decline $t_3 \approx 73$ days, and the strict adherence to the MMRD relation does not allow for faint and fast novae. This makes novae observable for a slightly longer period of time compared to the method used in this work. But overall, the differences in the shape of the simulated nova lightcurves cannot explain the inconsistencies in the results.

One of the three major requirements for a nova candidate to be identified in the PGIR pipeline is that the transient has to be 3 mags brighter than any 2MASS counterparts within a radius of $10''$ (De et al., 2021). From the positions and peak brightness of PGIR-detected novae listed in Table 1 of De et al. (2021), it appears that PGIR 20ekz and PGIR 20eig do not meet this requirement. They could have been discovered because the astrometry on individual epochs varies significantly (because of the $8.7''$ PGIR pixel scale), so the positions of a transient from a few observations can meet all of the requirements even when the median position does not. We estimated the degree to which this matters for the recovery fraction in a simulation by studying the 2MASS counterparts near the 10,000 positions of our simulated sample.

To mimic the PGIR detectors, we estimated peak observed brightness of 10,000 simulated novae only using the ASAS-SN site in Texas (similar in latitude to the single Palomar site of PGIR) and ignoring extinction (as the effects of extinction are much milder in PGIR's J band). We estimated the recovery fraction after requiring that the peak brightness be 3 mag brighter than any 2MASS counterpart within $10''$ of any nova. We then compared that result

to one where the positions were allowed to vary between epochs by randomly sampling a normal distribution of RA and Dec. 10 times. ASAS-SN and PGIR have similar pixel scales ($8''$ vs $8.7''$), so we sampled the positions from a normal distribution with $\sigma = 1.7''$, because the 95% quantile of the astrometric accuracy of ASAS-SN was found to be $3.4''$ (Yaron et al. 2019b; no similar analysis has been published for PGIR, to our knowledge). Letting the positions vary on individual epochs yields a detection efficiency roughly 7% higher than the static positions. Assuming a similar increase in the PGIR analysis could increase the recovery fraction to ∼24%, suggesting a derived nova rate of $R \approx 32$ yr^{-1}, consistent with this work at the 1.2σ level and consistent with the default PGIR rate at the 1.3σ level. Another way to look at how sensitive the PGIR rate is to the 2MASS requirement is by decreasing the PGIR sample from 11 to 9 novae (by excluding 20ekz and 20eig). As seen in Figure 8 of De et al. (2021), this would give larger Poissonian uncertainties, corresponding to a 1σ range of the Galactic nova rate between 27 yr^{-1} and 52 yr^{-1}, consistent with both rates within the uncertainties. So, the rates derived in this work are inconsistent at the 1σ level with the PGIR rate, but small changes in either model would appear to bring the results into agreement at a rate of ~ 30 per year.

4.5.3 Extragalactic Comparisons and Faint/Fast Novae

Because of uncertainties in galaxy stellar masses and the potential variation of nova rate with stellar population parameters, there are challenges associated with comparing indirectly derived rates from extragalactic nova surveys with direct rates from Galactic surveys. However, extragalactic surveys have historically been more complete in at least some dimensions, so the exercise has been common practice in the literature. The most recent survey of M31 suggested a Milky Way rate of $R = 34^{+15}_{-12}$ (Darnley et al., 2006), consistent with the

rates derived here. Another common practice is to estimate the linear correlation between the nova rate and the log luminosity of a sample of galaxies. della Valle & Livio (1994a) studied five galaxies to infer a Galactic nova rate of 24 yr^{-1}, Shafter et al. (2000) studied three galaxies to infer a Galactic nova rate of 27^{+10}_{-8} yr^{-1}, and Della Valle & Izzo (2020) compiled measurements from 14 galaxies to infer a Galactic nova rate of ~ 22 yr^{-1}. These estimates have large uncertainties, but they are notably all consistent with the most likely rate predicted in this work.

Shara et al. (2016) argues that extragalactic nova surveys underestimate nova rates because they neglect to account for faint and fast novae, but the present paper shows that missed faint fast novae are not an important source of uncertainty in the Galactic novae rate (see Section 4.3.2 and Figure 4.5) compared to other factors such as the foreground extinction. These simulations are consistent with the lack of discovery in ASAS-SN of a substantial population of faint fast novae after years of daily monitoring. While faint fast novae undoubtedly exist at some level and are a harder to detect, current Galactic data provide no evidence for a large, yet to be discovered population of these sources, and it is plausible that extragalactic studies have overestimated their importance.

4.6 Conclusions

In this work, we have presented the results of the first direct Galactic nova rate analysis using optical transient surveys with all-sky FOVs. The results predict a much lower rate than recent estimates, with the most likely model, built by combining ASAS-SN and *Gaia* observations, estimating a Galactic nova rate of $R = 26 \pm 5$ yr^{-1}. This rate is consistent with the derived rates from ASAS-SN and *Gaia* observations individually. Our analysis suggests

that rates above 40 yr^{-1} are unlikely unless: (i) novae have a much lower scale height than predicted from stellar density models (subjecting them to higher dust extinction), (ii) typical extinction is much higher than predicted from existing three-dimensional dust models, or (iii) the reporting efficiencies of ASAS-SN and *Gaia* are much lower than indicated from current evidence.

If the Galactic nova rate is < 30 yr^{-1}, does that have any broader implications for the Galaxy? Izzo et al. (2015) detected ^{7}Li absorption in V1369 Cen, and suggested that, based off the intensity of the line, novae could explain the overabundance of ^{7}Li by assuming a slow nova rate of 24 per year. On the other hand, Molaro et al. (2016) argues that only 2 novae per year would be necessary to explain the abundance of ^{7}Li in the Galaxy. So, it is possible that even a relatively low nova rate could still explain the Galactic abundances of ^{7}Li.

Our derived rate suggests that, over the past 5 years, observers have been discovering about half of the Galaxy's nova eruptions, on average. Between 2019–2021, we find that ASAS-SN and *Gaia* observations alone have recovered $\sim 54\%$ of Galactic novae, and individually, ASAS-SN recovers $\sim 33\%$ of novae and *Gaia* recovers $\sim 42\%$ of novae.

Though direct estimates of the Galactic nova rate from large time domain surveys allow for fewer assumptions regarding cadence, many assumptions about the pipelines still need to be made. This is likely the reason the rates derived in this work do not agree with the PGIR rate, but we find that small changes in the models can increase the agreement, with the largest overlap occurring around ~ 30 novae per year.

While it is important to improve our understanding of the efficiency of transient alert pipelines (perhaps though uninformed "injection" events, as performed by LIGO/Virgo; Abadie et al. 2012), we can also make progress by gathering additional data from surveys with

improved cadences and less sensitivity to dust. As seen in Figure 4.8, the number of Northern Hemisphere Galactic plane novae discovered exceeded that in the Southern Plane. Given that there are currently more operating surveys covering the Plane in the north compared to the south, and some northern surveys are less sensitive to dust (such as Palomar Gattini-IR), a red or near-IR high-resolution and moderate-cadence survey of the Southern Galactic plane would give close to all-sky coverage of the dusty regions of the Galaxy, allowing the role of dust in nova discovery to be better constrained. Luckily, planned near-IR surveys like the Dynamic REd All-sky Monitoring Survey (DREAMS; Soon et al. 2020) and the PRime-focus Infrared Microlensing Experiment[4] (PRIME), along with the multi-band optical Vera Rubin Observatory (Tyson, 2002), make the future prospects of southern hemisphere time-domain surveys bright. Depending on the observing strategy to cover the plane, these surveys should have the ability to detect novae not recovered by current observing capabilities. The degree to which these surveys increase the discovery rate will be the next big step in constraining the Galactic nova rate. With additional Southern Hemisphere observations, the transient community could discover up to $\sim 80\%$ of the Galactic nova population, leading to a tightly constrained Galactic nova rate.

Acknowledgements

AK, LC, EA, and KVS acknowledge financial support of NSF award AST-1751874 and a Cottrell fellowship of the Research Corporation. JS acknowledges support from the Packard Foundation. BJS, CSK, and KZS are supported by NSF grant AST-1907570. CSK and KZS are supported by NSF grant AST-181440. STH is funded by the Science and Technology

[4] http://www-ir.ess.sci.osaka-u.ac.jp/prime/index.html

Facilities Council grant ST/S000623/1. ZKR acknowledges funding from the Netherlands Research School for Astronomy (NOVA).

We thank the Las Cumbres Observatory and its staff for its continuing support of the ASAS-SN project. ASAS-SN is supported by the Gordon and Betty Moore Foundation through grant GBMF5490 to the Ohio State University, and NSF grants AST-1515927 and AST-1908570. Development of ASAS-SN has been supported by NSF grant AST-0908816, the Mt. Cuba Astronomical Foundation, the Center for Cosmology and AstroParticle Physics at the Ohio State University, the Chinese Academy of Sciences South America Center for Astronomy (CAS- SACA), and the Villum Foundation.

This work has made use of data from the European Space Agency (ESA) mission *Gaia* (`https://www.cosmos.esa.int/gaia`), processed by the *Gaia* Data Processing and Analysis Consortium (DPAC, `https://www.cosmos.esa.int/web/gaia/dpac/consortium`). Funding for the DPAC has been provided by national institutions, in particular the institutions participating in the *Gaia* Multilateral Agreement. Further details of funding authorities and individuals contributing to the success of the mission is shown at `https://gea.esac.esa.int/archive/documentation/GEDR3/Miscellaneous/sec_acknowl/`.

This work is in part based on observations obtained at the Southern Astrophysical Research (SOAR) telescope, which is a joint project of the Ministério da Ciência, Tecnologia e Inovações (MCTI/LNA) do Brasil, the US National Science Foundation's NOIRLab, the University of North Carolina at Chapel Hill (UNC), and Michigan State University (MSU).

The analysis for this work was performed primarily in `ipython` (Perez & Granger, 2007) using `numpy` (Oliphant, 2006; Van Der Walt et al., 2011), `Astropy` (Price-Whelan et al., 2018), `Matplotlib` (Hunter, 2007), and `scipy` (Virtanen et al., 2020).

We thank K. De for helpful conversations regarding Galactic novae and transient surveys

and Jo Bovy for help with the extinction models.

Chapter 5

Conclusions and Future Work

This thesis has made use of the ongoing all-sky observations of ASAS-SN and *Gaia* to discover classical novae in the Galaxy and estimate the frequency at which they are produced. Recent estimates of the Galactic nova rate predict an annual rate of ~ 60 but even with the advent of these all-sky observations the discovery rate remains relatively low at ~ 13 per year since 2017. This analysis suggests that recent predictions of the nova rate have overestimated the nova rate and find that the most plausible rate to be 26 ± 5 yr^{-1}. Here are the major conclusions from the analysis of transient surveys, Galactic stellar and dust density modeling, and the Galactic nova rate.

- The mean classical nova brightens by ~ 11 magnitudes during eruption, while the most common source of classical nova confusion, the dwarf nova, typically only brightens by ~ 5 magnitudes. The outburst amplitude distributions of these two transients overlap by roughly 15%.

- The amplitude of outburst is slightly negatively with the speed of a classical nova. This correlation is less strong than previously estimated (Warner, 1987). Conversely, these quantities are strongly positively correlated for dwarf nova outbursts.

- There is only small levels of confusion between the dwarf nova and the classical nova when reported by large sky transient surveys.

- All-sky 3D dust maps suggest that only ∼half of Galactic nova get bright enough to be observed by optical surveys like ASAS-SN.

- Dust maps combined with stellar density models suggest that there has been a severe deficit of novae discovered close the the Galactic plane. Only $\sim 25\%$ of discovered novae lie within two degrees of the Galactic plane. Comparing that to the nova model in this work, $\sim 70\%$ of Galactic novae should lie within $|b| < 2^\circ$. Only looking at the bright $g < 15$ mag novae in the model, $\sim 30\%$ are within $|b| < 2^\circ$. This is consistent with the observations: dust in the plane severely obscures about half of Galactic novae from being discovered in V- or g-band optical surveys.

- Nova rates derived from g- or V-band optical surveys are sensitive to the assumed positions of novae and reddening laws of at the $\sim 30\%$ level.

- Years of monitoring from ASAS-SN, an optical all-sky survey at a one day cadence, have not significantly increased the discovery rate of novae, nor have uncovered a sample of faint, fast novae not discovered in previous years.

- Recent monitoring of red/NIR surveys like PGIR and *Gaia* have uncovered a sample of highly reddened novae in the plane not discovered in previous years, increasing the discovery rate to 17 novae in 2021, the highest number on record.

- I have built a sophisticated model of novae and dust in the Galaxy to explore what fraction of the population ASAS-SN and *Gaia* recovered between 2019 and 2021. The results suggest that ASAS-SN recovered $\sim 33\%$, *Gaia* recovered $\sim 42\%$, and a joint effort of both surveys recovered $\sim 54\%$.

- Combining this model with the discovery rates from ASAS-SN and *Gaia* over this time

period and by using a Monte Carlo simulation, I have made the first estimations of the Galactic nova rate using all-sky transient surveys. The results from ASAS-SN, *Gaia*, and a joint effort by both surveys predicts rates of $R = 28 \pm 6$ yr^{-1}, $R = 22 \pm 5$ yr^{-1} , $R = 26 \pm 5$ yr^{-1}, respectively.

- The recovery fraction of faint fast novae in ASAS-SN and *Gaia* is only a factor of ~ 2 lower than novae that follow a putative MMRD correlation. The importance of faint, fast novae in deriving a nova rate has possibly been overinflated in the literature.

This thesis provides the second and third Galactic nova rate estimations from a large sky survey, but the results are inconsistent at the 1σ level with the first rate from PGIR of $R = 44^{+20}_{-8}$ yr^{-1}. I have explored possible errors in modeling transient pipelines and found that small changes can bring the results into agreement around ~ 30 yr^{-1}. At this time, it is difficult to determine if the annual Galactic nova rate is in the 20s, the 30s, or is > 40 because of the small sample of rates derived from large sky surveys. Rates in the 20s and 30s per year are in good agreement with the results of this thesis, but rates > 40 per year would suggest errors in the modeling.

The lack of high cadence red/NIR observations in the Southern Hemisphere is arguably the largest deficiency in Galactic nova searches, which could directly address the remaining systematic uncertainties in the nova modeling mentioned above. Fortunately, this issue should be addressed with surveys like the Dynamic REd All-sky Monitoring Survey (DREAMS; Soon et al. 2020), the PRime-focus Infrared Microlensing Experiment[1] (PRIME), and the Vera Rubin Observatory (Tyson, 2002). If these surveys observe the Southern Galactic plane as planned, the degree to which the nova discovery rate increases should elucidate

[1] http://www-ir.ess.sci.osaka-u.ac.jp/prime/index.html

much of the current disagreement in the literature. Additional completeness studies using these surveys will provide valuable insights to tightly constrain the Galactic nova rate.

BIBLIOGRAPHY

BIBLIOGRAPHY

Abadie, J., Abbott, B. P., Abbott, R., et al. 2012, PhRvD, 85, 082002, doi: 10.1103/PhysRevD.85.082002

Abdo, A. A., Ackermann, M., Ajello, M., et al. 2010, ApJS, 188, 405, doi: 10.1088/0067-0049/188/2/405

Ackermann, M., Ajello, M., Albert, A., et al. 2014, Science, 345, 554, doi: 10.1126/science.1253947

Adams, S. M., Kochanek, C. S., Beacom, J. F., Vagins, M. R., & Stanek, K. Z. 2013, ApJ, 778, 164, doi: 10.1088/0004-637X/778/2/164

Alard, C. 2000, A&AS, 144, 363, doi: 10.1051/aas:2000214

Alard, C., & Lupton, R. H. 1998, ApJ, 503, 325, doi: 10.1086/305984

Allen, C. W. 1954, MNRAS, 114, 387, doi: 10.1093/mnras/114.4.387

Arnould, M., & Norgaard, H. 1975, A&A, 42, 55

Aydi, E., Strader, J., Chomiuk, L., et al. 2019, The Astronomer's Telegram, 13068, 1

Aydi, E., Sokolovsky, K. V., Chomiuk, L., et al. 2020, Nature Astronomy, 4, 776, doi: 10.1038/s41550-020-1070-y

Bailer-Jones, C. A. L., Rybizki, J., Fouesneau, M., Mantelet, G., & Andrae, R. 2018, AJ, 156, 58, doi: 10.3847/1538-3881/aacb21

Beamin, J. C., Minniti, D., Saito, R. K., & Kurtev, R. 2013, The Astronomer's Telegram, 5212, 1

Bennett, M. B., Wrede, C., Chipps, K. A., et al. 2013, PhRvL, 111, 232503, doi: 10.1103/PhysRevLett.111.232503

Bland-Hawthorn, J., & Gerhard, O. 2016, ARA&A, 54, 529, doi: 10.1146/annurev-astro-081915-023441

Bode, M. F., & Evans, A. 2008, Classical Novae, Vol. 43

Bovy, J., Rix, H.-W., Green, G. M., Schlafly, E. F., & Finkbeiner, D. P. 2016, ApJ, 818, 130, doi: 10.3847/0004-637X/818/2/130

Bruch, A. 1984, A&AS, 56, 441

Burlak, M. A., & Henden, A. A. 2008, Astronomy Letters, 34, 241, doi: 10.1134/S1063773708040038

Capaccioli, M., Della Valle, M., D'Onofrio, M., & Rosino, L. 1989a, AJ, 97, 1622, doi: 10.1086/115104

—. 1989b, AJ, 97, 1622, doi: 10.1086/115104

Cardelli, J. A., Clayton, G. C., & Mathis, J. S. 1989, ApJ, 345, 245, doi: 10.1086/167900

Cautun, M., Benítez-Llambay, A., Deason, A. J., et al. 2020, MNRAS, 494, 4291, doi: 10.1093/mnras/staa1017

Chambers, K. C., Magnier, E. A., Metcalfe, N., et al. 2016, arXiv e-prints, arXiv:1612.05560. https://arxiv.org/abs/1612.05560

Chen, H.-L., Woods, T. E., Yungelson, L. R., Gilfanov, M., & Han, Z. 2016, MNRAS, 458, 2916, doi: 10.1093/mnras/stw458

Chomiuk, L., Metzger, B. D., & Shen, K. J. 2021a, ARA&A, 59, doi: 10.1146/annurev-astro-112420-114502

Chomiuk, L., Linford, J. D., Aydi, E., et al. 2021b, ApJS, 257, 49, doi: 10.3847/1538-4365/ac24ab

Ciardullo, R., Ford, H. C., Williams, R. E., Tamblyn, P., & Jacoby, G. H. 1990, AJ, 99, 1079, doi: 10.1086/115397

Clemens, J. C., Crain, J. A., & Anderson, R. 2004, in Proc. SPIE, Vol. 5492, Ground-based Instrumentation for Astronomy, ed. A. F. M. Moorwood & M. Iye, 331–340, doi: 10.1117/12.550069

Contreras Pena, C., Lucas, P. W., Saito, R. K., Minniti, D., & Kurtev, R. 2016, The Astronomer's Telegram, 8972, 1

Coppejans, D. L., Körding, E. G., Knigge, C., et al. 2016, MNRAS, 456, 4441, doi: 10.1093/mnras/stv2921

Darnley, M. J. 2019, arXiv e-prints, arXiv:1912.13209. https://arxiv.org/abs/1912.13209

Darnley, M. J., & Henze, M. 2019, arXiv e-prints, arXiv:1909.10497. https://arxiv.org/abs/1909.10497

Darnley, M. J., Ribeiro, V. A. R. M., Bode, M. F., Hounsell, R. A., & Williams, R. P. 2012, ApJ, 746, 61, doi: 10.1088/0004-637X/746/1/61

Darnley, M. J., Bode, M. F., Kerins, E., et al. 2006, MNRAS, 369, 257, doi: 10.1111/j.1365-2966.2006.10297.x

Darnley, M. J., Henze, M., Steele, I. A., et al. 2015, A&A, 580, A45, doi: 10.1051/0004-6361/201526027

Darnley, M. J., Henze, M., Bode, M. F., et al. 2016, ApJ, 833, 149, doi: 10.3847/1538-4357/833/2/149

De, K., Hankins, M., Kasliwal, M. M., et al. 2020a, The Astronomer's Telegram, 13790, 1

De, K., Hankins, M. J., Kasliwal, M. M., et al. 2020b, PASP, 132, 025001, doi: 10.1088/1538-3873/ab6069

De, K., Hankins, M., Andreoni, I., et al. 2020c, The Astronomer's Telegram, 14014, 1

De, K., Hankins, M., Kasliwal, M. M., et al. 2020d, The Astronomer's Telegram, 13790, 1

De, K., Kasliwal, M. M., Hankins, M. J., et al. 2021, The Astrophysical Journal, 912, 19, doi: 10.3847/1538-4357/abeb75

De, K., Kasliwal, M. M., Hankins, M. J., et al. 2021, arXiv e-prints, arXiv:2101.04045. https://arxiv.org/abs/2101.04045

Della Valle, M., & Izzo, L. 2020, arXiv e-prints, arXiv:2004.06540. https://arxiv.org/abs/2004.06540

della Valle, M., & Livio, M. 1994a, ApJL, 423, L31, doi: 10.1086/187228

—. 1994b, A&A, 286, 786

—. 1995, ApJ, 452, 704, doi: 10.1086/176342

Diehl, R., Halloin, H., Kretschmer, K., et al. 2006, Nature, 439, 45, doi: 10.1038/nature04364

Dilday, B., Howell, D. A., Cenko, S. B., et al. 2012, Science, 337, 942, doi: 10.1126/science.1219164

Drake, A. J., Gänsicke, B. T., Djorgovski, S. G., et al. 2014, MNRAS, 441, 1186, doi: 10.1093/mnras/stu639

Drimmel, R., Cabrera-Lavers, A., & López-Corredoira, M. 2003, A&A, 409, 205, doi: 10.1051/0004-6361:20031070

Duerbeck, H. W. 1987, SSRv, 45, 1, doi: 10.1007/BF00187826

Duerbeck, H. W. 2008, Novae: an historical perspective, 2nd edn., ed. M. F. Bode & A. Evans, Cambridge Astrophysics (Cambridge University Press), 1–15, doi: 10.1017/CBO9780511536168.003

Duerbeck, H. W. 2008, in Classical Novae, 2nd Edition. Cambridge Astrophysics Series, No. 43, Cambridge: Cambridge University Press, ed. M. F. Bode & A. Evans, 1–15

Flewelling, H. A., Magnier, E. A., Chambers, K. C., et al. 2016, arXiv e-prints, arXiv:1612.05243. https://arxiv.org/abs/1612.05243

Friedman, M., Budner, T., Pérez-Loureiro, D., et al. 2020, PhRvC, 101, 052802, doi: 10.1103/PhysRevC.101.052802

Gaia Collaboration, Prusti, T., de Bruijne, J. H. J., et al. 2016, A&A, 595, A1, doi: 10.1051/0004-6361/201629272

Gaia Collaboration, Spoto, F., Tanga, P., et al. 2018a, A&A, 616, A13, doi: 10.1051/0004-6361/201832900

Gaia Collaboration, Brown, A. G. A., Vallenari, A., et al. 2018b, A&A, 616, A1, doi: 10.1051/0004-6361/201833051

—. 2021, A&A, 649, A1, doi: 10.1051/0004-6361/202039657

Gallagher, J. S., I., & Code, A. D. 1974, ApJ, 189, 303, doi: 10.1086/152804

Gallagher, J. S., & Starrfield, S. 1978, ARA&A, 16, 171, doi: 10.1146/annurev.aa.16.090178.001131

Gänsicke, B. T., Dillon, M., Southworth, J., et al. 2009, MNRAS, 397, 2170, doi: 10.1111/j.1365-2966.2009.15126.x

Gehrz, R. D. 1988, ARA&A, 26, 377, doi: 10.1146/annurev.aa.26.090188.002113

Gravity Collaboration, Abuter, R., Amorim, A., et al. 2018, A&A, 615, L15, doi: 10.1051/0004-6361/201833718

Green, G. M., Schlafly, E., Zucker, C., Speagle, J. S., & Finkbeiner, D. 2019, ApJ, 887, 93, doi: 10.3847/1538-4357/ab5362

Green, G. M., Schlafly, E. F., Finkbeiner, D. P., et al. 2015, ApJ, 810, 25, doi: 10.1088/0004-637X/810/1/25

Gutierrez, L. A., Saito, R. K., & Minniti, D. 2016, The Astronomer's Telegram, 8551, 1

Hachisu, I., & Kato, M. 2014, ApJ, 785, 97, doi: 10.1088/0004-637X/785/2/97

Hameury, J. M. 2020, Advances in Space Research, 66, 1004, doi: 10.1016/j.asr.2019.10.022

Hameury, J. M., & Lasota, J. P. 2017, A&A, 602, A102, doi: 10.1051/0004-6361/201730760

Harrison, T. E., Johnson, J. J., McArthur, B. E., et al. 2004, AJ, 127, 460, doi: 10.1086/380228

Hatano, K., Branch, D., Fisher, A., & Starrfield, S. 1997, MNRAS, 290, 113, doi: 10.1093/mnras/290.1.113

Hellier, C. 2001, Cataclysmic Variable Stars

Hernanz, M., Jose, J., Coc, A., & Isern, J. 1996, ApJL, 465, L27, doi: 10.1086/310122

Hodgkin, S. T., Harrison, D. L., Breedt, E., et al. 2021, A&A, 652, A76, doi: 10.1051/0004-6361/202140735

Holoien, T. W. S., Brown, J. S., Vallely, P. J., et al. 2019, MNRAS, 484, 1899, doi: 10.1093/mnras/stz073

Howell, S. B., Szkody, P., & Cannizzo, J. K. 1995, ApJ, 439, 337, doi: 10.1086/175177

Hunter, J. D. 2007, Computing in Science & Engineering, 9, 90, doi: 10.1109/MCSE.2007.55

Ivezić, Ž., Kahn, S. M., Tyson, J. A., et al. 2019, ApJ, 873, 111, doi: 10.3847/1538-4357/ab042c

Izzo, L., Della Valle, M., Mason, E., et al. 2015, ApJL, 808, L14, doi: 10.1088/2041-8205/808/1/L14

Jayasinghe, T., Kochanek, C. S., Stanek, K. Z., et al. 2018a, MNRAS, 477, 3145, doi: 10.1093/mnras/sty838

—. 2018b, MNRAS, 477, 3145, doi: 10.1093/mnras/sty838

Jayasinghe, T., Stanek, K. Z., Kochanek, C. S., et al. 2019, MNRAS, 486, 1907, doi: 10.1093/mnras/stz844

—. 2020, MNRAS, 493, 4186, doi: 10.1093/mnras/staa499

José, J., & Hernanz, M. 1998, ApJ, 494, 680, doi: 10.1086/305244

José, J., Hernanz, M., & Iliadis, C. 2006, Nuclear Physics A, 777, 550, doi: https://doi.org/10.1016/j.nuclphysa.2005.02.121

Kafka, S. 2020, Observations from the AAVSO International Database, https://www.aavso.org

Kahabka, P., & van den Heuvel, E. P. J. 1997, ARA&A, 35, 69, doi: 10.1146/annurev.astro.35.1.69

Kalomeni, B., Nelson, L., Rappaport, S., et al. 2016, ApJ, 833, 83, doi: 10.3847/1538-4357/833/1/83

Kasliwal, M. M., Cenko, S. B., Kulkarni, S. R., et al. 2011, ApJ, 735, 94, doi: 10.1088/0004-637X/735/2/94

Kato, T. 2015, PASJ, 67, 108, doi: 10.1093/pasj/psv077

Kato, T., Maehara, H., & Uemura, M. 2012, PASJ, 64, 63, doi: 10.1093/pasj/64.3.63

Kato, T., Isogai, K., Wakamatsu, Y., et al. 2020, PASJ, 72, 14, doi: 10.1093/pasj/psz134

Kawash, A., Aydi, E., Strader, J., Chomiuk, L., & Sokolovsky, K. V. 2020, The Astronomer's Telegram, 14118, 1

Kawash, A., Aydi, E., Strader, J., Sokolovsky, K. V., & Chomiuk, L. 2021a, The Astronomer's Telegram, 14928, 1

Kawash, A., Chomiuk, L., Strader, J., et al. 2021b, arXiv e-prints, arXiv:2101.12239. https://arxiv.org/abs/2101.12239

Kawash, A., Chomiuk, L., Rodriguez, J. A., et al. 2021c, ApJ, 922, 25, doi: 10.3847/1538-4357/ac1f1a

Kawash, A., Chomiuk, L., Strader, J., et al. 2022, arXiv e-prints, arXiv:2206.14132. https://arxiv.org/abs/2206.14132

Kemp, A. J., Karakas, A. I., Casey, A. R., et al. 2022, arXiv e-prints, arXiv:2206.13729. https://arxiv.org/abs/2206.13729

—. 2021, MNRAS, 504, 6117, doi: 10.1093/mnras/stab1160

Kochanek, C. S., Shappee, B. J., Stanek, K. Z., et al. 2017, PASP, 129, 104502, doi: 10.1088/1538-3873/aa80d9

König, O., Wilms, J., Arcodia, R., et al. 2022, Nature, 605, 248, doi: 10.1038/s41586-022-04635-y

Kopylov, I. M. 1955, Izvestiya Krymskoj Astrofizicheskoj Observatorii, 13, 23

Kostov, A., & Bonev, T. 2018, Bulgarian Astronomical Journal, 28, 3. https://arxiv.org/abs/1706.06147

Kostrzewa-Rutkowska, Z., Jonker, P. G., Hodgkin, S. T., et al. 2018, MNRAS, 481, 307, doi: 10.1093/mnras/sty2221

Kozlowski, S., Poleski, R., Udalski, A., et al. 2012, The Astronomer's Telegram, 4323, 1

Kuin, N. P. M., Page, K. L., Mróz, P., et al. 2020, MNRAS, 491, 655, doi: 10.1093/mnras/stz2960

Landais, G., Ochsenbein, F., & Simon, A. 2013, Astronomical Society of the Pacific Conference Series, Vol. 475, TAPVizieR: A New Way to Access the VizieR Database, ed. D. N. Friedel, 227

Lasker, B. M., Lattanzi, M. G., McLean, B. J., et al. 2008, AJ, 136, 735, doi: 10.1088/0004-6256/136/2/735

Li, L., Shen, S., Hou, J., et al. 2018, The Astrophysical Journal, 858, 75, doi: 10.3847/1538-4357/aabaef

Liller, W., & Mayer, B. 1987, PASP, 99, 606, doi: 10.1086/132021

Lundmark, K. 1935, Meddelanden fran Lunds Astronomiska Observatorium Serie II, 74, 1

Lundmark, K. E. 1920, PhD thesis, Uppsala University, Sweden

Marshall, D. J., Robin, A. C., Reylé, C., Schultheis, M., & Picaud, S. 2006, A&A, 453, 635, doi: 10.1051/0004-6361:20053842

Mathis, J. S. 1990, ARA&A, 28, 37, doi: 10.1146/annurev.aa.28.090190.000345

Mclaughlin, D. B. 1945, PASP, 57, 69, doi: 10.1086/125689

Metzger, B. D., Zenati, Y., Chomiuk, L., Shen, K. J., & Strader, J. 2021, ApJ, 923, 100, doi: 10.3847/1538-4357/ac2a39

Minniti, D., Lucas, P. W., Emerson, J. P., et al. 2010, NewA, 15, 433, doi: 10.1016/j.newast.2009.12.002

Miroshnichenko, A. S. 1988, AZh, 65, 582

Molaro, P., Izzo, L., Mason, E., Bonifacio, P., & Della Valle, M. 2016, MNRAS, 463, L117, doi: 10.1093/mnrasl/slw169

Montenegro, K., Minniti, D., & Saito, R. K. 2015, The Astronomer's Telegram, 7241, 1

Mroz, P., & Udalski, A. 2014, The Astronomer's Telegram, 6406, 1

—. 2016, The Astronomer's Telegram, 9215, 1

Mróz, P., Udalski, A., Poleski, R., et al. 2015a, AcA, 65, 313. https://arxiv.org/abs/1601.02617

—. 2015b, ApJS, 219, 26, doi: 10.1088/0067-0049/219/2/26

Munari, U., Siviero, A., Dallaporta, S., et al. 2011, NewA, 16, 209, doi: 10.1016/j.newast.2010.08.010

Nataf, D. M., Gonzalez, O. A., Casagrande, L., et al. 2016, MNRAS, 456, 2692, doi: 10.1093/mnras/stv2843

Nelemans, G., Siess, L., Repetto, S., Toonen, S., & Phinney, E. S. 2016, ApJ, 817, 69, doi: 10.3847/0004-637X/817/1/69

Oliphant, T. E. 2006, A guide to NumPy, Vol. 1 (Trelgol Publishing USA)

Ortolani, S., Rafanelli, P., Rosino, L., & Vittone, A. 1980, A&A, 87, 31

Osaki, Y. 1996, PASP, 108, 39, doi: 10.1086/133689

—. 2001, Astronomical Society of the Pacific Conference Series, Vol. 245, Dwarf Nova and Accretion Disks, ed. T. von Hippel, C. Simpson, & N. Manset, 57

Otulakowska-Hypka, M., Olech, A., & Patterson, J. 2016, MNRAS, 460, 2526, doi: 10.1093/mnras/stw1120

Özdönmez, A., Ege, E., Güver, T., & Ak, T. 2018, MNRAS, 476, 4162, doi: 10.1093/mnras/sty432

Page, K. L., Kuin, N. P. M., & Darnley, M. J. 2020, The Astronomer's Telegram, 13731, 1

Pagnotta, A., & Schaefer, B. E. 2014, ApJ, 788, 164, doi: 10.1088/0004-637X/788/2/164

Pala, A. F., Gänsicke, B. T., Belloni, D., et al. 2022, MNRAS, 510, 6110, doi: 10.1093/mnras/stab3449

Patat, F., Chugai, N. N., Podsiadlowski, P., et al. 2011, A&A, 530, A63, doi: 10.1051/0004-6361/201116865

Patterson, J. 2011, MNRAS, 411, 2695, doi: 10.1111/j.1365-2966.2010.17881.x

Patterson, J., Uthas, H., Kemp, J., et al. 2013, MNRAS, 434, 1902, doi: 10.1093/mnras/stt1085

Perez, F., & Granger, B. E. 2007, Computing in Science Engineering, 9, 21

Pickering, E. C. 1893, Astronomische Nachrichten, 134, 101, doi: 10.1002/asna.18941340608

Pickering, W. H. 1895, The Observatory, 18, 436

Pojmański, G. 2001, in Astronomical Society of the Pacific Conference Series, Vol. 246, IAU Colloq. 183: Small Telescope Astronomy on Global Scales, ed. B. Paczynski, W.-P. Chen, & C. Lemme, 53

Prantzos, N. 2012, A&A, 542, A67, doi: 10.1051/0004-6361/201219043

Price-Whelan, A. M., Sipőcz, B. M., Günther, H. M., et al. 2018, AJ, 156, 123, doi: 10.3847/1538-3881/aabc4f

Robin, A. C., Reylé, C., Derrière, S., & Picaud, S. 2003, A&A, 409, 523, doi: 10.1051/0004-6361:20031117

Romano, D., Matteucci, F., Ventura, P., & D'Antona, F. 2001, A&A, 374, 646, doi: 10.1051/0004-6361:20010751

Rukeya, R., Lü, G., Wang, Z., & Zhu, C. 2017, PASP, 129, 074201, doi: 10.1088/1538-3873/aa6b4d

Saito, R. K., Dekany, I., Minniti, D., Catelan, M., & Angeloni, R. 2014, The Astronomer's Telegram, 6022, 1

Saito, R. K., Minniti, D., Angeloni, R., & Catelan, M. 2012, The Astronomer's Telegram, 4426, 1

—. 2013a, The Astronomer's Telegram, 4830, 1

—. 2013b, The Astronomer's Telegram, 4830, 1

Saito, R. K., Minniti, D., Angeloni, R., Dekany, I., & Catelan, M. 2015, The Astronomer's Telegram, 7124, 1

Saito, R. K., Minniti, D., Catelan, M., et al. 2016, The Astronomer's Telegram, 8602, 1

Saito, R. K., Minniti, D., Drew, J. E., Greimel, R., & Lucas, P. W. 2017, The Astronomer's Telegram, 10247, 1

Sale, S. E., Drew, J. E., Barentsen, G., et al. 2014, MNRAS, 443, 2907, doi: 10.1093/mnras/stu1090

Schaefer, B. E. 2010, ApJS, 187, 275, doi: 10.1088/0067-0049/187/2/275

—. 2018, MNRAS, 481, 3033, doi: 10.1093/mnras/sty2388

Schenker, K., Kolb, U., & Ritter, H. 1998, MNRAS, 297, 633, doi: 10.1046/j.1365-8711.1998.01529.x

Schlafly, E. F., & Finkbeiner, D. P. 2011, ApJ, 737, 103, doi: 10.1088/0004-637X/737/2/103

Schlafly, E. F., Green, G. M., Lang, D., et al. 2018, ApJS, 234, 39, doi: 10.3847/1538-4365/aaa3e2

Schlegel, D. J., Finkbeiner, D. P., & Davis, M. 1998, ApJ, 500, 525, doi: 10.1086/305772

Schreiber, M. R., Zorotovic, M., & Wijnen, T. P. G. 2016, MNRAS, 455, L16, doi: 10.1093/mnrasl/slv144

Selvelli, P., & Gilmozzi, R. 2019, A&A, 622, A186, doi: 10.1051/0004-6361/201834238

Shafter, A. W. 1997, ApJ, 487, 226, doi: 10.1086/304609

Shafter, A. W. 2002, in American Institute of Physics Conference Series, Vol. 637, Classical Nova Explosions, ed. M. Hernanz & J. José, 462–471, doi: 10.1063/1.1518246

—. 2017, ApJ, 834, 196, doi: 10.3847/1538-4357/834/2/196

Shafter, A. W., Ciardullo, R., & Pritchet, C. J. 2000, ApJ, 530, 193, doi: 10.1086/308349

Shafter, A. W., & Irby, B. K. 2001, ApJ, 563, 749, doi: 10.1086/324044

Shafter, A. W., Rau, A., Quimby, R. M., et al. 2009, ApJ, 690, 1148, doi: 10.1088/0004-637X/690/2/1148

Shafter, A. W., Darnley, M. J., Hornoch, K., et al. 2011, ApJ, 734, 12, doi: 10.1088/0004-637X/734/1/12

Shappee, B. J., Prieto, J. L., Grupe, D., et al. 2014, ApJ, 788, 48, doi: 10.1088/0004-637X/788/1/48

Shara, M. M., Doyle, T. F., Lauer, T. R., et al. 2016, ApJS, 227, 1, doi: 10.3847/0067-0049/227/1/1

Shara, M. M., Doyle, T., Lauer, T. R., et al. 2017a, ApJ, 839, 109, doi: 10.3847/1538-4357/aa65cd

Shara, M. M., Iłkiewicz, K., Mikołajewska, J., et al. 2017b, Nature, 548, 558, doi: 10.1038/nature23644

Sharov, A. S. 1972, Soviet Ast., 16, 41

Simion, I. T., Belokurov, V., Irwin, M., et al. 2017, MNRAS, 471, 4323, doi: 10.1093/mnras/stx1832

Smak, J. 1984, AcA, 34, 161

Sokolovsky, K., Korotkiy, S., & Lebedev, A. 2014, in Astronomical Society of the Pacific Conference Series, Vol. 490, Stellar Novae: Past and Future Decades, ed. P. A. Woudt & V. A. R. M. Ribeiro, 395. https://arxiv.org/abs/1303.3268

Soon, J., Adams, D., De, K., et al. 2020, in Society of Photo-Optical Instrumentation Engineers (SPIE) Conference Series, Vol. 11203, Advances in Optical Astronomical Instrumentation 2019, 1120307, doi: 10.1117/12.2539594

Sparks, W. M., & Sion, E. M. 2021, ApJ, 914, 5, doi: 10.3847/1538-4357/abf2bc

Starrfield, S., Bose, M., Iliadis, C., et al. 2020, ApJ, 895, 70, doi: 10.3847/1538-4357/ab8d23

Starrfield, S., Truran, J. W., & Sparks, W. M. 1978a, ApJ, 226, 186, doi: 10.1086/156598

—. 1978b, ApJ, 226, 186, doi: 10.1086/156598

Starrfield, S., Truran, J. W., Sparks, W. M., & Kutter, G. S. 1972, ApJ, 176, 169, doi: 10.1086/151619

Strope, R. J., Schaefer, B. E., & Henden, A. A. 2010, AJ, 140, 34, doi: 10.1088/0004-6256/140/1/34

Tajitsu, A., Sadakane, K., Naito, H., Arai, A., & Aoki, W. 2015, Nature, 518, 381, doi: 10.1038/nature14161

Tampo, Y., Naoto, K., Isogai, K., et al. 2020, PASJ, 72, 49, doi: 10.1093/pasj/psaa043

Toonen, S., Claeys, J. S. W., Mennekens, N., & Ruiter, A. J. 2014, A&A, 562, A14, doi: 10.1051/0004-6361/201321576

Tyson, J. A. 2002, in Society of Photo-Optical Instrumentation Engineers (SPIE) Conference Series, Vol. 4836, Survey and Other Telescope Technologies and Discoveries, ed. J. A. Tyson & S. Wolff, 10–20, doi: 10.1117/12.456772

Udalski, A., Szymański, M. K., & Szymański, G. 2015a, AcA, 65, 1. https://arxiv.org/abs/1504.05966

—. 2015b, AcA, 65, 1. https://arxiv.org/abs/1504.05966

van den Bergh, S. 1991a, PASP, 103, 1053, doi: 10.1086/132925

—. 1991b, PASP, 103, 609, doi: 10.1086/132860

van den Bergh, S., & Younger, P. F. 1987a, A&AS, 70, 125

—. 1987b, A&AS, 70, 125

Van Der Walt, S., Colbert, S. C., & Varoquaux, G. 2011, Computing in Science & Engineering, 13, 22

Vasini, A., Matteucci, F., & Spitoni, E. 2022, arXiv e-prints, arXiv:2204.00510. https://arxiv.org/abs/2204.00510

Virtanen, P., Gommers, R., Oliphant, T. E., et al. 2020, Nature Methods, 17, 261, doi: https://doi.org/10.1038/s41592-019-0686-2

Walter, F. M., Battisti, A., Towers, S. E., Bond, H. E., & Stringfellow, G. S. 2012, PASP, 124, 1057, doi: 10.1086/668404

Warner, B. 1987, MNRAS, 227, 23, doi: 10.1093/mnras/227.1.23

—. 1995, Cambridge Astrophysics Series, 28

Watson, C. L., Henden, A. A., & Price, A. 2006, Society for Astronomical Sciences Annual Symposium, 25, 47

Wyrzykowski, L., Udalski, A., Kozlowski, S., et al. 2014a, The Astronomer's Telegram, 6002, 1

—. 2014b, The Astronomer's Telegram, 6002, 1

Yaron, O., Gal-Yam, A., Ofek, E., & Sass, A. 2019a, Transient Name Server AstroNote, 37, 1

Yaron, O., Gal-Yam, A., Ofek, E., Sass, A., & Knezevic, N. 2019b, Transient Name Server AstroNote, 15, 1

Yaron, O., Prialnik, D., Shara, M. M., & Kovetz, A. 2005, ApJ, 623, 398, doi: 10.1086/428435

York, D. G., Adelman, J., Anderson, John E., J., et al. 2000, AJ, 120, 1579, doi: 10.1086/301513